Synchronization, Waves, and Turbulence in Systems of Interacting Chemical Oscillators

vorgelegt von
Diplom-Physikerin
Vanessa Casagrande

Von der Fakultät II - Mathematik- und Naturwissenschaften
der Technischen Universität Berlin
zur Erlangung des akademischen Grades
Doktor der Naturwissenschaft
– Dr. rer. nat. –
vorgelegte Dissertation

Promotionsausschuss:

Vorsitzender: Prof. Dr. E. Sedlmayr
Gutachter: Prof. Dr. H. Engel
Gutachter: Dr. M. Falcke
Gutachter: Prof. Dr. A.S. Mikhailov

Tag der wissenschaftlichen Aussprache: 22.02.2006

Berlin 2006
D 83

Kurzfassung

Die vorliegende Doktorarbeit beschäftigt sich mit wechselwirkenden nichtlinearen Oszillatoren. Es werden nichtlokal gekoppelte Oszillatoren untersucht, deren Wechselwirkung langreichweitig und abstandsabhängig ist. Zur mathematischen Modellierung der oszillatorischen Dynamik solcher Systeme wird die komplexe Ginzburg-Landau-Gleichung (CGLE) verwendet, die eine allgemeingültige Beschreibung von Reaktions-Diffusions-Systemen nahe der Hopf-Bifurkation liefert. Die CGLE wird zur Beschreibung der langreichweitigen Wechselwirkung mit einer zusätzlichen Gleichung gekoppelt, welche die langsame zeitliche Entwicklung einer weiteren diffundierenden passiven Komponente beschreibt. Aufgrund ihrer großen Diffusionskonstante ist die durch die passive Komponente vermittelte Kopplung nichtlokal. Das Ein-Oszillator-System weist Birhythmizität auf, d.h. zwei Grenzzyklen mit unterschiedlichen Amplituden und Frequenzen koexistieren. Die lineare Stabilitätsanalyse der Phasenapproximation des räumlich ausgedehnten Systems zeigt, dass die zwei Grenzzyklen unterschiedliche Stabilitätseigenschaften in Bezug auf die Propagation kleiner Störungen besitzen. Die numerische Lösung der Gleichungen zeigt zahlreiche Strukturen auf, wie homogene Oszillationen, Phasen- und Amplitudenturbulenz, aufbrechende Spiralen sowie Synchronisations- und Desynchronisationsausbrüche.

Wir schlagen vor, dass – neben bekannten Oszillationsvorgängen in der Biologie wie z.B. glycolytische Oszillationen oder Kalzium-Wellen – eine selbstorganisierte raum-zeitliche Strukturbildung im Bereich biologischer Systeme aufgrund von Synchronisation der Konformationszyklen der Enzyme zustande kommen kann. Ein Modell, in dem allosterische Enzyme durch Diffusion kleiner regulatorischer Produktmoleküle miteinander wechselwirken, wird vorgestellt. Jedes Enzym wird als Phasenoszillator beschrieben: Ein einzelner katalytischer Vorgang ist eine zyklische Sequenz von Konformationsänderungen. Durch eine solche Abfolge struktureller Änderungen kann ein Substratmolekül in ein Produktmolekül umgewandelt werden. Entweder bindet das abgegebene Produktmolekül an ein anderes Enzym, und beeinflußt damit dessen katalytische Aktivität, oder es zersetzt sich. Diese Rückkopplung bewirkt die Synchronisation der Enzymzyklen, so dass die Produktkonzentration mit einer Zeitperiode in der Größenordnung der Dauer einer einzelnen katalytischen Reaktion oszilliert. Die Enzympopulation kann auch in mehrere Gruppen zerfallen (Clusterbildung). In einem ausgedehnten System, in dem keine Durchmischung durch Produktdiffusion erfolgt,

tritt eine Kodimension-2 Hopf-Wellen-Bifurkation auf. Numerische Simulationen zeigen die Entstehung raum-zeitlicher Strukturen wie stehender oder propagierender Wellen, *Ripples*, Kreiswellenmuster und Spiralwellen.

Abstract

The aim of this thesis is to investigate systems of interacting nonlinear oscillators. We analyze nonlocally coupled oscillators where the interaction among the dynamical units is long-ranged and distance-dependent. In the proposed model, the oscillatory dynamics are given by the complex Ginzburg-Landau equation, which provides a general description of reaction-diffusion systems close to the Hopf bifurcation. The system is further coupled to a passive component which is diffusing as well, and inertial. This second field has a much larger diffusion constant than the first one, thus it provides an effective nonlocal coupling. The single oscillator-system displays birhythmicity, i.e. the coexistence of two stable limit cycles with different amplitudes and frequencies. Linear stability analysis of the phase approximation of the extended system shows that the two limit cycles have different stability properties against propagation of weak perturbations. Numerical solution of the equations displays patterns such as uniform oscillations, phase and amplitude turbulence, spiral breakup, bursts of synchronization, and bursts of desynchronization.

We suggest that, besides the known oscillatory phenomena in biology such as glycolytic oscillations and calcium waves, a novel type of self-organized spatio-temporal behavior could arise from synchronization among enzyme molecules. We propose a system of product-activated allosteric enzymes interacting through diffusion of small product molecules with regulatory function. We describe an enzyme as a phase oscillator: An individual catalytic event is a circular motion in the enzyme's conformational space. This sequence of structural changes allows conversion of one substrate molecule into one product molecule. The released product can then either bind to another enzyme and regulate its activity, or decay. This feedback mechanism causes synchronization of the enzymatic cycles, resulting in oscillations of the product concentration on the time scale of the duration of an individual catalytic reaction. The enzyme population can also split into clusters. In the extended system where product diffusion does not allow complete mixing, a codimension-2 Hopf-wave bifurcation is found. Numerical simulations reveal the existence of patterns such as standing and travelling waves, ripples, pacemakers, and spirals.

Contents

Chapter 1

Introduction

Self-organization is an intriguing phenomenon: It denotes the capability of a system to develop an ordered state. Such an *order* can be found in the temporal evolution of the system (for example, the emergence of an oscillatory trend), or even in the formation of spatially organized structures (like propagation of concentration waves in oscillatory chemical reactions). The spontaneous emergence of order is fascinating, because it appears to contradict the expectation that any system evolves towards a stationary, homogeneous state. Such a state is perceived as the normal and most likely condition for any physico-chemical system, because the second law of thermodynamics predicts spontaneous evolution towards disorder for closed systems. However, many dynamical systems of major interest are not closed at all: They can only be understood by considering their property of being persistently interacting with the external environment. Such exchange of energy and matter renders self-organization possible. The system is kept *active* and prevented from falling into an inert equilibrium state [1].

All living beings owe their functional activity to such an exchange, which is known as *metabolism*. In this way, they manage to *export entropy* outwards, and keep order inside. As clearly formulated by Schrödinger [2]: “What an organism feeds upon is negative entropy. Or, to put it less paradoxically, the essential thing in metabolism is that the organism succeeds in freeing itself from all the entropy it cannot help producing while alive”.

The investigation of systems in out-of-equilibrium conditions has become a very important field of research. Many different systems are known to be able to display pattern formation when kept in an active state. The examples include chemical reaction-diffusion systems [3, 4], electrochemical systems [5], hydrodynamical systems [6, 7], semiconductors [8], granular media [9], and optical systems [10, 11]. Living organisms are regarded as

an especially interesting class of self-organizing systems [12–14], as it is proven by the large number of studies on glycolytic oscillations [15–21], circadian rhythm [22–24], dynamics of the cardiac tissues [25, 26], collective behavior of microorganisms [27], and inter- and intracellular calcium dynamics [28–31]. Moreover, the application of the knowledge of dynamical systems in biology and medicine is giving rise to new therapeutic approaches, such as the treatment of Parkinson's disease by means of neuronal desynchronization [32, 33], or the indications for the development of new drugs based on the collective dynamical instabilities in living cells [31].

The theoretical modeling of these phenomena has highlighted the existence of general mechanisms underlying self-organization in all of these different systems. This observation is the basis of an interdisciplinary approach denoted as *synergetics* which was introduced by H. Haken [34]. The fundamental idea is that self-organization arises as a consequence of interactions of dynamical units. The cooperation of such dynamical units is characterized by some universal features, regardless of the peculiar details characterizing the specific system.

Thus, interactions among individual active elements play a central role. A relevant feature of such coupling, in the case of spatially extended systems, is its range. The two opposite cases of globally coupled systems (where the interaction uniformly affects all elements) and locally coupled systems (where each element directly influences only its neighbors) have been extensively studied [35–42].

Recently, Kuramoto *et al.* have stressed that there is also an intermediate regime, which can be defined as *nonlocal coupling*, where the descriptions provided in the two other cases break down [43–49]. One speaks about nonlocal coupling when the interaction range is larger than the distance between two neighboring active units, but still significantly smaller than the extension of the whole system. Such nonlocal coupling is found to arise in a general way when a population of dynamical elements is coupled through an additional diffusive substance. This regime is featured by the presence of exotic behaviors like the emergence of spatially discontinuous patterns, and requires a new approach.

In this thesis, we introduce a model where local and nonlocal coupling are simultaneously acting: An active oscillatory field is coupled to a second, passive field; both species are diffusing, but the second one has a much larger diffusion constant. This causes the coupling through it to be nonlocal. Moreover, the nonlocal coupling is assumed to be inertial. We investigate the model both analytically and numerically.

In the domain of biological systems, nonlocal coupling can be present as well. A known

example is a system of living cells, acting as dynamical units, communicating nonlocally with each other through some diffusive chemicals [43]. However, the same dynamics can be figured on a completely different scale. Single proteins behave in some cases as nonlinear oscillators [50, 51], and can therefore be viewed as active elements. Moreover, their functioning can be affected by the presence of small molecules with regulatory function. Thus, a population of proteins, for instance enzymes, can be interacting through diffusion of small regulatory molecules. This system has been theoretically investigated as a prototype model to explore the possibility of self-organization phenomena on a molecular level. In particular, the case of a small system with homogeneous distribution of regulatory molecules was studied [52–56]. It was found that the enzymes can undergo synchronization: the interaction is able to drive them to operate coordinately. This gives rise to oscillations which are essentially different from the above-mentioned periodic phenomena such as glycolysis and calcium waves. While those oscillations emerge from slow temporal variations of the reaction equilibrium conditions, the synchronization takes place on a molecular level here. It requires microscopic self-organization and out-of-equilibrium conditions for individual proteins [57].

In this work, we examine the case of a larger reaction volume where not only temporal variations of the system state, but also spatio-temporal patterns can be observed. The system consists of a population of allosteric enzymes. They catalyze a single reaction whose result is the formation of a product molecule. This molecule in turn is able to regulate the catalytic activity of the enzymes. The system is described by means of delayed partial differential equations. We analyze the bifurcation scenario and the one- and two-dimensional patterns emerging in the system.

The thesis is organized as follows. In Chapter 2 nonlinear oscillators are presented. We introduce the concept of self-sustained oscillations and give a description of the reduction method known as *phase dynamics approximation*. We describe the phenomenon of *birhythmicity*. We introduce the concept of *systems of interacting oscillators* focusing in particular on the distinction between *local, global*, and *nonlocal* coupling. Some of the main theoretical and experimental results on the three different interaction types are reviewed.

In Chapter 3 we present a model for a system of interacting oscillators with inertial nonlocal coupling, where the oscillatory dynamics are provided by the *complex Ginzburg-Landau equation* (CGLE). We analyze the single oscillator behavior by showing that it displays birhythmicity: there is one *rapid* and one *slow* limit cycles. We introduce the phase dynamics approximation for the interacting system to investigate diffusional instabilities. We show numerical results for the one- and two-dimensional systems. Among other patterns, we

emphasize the presence of a new type of intermittent turbulence which can emerge in the form of *bursts of synchronization* on a turbulent background or *bursts of desynchronization* on a synchronized background.

In Chapter 4 we first review some known examples of self-sustained oscillations in biological systems. We focus on the possibility of self-organized synchronization of enzymes operating as molecular machines in a living cell. We give an overview of the basic concepts of enzyme dynamics, with particular emphasis on the property of *allostery*, and on the role of conformational transformations.

In Chapter 5 we present a model for a system of product-activated allosteric enzymes coupled through product diffusion. We discuss the characteristic time and length scales of the system. We study the bifurcation scenario of the mean-field model to investigate the conditions for the occurrence of synchronization. In particular, we focus on the emergence of a codimension-2 Hopf-wave bifurcation in the extended system, where complete mixing of the regulatory molecules cannot be assumed. We show typical one- and two-dimensional patterns obtained through numerical simulations.

The results are summarized in Chapter 6.

Chapter 2

Background

2.1 Oscillations in active nonlinear systems

Systems operating far from thermodynamical equilibrium are characterized by strong energy flows. Energy is consumed, dissipated and continuously supplied to such a system, so that a thermodynamical description, based on the conservation of physical quantities at equilibrium states, is not suitable to understand their nature. To stress their difference with respect to conservative systems, they were originally called *dissipative systems* [1], but the name *active systems* is used as well, which seems to better convey the important feature that energy is not only consumed, but also supplied, in order to maintain a certain degree of activity.

A fascinating feature of active systems is their capability to show oscillatory dynamics, in the form of self-sustained oscillations. Oscillatory behavior is also present in Hamiltonian systems, as the most immediate example of a linear pendulum reveals. Nonetheless, the nature of oscillations is essentially different in the two cases.

Let us compare the dynamics of these systems in the phase space (see Fig. 2.1). In the case of the linear pendulum, the initial condition will select one orbit in the phase space. The periodic motion is reflected by the fact that the trajectory is a closed curve. The initial condition, i.e. the perturbation applied to the rest state, selects the amplitude of the oscillations and the energy, which is conserved during the motion and is represented by the area enclosed in the phase-space trajectory.

Self-oscillations in active systems represent instead *attractors* in the phase space. This means that, starting from any initial condition, the system will eventually end up by performing a periodic motion on a given orbit. This orbit only depends on the parameters of the system, and, since it will be reached from any initial state, it is called a *limit cycle*. A limit

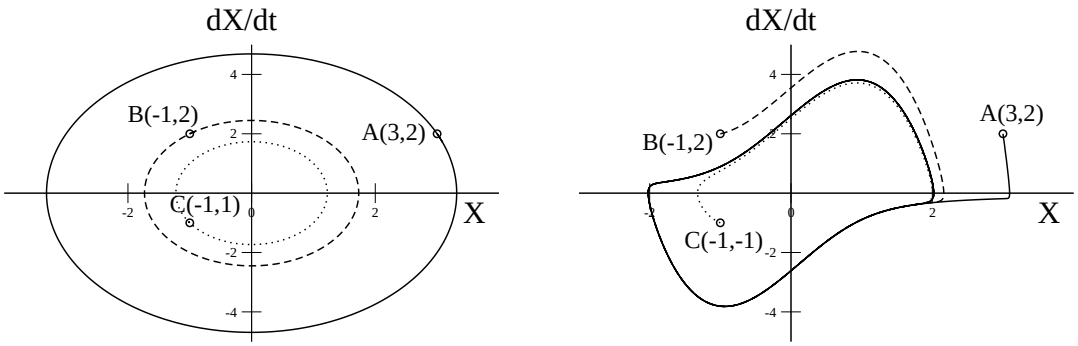

Figure 2.1: Trajectories in the phase space for a Hamiltonian system (harmonic pendulum: left) and a dissipative system (Van der Pol oscillator: right). The motion equations of the harmonic pendulum are: $\frac{\mathrm{d}^2X}{\mathrm{d}t^2} = -\omega X, E = \frac{1}{2}\left[\omega^2X^2 + \left(\frac{\mathrm{d}X}{\mathrm{d}t}\right)^2\right] - 1$. The equation of the Van der Pol oscillator is: $\frac{\mathrm{d}^2X}{\mathrm{d}t^2} = -\mu(X^2-1)\frac{\mathrm{d}X}{\mathrm{d}t} - X$. A,B,C are three different initial conditions.

cycle reached from three different initial conditions is shown for the Van der Pol oscillator in Fig. 2.1. These self-sustained oscillations are only possible because of the interplay of energy supply and energy dissipation in the system. The balance between the energy income and outcome determines the amplitude of the oscillations. Mathematically, such systems are described by means of nonlinear equations.

Active nonlinear systems, capable to display self-sustained oscillations, are the subject of the present work. Below we consider in more detail such a limit-cycle oscillator, following references [37, 39].

Let us first take a generic dynamical system, described by the ordinary differential equation:

$$\frac{\mathrm{d}\mathbf{X}}{\mathrm{d}t} = \mathbf{F}(\mathbf{X}). \tag{2.1}$$

Here $\mathbf{X}$ is a vector field whose components $\{X_1, X_2, \ldots, X_n\}$ represent, for instance, concentrations of different chemical species. The vector function $\mathbf{F}(\mathbf{X})$ describes interaction between different components and is in general a nonlinear function. The dynamics of the field $\mathbf{X}$ also depends on some independent parameters, representing external conditions or intrinsic characteristics of the system. In the present case, we assume that the relevant parameter is unique (denoted in the following by p), and we call it the *control parameter*.

Thus, (2.1) should be written as:

$$\frac{\mathrm{d}\mathbf{X}}{\mathrm{d}t} = \mathbf{F}(\mathbf{X}; p). \tag{2.2}$$

Depending on the value of p, the dynamics of the field $\mathbf{X}$ might change. For instance, the stationary state:

$$\mathbf{X}(t) = \mathbf{X}_0 = \text{const} \tag{2.3}$$

defined by the condition:

$$\mathbf{F}(\mathbf{X}; p) = 0 \tag{2.4}$$

might change its stability properties. By assumption, there is a critical value of p at which it happens. This specific value p_c is called a *bifurcation point*. When $p < p_c$ (Fig. 2.2(a)) the system has a stable fixed point $\mathbf{X}_0$: All N complex eigenvalues λ_j of the Jacobian matrix J defined by:

$$J_{ik} = \frac{\partial F_i}{\partial X_k} \tag{2.5}$$

have negative real parts. That is, any perturbation of the form:

$$\varepsilon(\lambda)\mathrm{e}^{\lambda t} \tag{2.6}$$

applied to the stationary state would decay, and the system would eventually get back to the fixed point. At $p = p_c$ (Fig. 2.2(b)) the stationary point looses its stability: The real part of at least one eigenvalue becomes positive, so that the associated perturbation is no longer decaying, but growing with time. We consider a bifurcation where this happens simultaneously for a pair of complex conjugated eigenvalues, which are called the *bifurcating eigenvalues*.

The new stationary solution is then given by a periodic orbit whose amplitude is vanishing at the bifurcation point and increasing as p becomes larger than p_c (Fig. 2.2(c)), the frequency of the oscillations is given by the imaginary part of the bifurcating eigenvalues. This bifurcation is known as the *Hopf bifurcation*.

Close to the bifurcation point, it is possible to treat the system by means of a perturbative expansion, the distance $p - p_c$ being a small parameter which characterizes the state of the system.

It turns out that, in the vicinity of the bifurcation, the dynamics of the system can be expressed as a composition of a slow mode and some much faster oscillations. It can be shown that the real part of the bifurcating eigenvalue is of order $p - p_c$, so that a slow time scale:

$$\tau = (p - p_c)t \tag{2.7}$$

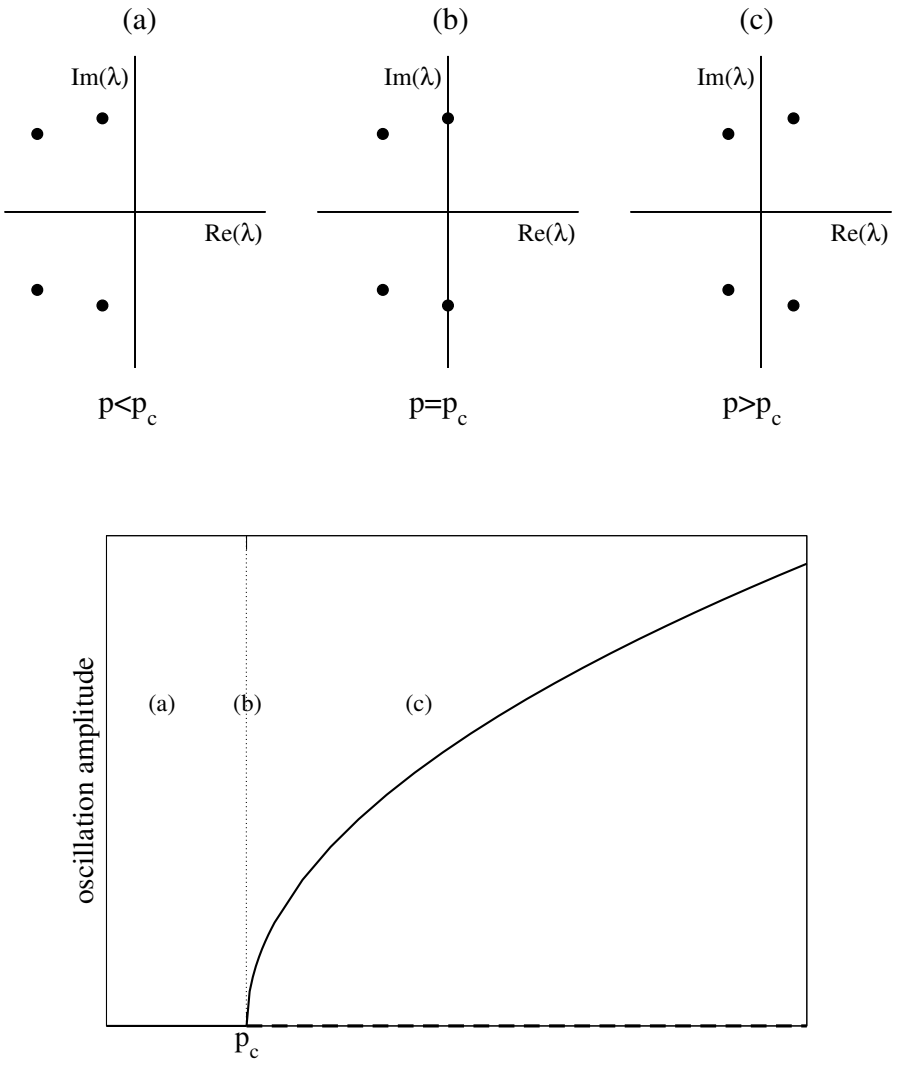

Figure 2.2: At the Hopf bifurcation, a pair of complex conjugate eigenvalues crosses the imaginary axis. (a) Before the bifurcation point ($p < p_c$), a stationary stable state exist. (b) At the bifurcation ($p = p_c$) it looses its stability. (c) The new stationary solution is a limit cycle whose amplitude increases as the square root of the distance from the bifurcation point. The frequency of the limit cycle equals the imaginary part of the eigenvalue (Imλ).

can be introduced.

As a result, the dynamics of the system will be expressed as:

$$\mathbf{X}(t) = \mathbf{X}_0 + \sqrt{p - p_c}\,[W(\tau)\mathbf{U}\exp(i\omega_0 t) + \text{c.c.}]\,, \tag{2.8}$$

where $W(\tau)$ is the slowly varying *complex amplitude*. Before going into the details of its dynamics, let's first observe that Eq. (2.8) reveals that our dynamical system $\mathbf{X}(t)$ close to the bifurcation is performing some periodic motion around the unstable fixed point $\mathbf{X}_0$. This periodic motion consists of a fast oscillating process with frequency ω_0 and amplitude $|\mathbf{U}|$, modulated by a slowly varying envelop $W(\tau)$. The amplitude of the oscillations scales as the square root of the distance from the bifurcation point.

In what concerns the complex amplitude, it turns out that its evolution is given by the following ODE:

$$\frac{\mathrm{d}W}{\mathrm{d}t} = (1 + \mathrm{i}\omega)W - (1 + \mathrm{i}\alpha)|W|^2 W \tag{2.9}$$

which is known as the *Stuart-Landau equation*.

It describes a circular motion on the complex plane with unit amplitude and constant frequency $\omega - \alpha$, representing the simplest nonlinear oscillator. By expressing the complex variable W in terms of two real quantities - the amplitude ρ and the phase Φ - as:

$$W(t) = \rho(t)\mathrm{e}^{i\Phi(t)} \tag{2.10}$$

the solution of (2.9) can be written as:

$$\begin{cases} \rho(t) & = 1 \\ \Phi(t) & = (\omega - \alpha)t \end{cases} \tag{2.11}$$

The most important point to be stressed at this stage is that the emergence of a slow time scale as well as the dynamics of the envelope W expressed by Eq. (2.9) are universal and do not depend on the specific dynamical system under consideration. The dependence on the details of a particular system are contained in the parameters of Eqs. (2.8) and (2.9). These parameters $\omega_0, \mathbf{U}, \omega$, and α are uniquely determined by the function $\mathbf{F}(\mathbf{X}; p)$.

The universal behavior of systems close to a bifurcation point is not restricted to the Hopf bifurcation, and is a fact which plays a fundamental role in all the theory of dynamical systems. In the present case, the outline of the derivation of the Stuart-Landau equation was aimed to define the objects which we call *oscillators*, by sketching the guidelines of one of the most general ways in which oscillatory dynamics my appear.

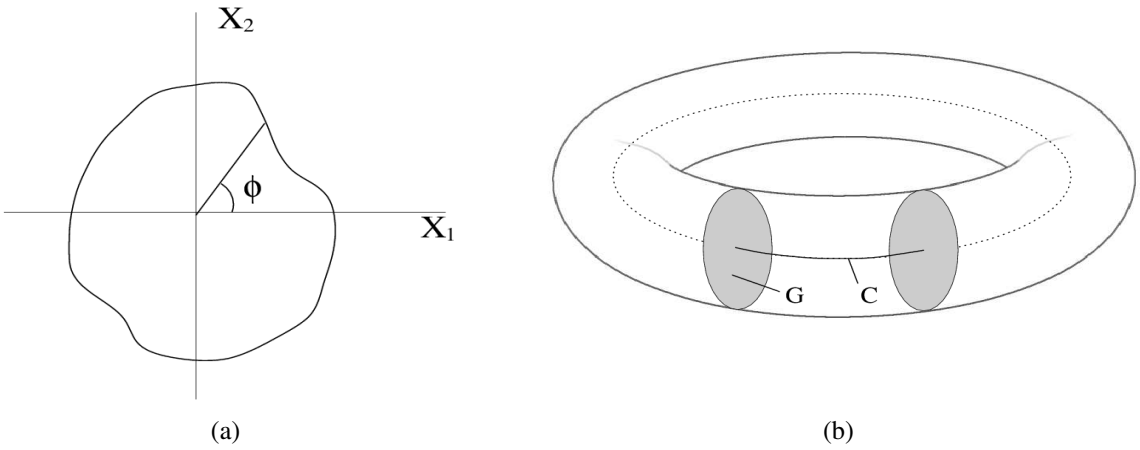

(a) (b)

Figure 2.3: (a) A phase variable constantly increasing with time can also be defined for unharmonic limit cycles. (b) The definition of phase can be extended to the neighborhood G of a limit cycle C, so that it can also be used to describe the dynamic of a perturbed limit cycle oscillator. Reproduced from [37].

When an oscillator is as simple as in Eq. (2.9), it can be viewed as a clock performing cyclic motion with constant velocity. In such a case, we can reduce the degrees of freedom of the system to only one important variable: the phase. As it has already been observed, for Eq. (2.9) the oscillation amplitude does not vary (it is constant and equal to unity), so that the state of the oscillator is completely determined once its angular position within the cycle is given. This is the information the phase variable Φ provides us with. In the present case, the phase description of our oscillator is:

$$\dot{\Phi} = \text{const.} \tag{2.12}$$

Remarkably, a phase variable with the same dynamics as in Eq. (2.12) may be defined for any stable periodic orbit, not necessarily displaying circular harmonic motion. Moreover, such definition can be generalized to a neighborhood of the limit cycle in the phase space, in such a way that a phase description can still be used for slightly perturbed limit cycle oscillators (see Fig. 2.3). In his first paper [35] Winfree used the name *generalized relaxation oscillators*,[1] and defined them as "devices which execute their fluctuations at a variable rate but within strictly fixed limits of amplitude".

Despite the simplicity of the phase dynamics description, phase oscillators can also be

[1]This denomination has however been abandoned in favor of the term *phase oscillators*. Indeed, at present the name *relaxation oscillators* is rather used to indicate strongly unharmonic oscillations.

used to model complex processes. For example, under specific conditions even molecular machines can be described as phase oscillators. A single protein is a complex molecule with a large number of degrees of freedom, which can undergo structural changes. In some cases, however, these *conformational motions* follow a well defined path. Such path in the high-dimensional space of all possible conformational states of the molecule is an analog of a limit cycle of a dynamical system. This analogy will be discussed in more detail in Chapter 4.

The concept of a simple clock is however not always suitable to describe real oscillations in biological and chemical systems. Indeed, the oscillatory behavior can also manifest itself through much more complicated dynamics. Let us return to the discussion of the Stuart-Landau equation (2.9). We have observed that this equation describes the system in the vicinity of a Hopf bifurcation. Further variation of the control parameter p can lead to new bifurcations. One of the typical cases is the period-doubling bifurcation: The oscillations become more complicated and the minimal repeated temporal pattern consists of two subsequent oscillations (see Fig. 2.4). A sequence of period-doublings can occur, thus leading to an increase of the oscillation period. For still larger values of the control parameter, periodicity of the motion is lost and the trajectory is chaotic. In the case of a period-doubled trajectory or of a chaotic oscillator, the phase description is not suitable because the position of the system in the attractor cannot be determined by means of a single phase coordinate.

Oscillatory dynamic is not the only possible outcome of nonlinear equations. Indeed, nonlinear systems are in general classified within three categories: *bistable, excitable*, and *oscillatory* [39, 40]. Bistable systems are characterized by the existence of two different stable states. Excitable systems posses a unique stable fixed point; however, if they are affected by a perturbation which overcomes a certain threshold amplitude, they are able to perform an excursion in the phase space before returning to the stable fixed point. That is, they do not relax immediately to the stationary state, but keep the excitation for a finite time.

2.2 Birhythmicity

A different example of complex oscillations is provided by the case of *birhythmicity*. The word *birhythmicity* was first introduced by Decroly and Goldbeter [58] to describe the coexistence for the same parameters of two different stable limit cycles. The system they have studied was a biochemical two-step reaction. The product of the first reaction is used as substrate by the second reaction. Each step is catalyzed by an allosteric enzyme (cf. Sec.

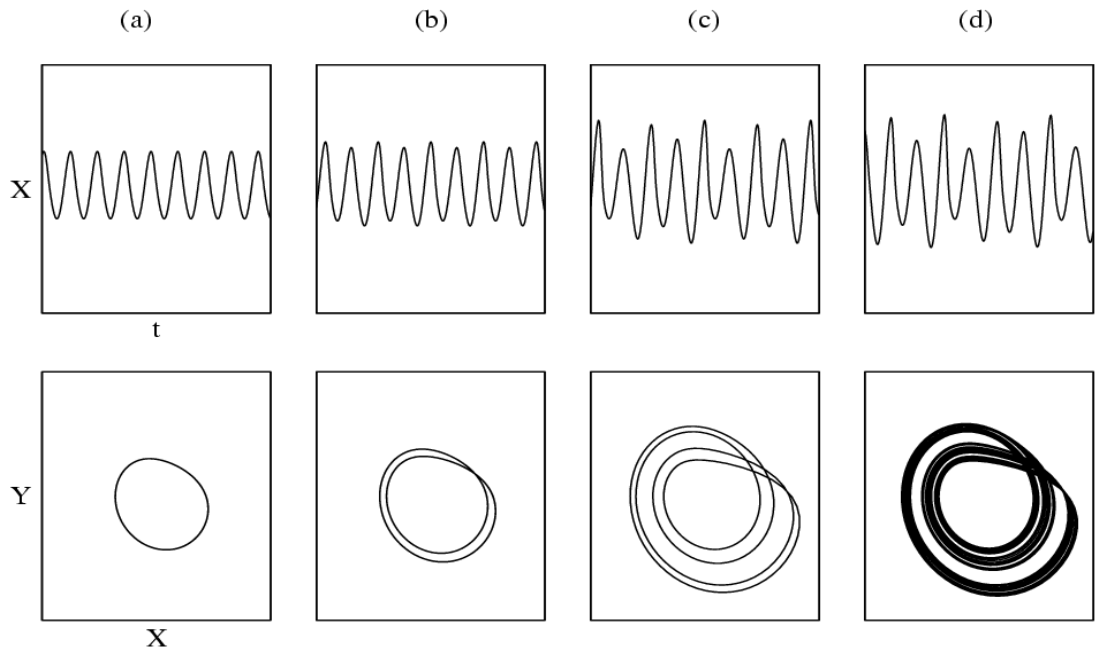

Figure 2.4: Example of a sequence of period-doubling bifurcations leading to turbulence. A set of numerical solutions of the Rössler system: $\dot{X} = -(Y + Z), \dot{Y} = X + \frac{Y}{5}, \dot{Z} = \frac{1}{5} + Z(X - \mu)$ is shown. The control parameter μ is set equal to 2.8(a), 2.9(b), 4.1(c), 4.25(d). Between (a) and (b) a period-doubling bifurcation occurs: The minimal pattern to be repeated in the time-series consists of two successive oscillations with different amplitudes. This is seen in the (X, Y) phase-plane. A simple closed orbit is replaced by a trajectory where the $[0 - 2\pi)$ range of the angular coordinate must be covered twice before it gets closed. The trajectory is not self-intersecting in the three-dimensional (X, Y, Z) plane. At higher values of μ, further period-doublings occur, and the trajectory ends up by being aperiodic.

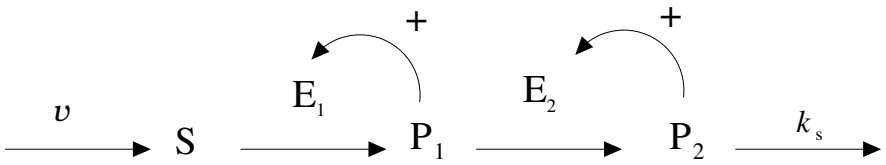

Figure 2.5: Two-step biochemical reaction [58]. A substrate (S) is supplied at rate v and converted into a product (P_1) through a reaction catalyzed by enzyme E_1. The catalytic activity of E_1 is enhanced by the increasing concentration of P_1 (i.e. E_1 is allosterically activated by its own product P_1). P_1 is then converted to P_2 through the reaction catalyzed by E_2, which is in turn an allosteric enzyme activated by P_2. The latter is then removed at constant rate k_s.

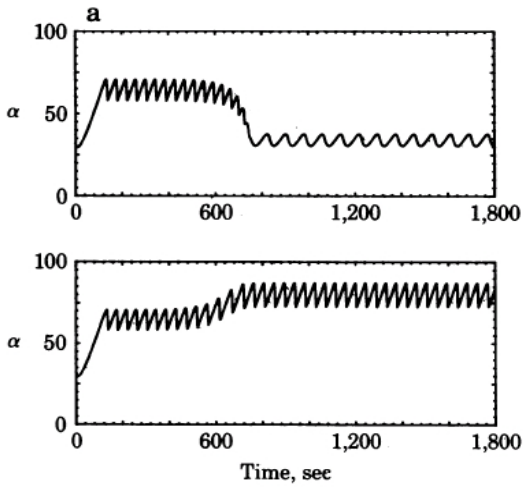

Figure 2.6: Bistability of oscillatory modes [58]. The time series of the substrate concentration is displayed. Starting from slightly different initial conditions, after a transient of about 700 s, two different limit cycles are reached by the system.

4.2.1) activated by its own reaction product. The initial substrate is supplied at a constant rate and the final product is continuously removed. The reaction scheme is sketched in Fig. 2.5. Choosing the product removal rate k_s as the control parameter, one can see that the system undergoes a cascade of period-doubling bifurcations leading to chaotic dynamics. But in a relatively narrow region before the occurrence of such period doublings, the system shows coexistence of two stable limit cycles. Numerical investigations have shown that two types of oscillations (which differ from each other by their amplitudes and frequencies) can be obtained by starting from different initial conditions (Fig. 2.6).

One year later, Alamgir and Epstein [59] described an experiment in a continuous stirred tank reactor where two chemical reactions were coupled to each other with the same scheme proposed by Decroly and Goldbeter. Two reactions were chosen which were already known to display oscillatory dynamics, namely the ClO_2^-–I^-[11] and the BrO_3^-–I^-[4] reactions. The two reactions interacted with each other via two different couplings (iodide reacts with bromate to yield bromide, and furthermore the reaction ClO_2^--BrO_3^--Br^- is oscillatory itself). Like in the theoretical predictions in Ref. [58], the systems displayed birhythmicity in a narrow

parameter region before the onset of chaotic oscillations, where the control parameter was the removal rate of I^-. The reaction could be driven by on-time perturbations from one to the other oscillatory state.

After that, a large number of models showing birhythmicity was proposed, mostly in the context of oscillations in biological systems [12]. In the domain of chemical oscillators, an interesting theoretical example was presented by Hocker and Epstein [60]. The system consists of two coupled subsystems, each of them of the FitzHug-Nagumo type. The FitzHugh-Nagumo systems can have a unique stable fixed point or display either bistability or oscillatory dynamics depending on the parameters. If the two coupled systems are such that one of them is bistable while the other is oscillatory, birhythmicity can arise, provided that the coupling between the two systems is not too strong. As in [58], under further increase of the control parameter (here, the coupling strength) chaotic behavior is found. Eventually, very strong coupling suppresses all exotic dynamics by driving the system to a unique simple limit cycle.

Birhythmicity in the famous Belousov-Zhabotinsky reaction [61–66] has not been intensively studied. Exceptions are the experimental observations by Lamba and Hudson [67] and a theoretical study based on the Oregonator model [68].

Recently, Stich et al. [69–71] have investigated the behavior of systems at the onset of birhythmicity. A systematic derivation of the normal form of the pitchfork-Hopf bifurcation was performed. This bifurcation corresponds to the simultaneous appearance of bistability and oscillations (see Fig. 2.7) leading to the coexistence of two stable limit cycles. Through variation of a control parameter, a stable fixed point looses its stability and oscillations arise. Through variation of a second parameter, the fixed point becomes unstable by the appearance of two other stable stationary points. The simultaneous variation of both parameters leads to the emergence of two different stable limit cycles.

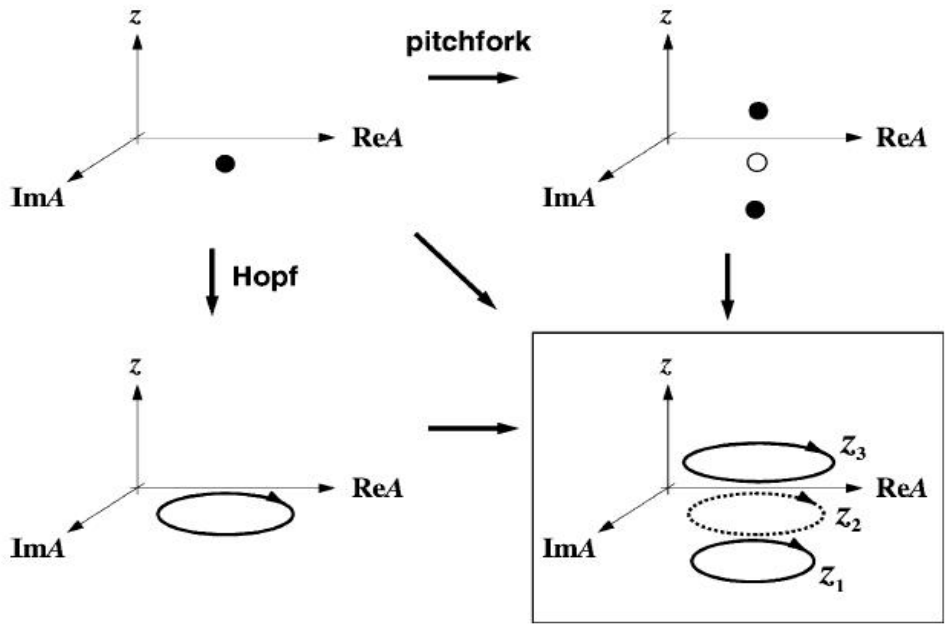

Figure 2.7: Schematic representation of the pitchfork-Hopf bifurcation (from [70]). Solid dots represent stable fixed points, open dots unstable fixed points, solid circles stable limit cycles, dashed circles unstable limit cycles.

2.3 Systems of interacting oscillators

Next we consider a set of N interacting oscillatory elements. Such a system is described by a set of N coupled evolution equations:

$$\frac{\mathrm{d}\mathbf{X}_m}{\mathrm{d}t} = \mathbf{F}_m(\mathbf{X}_m) + \mathbf{G}_m(\mathbf{X}_1, \mathbf{X}_2, \ldots, \mathbf{X}_N), \quad m = 1, \ldots, N. \tag{2.13}$$

The function $\mathbf{F}_m$ gives the local dynamics of the individual oscillator $\mathbf{X}_m$. We have named $\mathbf{G}_m$ the coupling function representing the interaction exerted on the oscillator m by the rest of the system. In this picture, the system is seen as a collection of distinct subunits, possibly representing separated objects, influencing each other by means of some interaction.

The coupling function $\mathbf{G}_m$ can often be expressed as a composition of pairwise terms, and Eq. (2.13) can therefore be written as:

$$\frac{\mathrm{d}\mathbf{X}_m}{\mathrm{d}t} = \mathbf{F}_m(\mathbf{X}_m) + \sum_{k=1}^{N} \mathbf{g}_{mk}(\mathbf{X}_m, \mathbf{X}_k). \tag{2.14}$$

Let us consider a system where the oscillators are located on a regular one-dimensional lattice. Such an array is thus characterized by the total number of oscillators N and by the distance h separating two neighboring oscillators, the total length of the chain is thus $L = Nh$.

The continuum limit is obtained when the space separating the oscillators becomes vanishingly small, while the total size of the system is kept constant:

$$N \rightarrow \infty \tag{2.15}$$

$$h \rightarrow 0 \tag{2.16}$$

$$L = Nh = \text{const.} \tag{2.17}$$

The system consists then of an infinite number of oscillators, with continuous spatial distribution. Such continuous picture is much more convenient, for example, for the description of oscillating chemical reactions. In this case, the reaction solution is an extended continuous medium, whose local dynamics are of the oscillatory type.

A convenient way to classify different types of interactions in systems of oscillators is according to the range over which the interaction extends. We shall distinguish between local, global, and nonlocal couplings. Below we consider these three types separately, assuming for simplicity that the oscillators are arranged in a regular one-dimensional array.

2.3.1 Local coupling and the complex Ginzburg-Landau equation

Let us consider a one-dimensional system of identical oscillators, that is the local dynamics $\mathbf{F}_m$ is the same for each element: $\mathbf{F}_m = \mathbf{F}$ for $m = 1, 2, \ldots, N$.

The interaction is *local* when each oscillator only experiences the influence of its first neighbors. That is, the equations describing the system are:

$$\frac{\mathrm{d}\mathbf{X}_m}{\mathrm{d}t} = \mathbf{F}(\mathbf{X}_m) + \sum_{k=m-1}^{m+1} \mathbf{g}_{mk}(\mathbf{X}_m, \mathbf{X}_k). \tag{2.18}$$

In many cases, the interaction $\mathbf{g}_{mn}$ is a spatially constant, linear function which can be written as:

$$\frac{\mathrm{d}\mathbf{X}_m}{\mathrm{d}t} = \mathbf{F}(\mathbf{X}_m) + \sum_{k=m-1}^{m+1} \mathbf{K}(\mathbf{X}_k - \mathbf{X}_m), \tag{2.19}$$

where $\mathbf{K}$ is a constant $n \times n$ matrix where n is the dimension of the vector field $\mathbf{X}$.

This type of coupling is by far the most common, as it arises in a natural way for a large number of physical systems [3, 37]. Let us consider the coupling terms in Eq. (2.19):

$$\mathbf{K}(\mathbf{X}_{m+1} - \mathbf{X}_m + \mathbf{X}_{m-1} - \mathbf{X}_m). \tag{2.20}$$

In order to take the continuum limit, we must substitute the discrete array index m with a continuous one dimensional coordinate x, the distance between two neighbors is the parameter h introduced above. First, we define a new interaction matrix as:

$$\mathbf{D} \equiv h^2\mathbf{K}. \tag{2.21}$$

Thus we get for Eq. (2.20):

$$\frac{\mathbf{D}}{h^2}[\mathbf{X}(x+h) + \mathbf{X}(x-h) - 2\mathbf{X}(x)]. \tag{2.22}$$

Now the limit $h \to 0$ has to be considered, which simultaneously entails (2.15, 2.16, 2.17). To the first orders in h we obtain for Eq. (2.22):

$$\frac{\mathbf{D}}{h^2}\left[\mathbf{X}(x) + h\frac{\partial \mathbf{X}}{\partial x} + \frac{h^2}{2}\frac{\partial^2 \mathbf{X}}{\partial x^2} + \mathbf{X}(x) - h\frac{\partial \mathbf{X}}{\partial x} + \frac{h^2}{2}\frac{\partial^2 \mathbf{X}}{\partial x^2} - 2\mathbf{X}(x)\right] = \mathbf{D}\frac{\partial^2 \mathbf{X}}{\partial x^2}. \tag{2.23}$$

Thus, the continuous version of system (2.19) reads:

$$\frac{\partial \mathbf{X}}{\partial t}(x,t) = \mathbf{F}(\mathbf{X}(x,t)) + \mathbf{D}\nabla^2\mathbf{X}(x,t) \tag{2.24}$$

which is a system of diffusively coupled oscillators. Often, if the components of $\mathbf{X}$ represent concentrations, the matrix $\mathbf{D}$ will be diagonal.

Models of the type (2.24) are called *reaction-diffusion systems* since they are mostly used to describe chemical reactions. In this case, the components of the field $\mathbf{X}$ represent concentrations of different chemical species. The term $\mathbf{F}(\mathbf{X}(x,t))$ includes then contributions from various local reactions. For instance, a contribution of the type $\alpha X_1(x,t)X_2(x,t)$ describes a reaction between components X_1 and X_2 occurring at constant rate α, a contribution $\beta X_1^2(x,t)$ corresponds to an autocatalytic reaction with rate β, while $-\gamma X_2$ means that component X_2 has a first-order decay kinetics with the constant rate γ. On the other hand, $\mathbf{D}\nabla^2\mathbf{X}(x,t)$ accounts for diffusion, which is the macroscopic manifestation of the Brownian motion of individual molecules [72–76] and is therefore responsible for matter transport.

Kuramoto starts his famous book [37] with the words: "Mathematically, a reaction-diffusion system is obtained by adding some diffusion terms to a set of ordinary differential equations which are first-order in time". Like in the case of a single oscillator, for extended systems with diffusional coupling it is possible to derive the normal form at the Hopf bifurcation point, that is the universal dynamics of reaction-diffusion systems close to the emergence of *uniform oscillations*. The result is the well known *complex Ginzburg-Landau equation* (CGLE) [37]:

$$\frac{\partial W}{\partial t} = (1+\mathrm{i}\omega)W - (1+\mathrm{i}\alpha)|W|^2W + (1+\mathrm{i}\beta)\nabla^2 W. \tag{2.25}$$

It admits a solution in the form of homogeneous oscillations, corresponding to the single element behavior described by Eq. (2.11). However, linear stability analysis shows that such oscillations can be unstable against the growth of spatial modulations. This instability, due to diffusion, is found when the parameters satisfy the Benjamin-Feir condition [37, 40]:

$$1 + \alpha\beta < 0. \tag{2.26}$$

The CGLE has a very rich spatiotemporal behavior [77]: It can display coherent structures [78], spirals [79], intermittent chaos [80], and turbulence [81, 82].

Local coupling provides the system with the notion of vicinity and distance: each element directly interacts only with its neighbors, which then transmit the interaction to their own neighbors. Thus, a localized perturbation spreads through the system affecting first its close proximity and later reaching the farther parts of the system. This is a crucial property of reaction-diffusion systems. Let us consider, for instance, a system where birhythmicity (cf. Sec. 2.2) is present. While for a single oscillator the birhythmicity manifests itself as

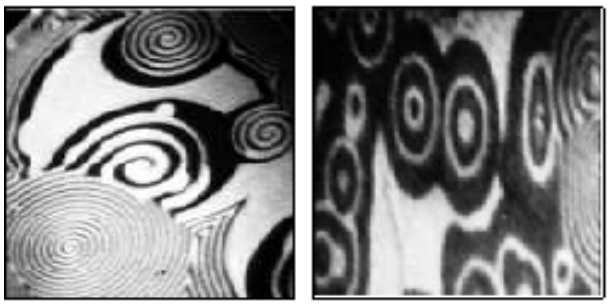

Figure 2.8: PEEM images of the reaction surface in catalytic CO oxidation on Pt(110). Dark (bright) areas correspond to oxygen (CO) covered domains. Among the most characteristic diffusion induced-patterns, rotating spirals (left) and target waves (right) can be observed. From [83].

bistability between two different oscillatory modes, in a system of interacting elements coupled through diffusion it can give rise to a rich variety of phenomena. Stich et al. [69–71] have observed spontaneous formation of pacemakers as a result of birhythmicity in the extended system. In this system, a stable oscillating core can form, which is able to emit waves towards the rest of the medium, entrained by a different frequency.

The inclusion of diffusional terms is thus necessary to model self-organization phenomena which are characterized by the presence of a spatial structure. As an example, the catalytic CO oxidation on Pt(110) can be considered, which is one of the best studied self-oscillating surface reactions [84]. In this reaction, molecules of oxygen and carbon monoxide, which are present in a chamber in the gas phase, can adsorb on a monocrystalline Pt(110) surface. The crystal carries out a catalytic function, thus providing a substrate where the oxidation reaction CO+O $\rightarrow$ CO_2 can take place. CO_2 molecules desorb from the surface and get back into the gas. If the gases are continuously pumped into the chamber, monitoring the CO and O coverages at the surface reveals self-sustained oscillations, i.e. the periodic alternation between a reactive (mainly oxygen-covered) state and a passive (mainly CO-covered) state. The temporal behavior of this system is already very rich: self-sustained oscillations, period doubling bifurcations, and chaos have been reported [85, 86]. Such temporal behavior is accurately reproduced by a three-component model of ordinary differential equations [87]. However, as experimental techniques allowing spatial resolution on the micrometer scale were employed, it became clear that temporal oscillations are accompanied by inhomogeneous coverages of the reaction surface. This has unveiled the wealth of spatio-temporal patterns displayed by the reaction, which includes traveling waves, propagating pulses, rotating spirals, target waves, and turbulence [88–90], see an example in Fig. 2.8. The presence of such spatio-temporal structures is due to the local diffusion of CO molecules through the surface: Once adsorbed, a CO molecule is able to migrate to a neighbor site on the crystal surface. However, the characteristic length of such diffusional motion is very small as compared to the total size of the reaction surface, in such a way that it cannot allow for a

homogeneous distribution of the adsorbed molecules. The mathematical modeling of such spatio-temporal patterns requires then the inclusion of diffusion terms, yielding a system of partial differential equations. For the CO oxidation reaction this has been done [91, 92], and the reaction-diffusion model has been found to appropriately account for the spatial behavior of the reaction.

2.3.2 Global coupling

When any two oscillators of the system directly affect each other, the coupling is said to be *all-to-all*. If, in particular, each element gives an identical contribution to the interaction, the system is *globally coupled*, which means that the coupling function $\mathbf{g}_{mn}$ of Eq. (2.14) is the same for any pair of oscillators:

$$\frac{\mathrm{d}\mathbf{X}_m}{\mathrm{d}t} = \mathbf{F}_m(\mathbf{X}_m) + \sum_{k=1}^{N} \mathbf{g}(\mathbf{X}_m, \mathbf{X}_k). \tag{2.27}$$

In many cases, the interaction in such a system can also be written in terms of the mean field:

$$\frac{\mathrm{d}\mathbf{X}_m}{\mathrm{d}t} = \mathbf{F}_m(\mathbf{X}_m) + \mathbf{G}(\langle\mathbf{X}\rangle, \mathbf{X}_m), \tag{2.28}$$

where $\langle\mathbf{X}\rangle$ denotes the average over the oscillators population defined as $\langle\mathbf{X}\rangle = \frac{1}{N}\sum_{k=1}^{N}\mathbf{X}_k$.

The effects of global coupling have been extensively studied [38, 41]. The first contributions by Winfree [35] and Kuramoto [36] were devoted to the analysis of systems of oscillators affected by weak coupling that can be described in the phase dynamics approximation. In particular, the paradigmatic model of globally coupled phase oscillators, known as the *Kuramoto model*, reads:

$$\frac{\mathrm{d}\Phi_m}{\mathrm{d}t} = \omega_m + \frac{G}{N}\sum_{k=1}^{N}\sin(\Phi_k - \Phi_m). \tag{2.29}$$

The behavior of this system has been described making use of order parameters which give informations about the synchronization of the system [36, 37, 42]. The oscillators are synchronized if they lock to a common frequency. For system (2.29), it turns out that there is a critical value of the coupling strength G below which synchronization is not possible. For couplings that are stronger than this critical value, synchronization takes place as a phase transition phenomenon: Oscillators whose native frequencies ω_m are close to the average frequency Ω of the population become entrained. This gives rise to the nucleation of a cluster of synchronized elements, which tends to grow and eventually saturates. The stationary

size of the synchronized cluster raises as the interaction increases. For finite values of the coupling strength G, there will always be a group of drifting oscillators which are not entrained because their native frequencies are too far apart from the average Ω. In the limit $G \to \infty$, the whole population becomes *fully synchronized* which means that not only the frequencies of all the oscillators are locked, but they also have all the same phase at each moment. Note that, in the simpler case where all oscillators in Eq. (2.29) are identical (i.e. they all have the same native frequency ω), the system becomes fully synchronized for any positive value of G.

Recently, an experimental confirmation of Kuramoto's theory of phase transition to synchronization has been provided in a system of globally coupled electrochemical oscillators [93]. The theoretical predictions about the dependence of the order parameter on the coupling intensity have been confirmed.

More complex behavior is found to arise, if one considers interaction functions containing higher harmonics [94–97]. Let us take for example a system of identical phase oscillators, all having the same natural frequency, interacting through a generic periodic function [95]:

$$\frac{\mathrm{d}\Phi_m}{\mathrm{d}t} = \omega_m + \frac{1}{N}\sum_{k=1}^{N} F(\Phi_k - \Phi_m), \tag{2.30}$$

where:

$$F(\Phi_k - \Phi_m) = \sum_{j=0}^{\infty}\{a_j \sin\left[j(\Phi_k - \Phi_m)\right] + b_j \cos\left[j(\Phi_k - \Phi_m)\right]\}. \tag{2.31}$$

If some of the a_j and b_j coefficients for $j > 1$ do not vanish, the phenomenon of *phase clustering* can occur. The oscillators organize themselves in distinct groups, each group being characterized by full synchronization, while the elements of two different clusters maintain a constant phase difference. The phenomenon of clustering as an effect of global coupling has also been observed experimentally in the photo-sensitive the Belousov-Zhabotinsky reaction [98].

A different type of clustering behavior is found if, instead of considering phase oscillators, also the amplitude degree of freedom is allowed to come into play [99, 100]. In fact, within the phase dynamics approximation, all oscillators necessarily follow the same orbit, and can only differ by their instantaneous frequencies and phases. This situation changes if limit cycle oscillators are considered. An example can be provided by globally coupled elements of the Stuart-Landau type (Eq. (2.9)) [100]:

$$\frac{\mathrm{d}W_m}{\mathrm{d}t} = (1 + \mathrm{i}\omega)W_m - (1 + \mathrm{i}\alpha)|W_m|^2 W_m + G(1 + \mathrm{i}\beta)(\langle W\rangle - W_m), \tag{2.32}$$

where $\langle W \rangle = \frac{1}{N} \sum_{m=1}^{N} W_m$. The phase dynamics approximation in the limit of weak coupling for system (2.32) does not show phase clustering. However, for finite coupling, the system breaks up into a number of macroscopic clusters, such that all the oscillators within a given cluster have the same complex amplitude, which however differs from one cluster to the other. In this case, the groups of synchronized oscillators follow different orbits in the phase space. For large values of the coupling constant G, the fully synchronized state is stable. Remarkably, systems of the type (2.32) can also display chaotic behavior, although the individual oscillators are identical and non chaotic.

Systems of chaotic oscillators with global coupling have been studied as well [101–103], showing that clustering, collective chaos, and synchronization phenomena are possible.

In many systems, both local and global couplings are simultaneously present. For example, in surface chemical reactions, local interactions are due to diffusion of the adsorbed molecules, while a coupling arising from the influence of the gas phase in the chamber acts globally on the reaction surface. Such kind of systems have been the subject of many studies. Let us focus again on the catalytic CO oxidation on Pt(110). Experimental observations have given indications that global coupling is responsible for the emergence of otherwise unseen spatio-temporal patterns such as standing waves [104, 105], and cellular structures [106]. Theoretical modeling and numerical simulations have not only confirmed this interpretation, but also revealed the possibility of other patterns due to global interactions. Abstract models making use of the globally coupled CGLE [92, 106–108] have been successful in reproducing qualitatively the observed patterns, thus clarifying the role played by the global coupling. Realistic modeling of the specific reaction with the inclusion of gas-phase coupling [92, 109–114] has permitted to investigate in more detail the behavior of the system for different parameters. Bifurcation analysis and numerical integration of such realistic model have also predicted the existence of cluster solutions and phase flips.

It has been observed that, also in the presence of global coupling, a kind of turbulence is possible that is qualitatively different from turbulence induced by diffusion, being characterized by intermittency and by the presence of long-range order [92, 108]. However, global coupling has mostly the effect to drive the system to an ordered state. For this reason, it has been used to implement a feedback control method through which suppression of turbulence could be achieved [115]. This method makes use of external regulation of the gas pressure: the global coupling is tuned and adapted according to a signal originating from the reaction surface. Moreover, a time-delay between the signal and the applied coupling can be used as an additional adjustable parameter. Experiments on the CO oxidation with this time-delayed

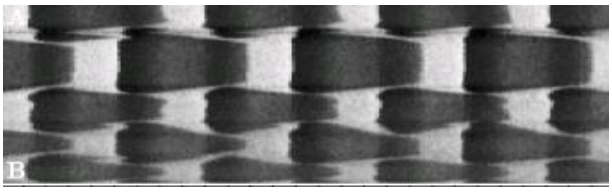

Figure 2.9: After [116]: Space (vertical coordinate)-time (horizontal coordinate) plot showing the formation of clusters giving rise to the characteristic spot-like structure in a system with both global and diffusional coupling in the CO oxidation on Pt(110).

global feedback [115, 116] have revealed that chemical turbulence can be controlled and the system can be driven to patterns such as uniform oscillations, clusters (see Fig. 2.9), standing waves, and intermittent turbulence. The experimentally seen behavior is in very good agreement with theoretical predictions where the same feedback scheme was applied to the CGLE [117, 118] and to the realistic reaction model [119, 120].

2.3.3 Nonlocal coupling

Both local and global coupling can be seen as limiting cases of a more general interaction type, which we will call *nonlocal coupling*, although it is often referred to as *long-range coupling* as well. Systems with nonlocal coupling are affected by a distance-dependent interaction, and, assuming identical local dynamics for all oscillators, can be written as:

$$\frac{\mathrm{d}\mathbf{X}_m}{\mathrm{d}t} = \mathbf{F}(\mathbf{X}_m) + \sum_{k=1}^{N} \mathbf{G}(m-k)(\mathbf{X}_k - \mathbf{X}_m), \quad m = 1, \ldots, N, \tag{2.33}$$

or, in a continuous version for a one-dimensional extended system of size L:

$$\frac{\partial \mathbf{X}(x)}{\partial t} = \mathbf{F}(\mathbf{X}(x)) + \int_L \mathbf{G}(x-x')\,[\mathbf{X}(x') - \mathbf{X}(x)]\,\mathrm{d}x'. \tag{2.34}$$

The nonlocal function $\mathbf{G}$ can take different forms, depending on the specific system. Some examples of possible coupling functions are shown in Fig. 2.10. In all cases, the oscillator located in x feels the influence of all other oscillators of the system with a distance-dependent strength. Since the coupling intensity tends to zero for remote elements, it is possible to define an effective interaction range l, such that oscillators which are separated by a larger distance are practically non-interacting. The above described couplings can thus be recovered in the following limits: (i) global coupling arises when $l \to \infty$, i.e. when the interaction range is much larger than the system size, so that each oscillator affects all others with constant intensity, (ii) local coupling corresponds to the limit $l \to 0$, i.e. each oscillator only affects its adjacent elements. There are several cases where effective coupling nonlocality cannot be overlooked, and neither the local nor the global coupling limit can be assumed. For example,

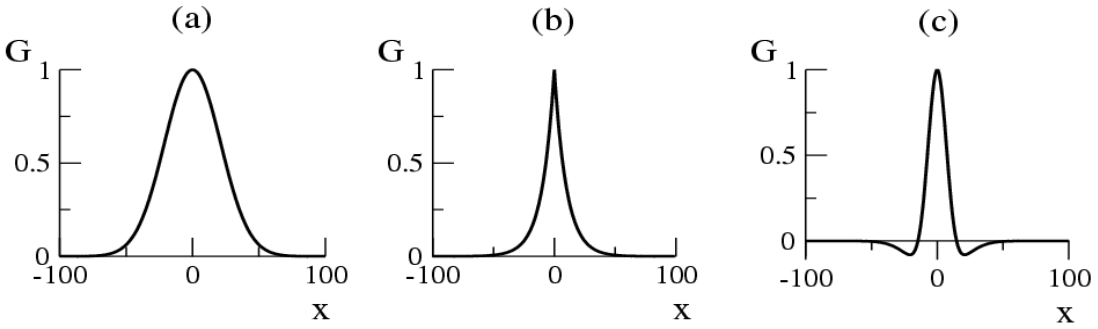

Figure 2.10: Three examples of possible nonlocal coupling functions for system (2.34). (a) Gaussian: $G(x) \propto \mathrm{e}^{-x^2}$; (b) Exponential: $G(x) \propto \mathrm{e}^{-|x|}$; (c) Non-monotonic $G(x) \propto \frac{1}{a^2}\mathrm{e}^{-\frac{x^2}{a^2}} - \frac{1}{b^2}\mathrm{e}^{-\frac{x^2}{b^2}}$.

nonlocal coupling generally arises whenever electric interactions are present. Two important examples are provided by electrochemical and neural systems.

Pattern formation in electrochemical systems is being extensively studied [5, 121]. In this case, the patterns are self-organized non-equilibrium spatial structures of the potential at the interface between the electrode and the electrolyte, the so-called double-layer potential. One characteristic feature of electrochemical systems which makes them essentially different from other pattern-forming media, is that spatial interactions cannot be described in terms of diffusional coupling. Indeed, here the main spatial coupling is caused by *migration currents*, which are due to motion of the ions through the electrolyte as a consequence of spatial gradients of the potential. For this reason, they are not included in the class of reaction-diffusion systems, but are rather referred to as *reaction-migration* systems. Coupling due to migration currents is known to be essentially nonlocal, moreover, its range can be tuned through the adjustment of the geometry of the electrochemical cell [122]. A formalism has been introduced, which highlights the nonlocal nature of such interactions [123, 124]. Namely, it has been shown that the evolution equation for the double-layer potential u can be written in the form of an integro-differential equation:

$$\frac{\partial u(x)}{\partial t} = F(u(x); \mathbf{p}) + \kappa \int_L H(x - x')[u(x') - u(x)]\mathrm{d}x', \tag{2.35}$$

where x is the one-dimensional spatial coordinate (in this case, the electrode has the structure of a ring) and $\mathbf{p}$ are other parameters related to the geometry of the electrochemical cell and to the applied voltage. The coupling function $H(x - x')$ depends on the system's conformation and has been calculated for several common cases. An example is shown in Fig. 2.11.

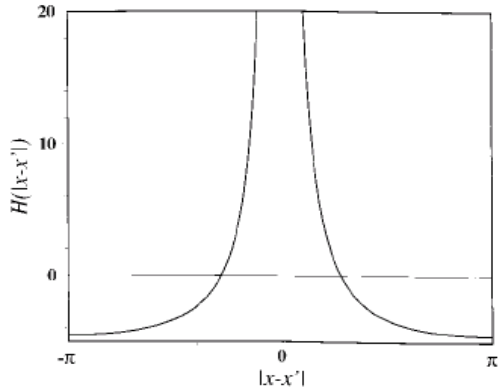

Figure 2.11: Nonlocal coupling function $H(x-x')$ for an electrochemical system governed by Eq.(2.35). The shape of the function can be roughly related to the electrostatic inverse-quadratic force law $F_e \sim 1/|x-x'|^2$. After [125].

Coupling nonlocality has important effects on the resulting patterns: In the bistable regime, remote triggering of waves [125], as well as front acceleration [122] have been reported, while in the oscillatory regime traveling pulses, target patterns [123], standing waves [126], and asymmetric target patterns [127, 128] have been observed and in some cases reproduced by numerical simulations.

Neural systems provide another example of nonlocally interacting systems. In fact, cortical networks are made of a large number of individual neurons communicating through spatially structured connections [129] which are essentially of electric nature. This makes the mathematical description in terms of equations like Eq. (2.34) particularly suitable [14]. Indeed, neural networks are regarded as an example of pattern-forming systems, since the spatio-temporal structure of neuronal activity shows oscillations, wave propagation, front propagation, and traveling pulses [129].

In surface chemical reactions like the already mentioned CO oxidation on Pt(110), two different types of nonlocal coupling can arise on very different length scales. The first one is once again of electrical origin, and is due to interactions between the adsorbed molecules. Such kind of interactions are neglected in the reaction-diffusion models that focus on pattern formation on the micrometer length scale, where the adsorbate can be seen as a non-interacting ideal gas. However, patterns also occur on a nanometer length scale, through the formation of agglomerates of a small number of atoms [130, 131]. To give an appropriate description of the phenomena occurring on such a small length scale, it is necessary to explicitly introduce interactions among the adsorbed atoms, which are called *lateral interactions*. Such interactions are nonlocal since they extend over several lattice lengths, i.e. each adsorbed atom is affected with a distance-dependent strength by the surrounding atoms, and not only by its first neighbors. Taking into account these lateral nonlocal interactions, mesoscopic modeling can be achieved, which allows to describe the spatio-temporal evolution of

patterns on the nanometer scale [132–134].

However, also on the macroscopic length scale, on the description level of classical reaction-diffusion systems, a nonlocal coupling can be present. It is due to the effect of inhomogeneous temperature distribution on the reaction surface, which gives rise to heat conduction phenomena. In many cases, such coupling can be neglected, and the reaction can be assumed to proceed on an isothermal surface. However, it is well known that the isothermal assumption does not hold under experimental conditions like high pressure of the gas ($10^{-2} - 10^{-3}$ mbar) or catalysis on very thin (2000-3000 Å) crystals (see [84] and also the review by Eiswirth and Ertl in [3]). When heat conduction comes into play, it performs a nonlocal coupling because the heat conduction constant is much larger than the diffusion constant of the particles on the surface. In [135] the first one has been estimated as $D_T = 0.26$ cm^2/s and the second one as $D_u = 5 \times 10^{-8}$ cm^2/s. Moreover, when the gas pressure is very high, particles diffusion becomes irrelevant due to the very high occupation ratio of the adsorption sites, which limits the chances for a particle to hop. Thus, in this case, one can often say that nonlocal thermal coupling is the only effective spatial interaction.

Many experimental observations have been published, where thermal effects play a primary role, both for the CO oxidation at high pressures [89, 90] or on thin catalysts [136], and for other catalytic reactions (see [137] and references therein). In what concerns the theoretical modeling of such phenomena, a number of works have appeared [135, 138, 139], where the kinetic terms describing the reaction are complemented by an additional heat conduction equation of the type:

$$\frac{\partial T}{\partial t} = D_T \nabla^2 T + f(T, \mathbf{u}), \tag{2.36}$$

where the components of $\mathbf{u}$ are the time- and space-dependent coverages, and the second term on the right-hand side contains the thermal effects due to the reactions as well as the heat exchange with the environment.

Note that, although the coupling term in Eq. (2.36) is formally a diffusional interaction, it acts as a nonlocal coupling due to the very large diffusion constant. In fact, it can be shown that such coupling can be written in an integral form like in Eq. (2.34), as we will do explicitly for the nonlocally coupled Ginzburg-Landau equation in Chapter 3.

In the last ten years, the theoretical study of nonlocal coupling has been undertaken by means of more abstract models, in order to capture the essential features of coupling nonlocality which are not related to system-dependent properties [43–49, 140–149].

As a prototype model of coupled oscillators with purely nonlocal interaction, a discrete

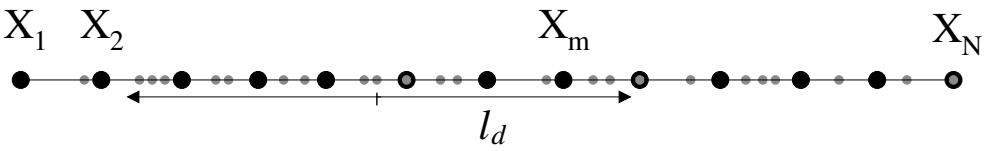

Figure 2.12: Discrete system whose continuous version is described by eq. (2.37)-(2.38). Black dots are cells whose position is fixed in space on a regular one-dimensional array. Small gray dots represent a substance which is released by the cells and diffuses through the extension of the system, affecting the dynamics of the other cells. l_d is the diffusion length.

set of dynamical units exchanging a diffusive substance was considered [43]. The oscillators are fixed on a lattice, they do not move and they do not directly interact with each other. They can be seen as biological cells displaying cyclic dynamics. The cells secrete a diffusive substance, which is in turn able to influence the cell's functioning. Thus, the substance makes the oscillators interact through a feedback mechanism whose range depends on the diffusion length. This coupling is nonlocal if diffusion is such that the substance released by one cell can reach and affect not only its neighbors, but even cells which are located far away from it. The system is sketched in Fig. 2.12. A simple model for the continuous version of this system is [46]:

$$\frac{\partial \mathbf{X}}{\partial t} = \mathbf{F}(\mathbf{X}) + K(\mathbf{Z} - \mathbf{X}) \tag{2.37}$$

$$\tau \frac{\partial \mathbf{Z}}{\partial t} = \mathbf{X} - \mathbf{Z} + l^2 \nabla^2 \mathbf{Z}. \tag{2.38}$$

The local dynamics of the first field $\mathbf{X}$ is assumed to be oscillatory, and no direct diffusional coupling for this field is present. The second field, representing the secreted substance, is instead responsible for the nonlocal coupling: it has a passive dynamics, in the sense that it "follows" the first variable, without being able to display self-sustained oscillations by itself.

Eq. (2.38) is a simple linear equation and can be solved by means of a Green function, thus expressing $\mathbf{Z}(x,t)$ as a functional of the oscillatory field, i.e.:

$$\mathbf{Z}(x,t) = \int_{-\infty}^{\infty} \int_{0}^{t} G(x - x', t - t') \mathbf{X}(x', t') \mathrm{d}x' \mathrm{d}t'. \tag{2.39}$$

This permits to write the system as a closed equation for $\mathbf{X}$, whose dynamics is thus given by an integro-differential equation. In the limit $\tau \to 0$, it is given by [46]:

$$\frac{\partial \mathbf{X}}{\partial t} = \mathbf{F}(\mathbf{X}) + \frac{K}{2l} \int_{-\infty}^{+\infty} \mathrm{d}x' \exp\left(-\frac{|x - x'|}{l}\right) \left[\mathbf{X}(x', t) - \mathbf{X}(x, t)\right]. \tag{2.40}$$

This is a nonlocally coupled oscillatory field, where l is the interaction range. We have mentioned at the beginning of this Section that the coupling is effectively nonlocal only for

appropriate values of the interaction range. This argument can be made more quantitative. Let's consider Eq. (2.40). We told that the nonlocal coupling reduces to the local diffusional coupling for small l. We can make an expansion of the term $\mathbf{X}(x')$ inside the integral:

$$\mathbf{X}(x') = \mathbf{X}(x) + \left.\frac{\partial \mathbf{X}}{\partial x}\right|_x (x'-x) + \left.\frac{\partial^2 \mathbf{X}}{\partial x^2}\right|_x (x'-x)^2 + \cdots + \frac{1}{n!}\left.\frac{\partial^n \mathbf{X}}{\partial x^n}\right|_x (x'-x)^n. \quad (2.41)$$

The first term cancels with $-\mathbf{X}(x,t)$ in Eq. (2.40) and we are left with a sum of terms of the type:

$$\frac{1}{n!}\int_{-\infty}^{+\infty} \mathrm{d}y\; y^n \exp\left(-\frac{|y|}{l}\right) = \begin{cases} \dfrac{l^{n+1}}{n!} & \text{n even} \\ 0 & \text{n odd.} \end{cases} \quad (2.42)$$

Since l is small, the nonzero contributions from the even n's are rapidly vanishing with increasing n, and we can safely truncate the series to the second order, which yields for Eq. (2.40):

$$\frac{\partial \mathbf{X}}{\partial t} = \mathbf{F}(\mathbf{X}) + Kl^2 \frac{\partial^2 \mathbf{X}}{\partial x^2}. \quad (2.43)$$

In conclusion, the nonlocally coupled system (2.37, 2.38) can be in principle approximated by the ordinary reaction-diffusion system of Eq. (2.43) in the case where the diffusion length l of the nonlocal field is small. For the resulting closed system after adiabatic elimination of the nonlocal field, the diffusion length is rescaled as:

$$l' = \sqrt{K} l, \quad (2.44)$$

where the quantity l' gives an indication on the typical wavelength of the patterns arising for system (2.43). If K tends to zero, then:

$$l' \ll l, \quad (2.45)$$

which means that the field $\mathbf{X}$ has a spatial structure on a length scale which is much smaller than the effective range l of the coupling provided by the diffusive field $\mathbf{Z}$. In this case, the resulting pattern will not have the smooth structure which is typical of ordinary diffusionally coupled systems.

Indeed, the main findings on this class of systems are related to the appearance of discontinuous patterns (see Figs. 2.13 and 2.14). As we have already pointed out, the considered systems are characterized by the absence of direct diffusional coupling of the oscillators, and it turns out that nonlocal coupling, although it may arise from diffusional dynamics, can display features which are qualitatively different from the usual diffusion. In particular, this

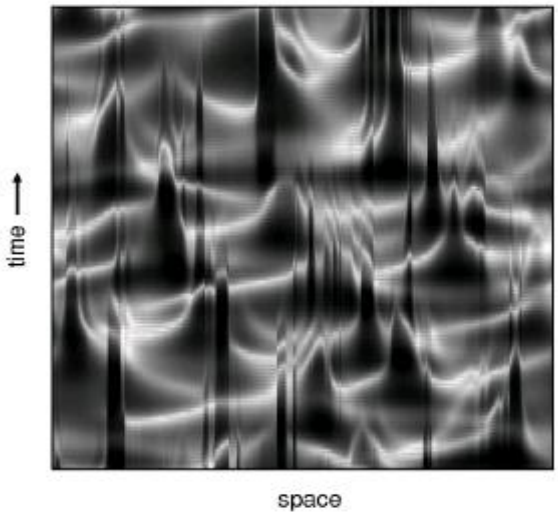

Figure 2.13: Monument-like structures displaying fractal nature in a nonlocally coupled system. The active field is displayed in gray scale where darker (brighter) gray corresponds to larger (smaller) values of the field. After [45].

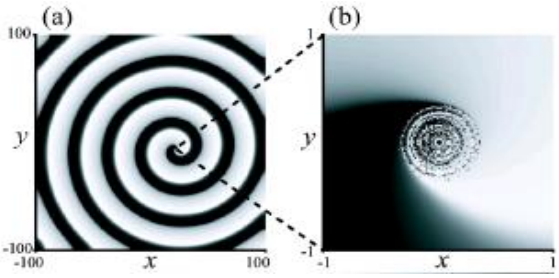

Figure 2.14: Loss of spatial continuity of a 2D pattern at the core of a spiral wave in a system with nonlocal coupling. After [48].

happens when condition (2.45) is satisfied, what Kuramoto refers to as *breakdown of the diffusive coupling approximation*. This results in the loss of spatial continuity of the patterns, as it was shown by numerical simulations [43, 46, 48, 144]. This qualitative feature has also been quantitatively analyzed, and it was found that in the case of breakdown of the diffusive coupling approximation, the spatial correlations of the oscillatory field show a power-law decay [44, 140, 143] typical of scaleless dynamical regimes [45]. This can also result in the emergence of turbulence even in the Benjamin-Feir stable regime [144].

Furthermore, addition of a small diffusive term for the oscillatory field was considered, and the normal form of such diffusing and nonlocally coupled field close to the Hopf bifurcation was derived, yielding a nonlocally coupled Ginzburg-Landau equation [47]. The addition of small diffusion has the effect to remove spatial discontinuities, by stabilizing the system towards short-wavelength perturbations. However, even in this case, a very special type of turbulence (reminding of turbulence in seismic systems) may appear [47, 147].

Recently, a formalism has been developed, to extend the order parameters used for globally coupled systems to the more general case of nonlocal coupling [49, 146, 149]. In this context, the conditions for the simultaneous presence of coherent and incoherent domains

(which has been named *chimera state*) are being clarified.

Moreover, nonlocal coupling has been introduced in the FitzHugh-Nagumo model [148, 150]. Here, it gives rise to a codimension-two Turing-wave bifurcation which generates so-called drifting patterns domains, defined as moving localized patches of traveling waves embedded in a stationary background (or vice-versa).

In all cases, nonlocal coupling is found to be responsible for the emergence of new structures that have been seen neither in globally nor in locally interacting media. However, the gap between the experimental observations which have been related to the specificity of nonlocal coupling and the general theory still needs to be bridged.

Chapter 3

Complex Ginzburg-Landau equation with nonlocal inertial coupling

3.1 The model

Provided with the above-mentioned motivations, our aim is to study a reaction-diffusion model, where an active oscillatory and diffusive field is coupled to a passive temperature-like field. This second field shall have a much larger diffusion constant than the first one, thus providing the system with a nonlocal coupling. Since direct diffusional coupling of the oscillatory field is also present, spatial interactions on two different scales are considered. Moreover, the coupling through the passive field is assumed to be inertial, like it would be for the case of a surface reaction with nonlocal coupling due to heat conduction. However it is important to stress that the proposed model is not meant to reproduce the kinetics of any specific experimental system, but has to be seen as a generic oscillatory system with nonlocal inertial interactions.

The dynamics of individual oscillators $\eta(x,t)$ are given by the complex Ginzburg-Landau equation (CGLE). This oscillatory field is linearly coupled to another complex-valued diffusive field z. The system reads:

$$\dot{\eta} = (1+\mathrm{i}\omega)\eta - (1+\mathrm{i}\alpha)|\eta|^2\eta + (1+\mathrm{i}\beta)\nabla^2\eta + K(z-\eta) \tag{3.1}$$

$$\tau\dot{z} = \eta - z + l^2\nabla^2 z. \tag{3.2}$$

The equations are brought into a dimensionless form by choosing the characteristic diffusion length in the oscillatory subsystem as the length unit and taking the characteristic relaxation time scale of the oscillators as the time unit. The parameters τ and l determine characteristic time and length scales of the additional field z. We assume that this field is inertial ($\tau \gg 1$)

and slowly varying in space ($l \gg 1$). The resulting diffusion constant D must also be larger than the diffusion constant of the oscillatory field, so $l^2/\tau \gg 1$.

Although the inertiality condition $\tau \gg 1$ is in contrast with the slowing-down in the vicinity of the bifurcation point (see Sec. 2.3.3), we are allowed to assume it since our system is not close to the Hopf bifurcation, but rather, as we already mentioned, in a generic oscillatory state.

Now we want to explicitly derive the integral form of the nonlocal coupling from the diffusive equation (3.2). That is, we want to find the Green function $G(x,t)$ which allows to write the variable z as:

$$z(x,t) = \int_{-\infty}^{\infty}\int_{0}^{t} G(x-x',t-t')\eta(x',t')\mathrm{d}x'\mathrm{d}t'. \tag{3.3}$$

First, we substitute Eq. (3.3) into Eq. (3.2):

$$\begin{aligned}
&\tau\frac{\partial}{\partial t}\int\int G(x-x',t-t')\eta(x',t')\mathrm{d}x'\mathrm{d}t' = \\
&\eta(x,t) - \int\int G(x-x',t-t')\eta(x',t')\mathrm{d}x',\mathrm{d}t' + \\
&+l^2\frac{\partial^2}{\partial x^2}\int\int G(x-x',t-t')\eta(x',t')\mathrm{d}x',\mathrm{d}t'.
\end{aligned} \tag{3.4}$$

The latter can be rewritten as an equation for the integrating functions, where η can be eliminated:

$$\frac{\partial}{\partial t}G(x,t) - D\frac{\partial^2}{\partial x^2}G(x,t) + \frac{1}{\tau}G(x,t) = \frac{1}{\tau}\delta(x,t), \tag{3.5}$$

where $D = \frac{l^2}{\tau}$. Now we follow a standard technique [151] by defining a functional transformation T which is a composition of the Fourier transform for the space variable and a Laplace transform for the time variable:

$$T(f(x,t)) \equiv \tilde{f}(q,s) = \int_{-\infty}^{\infty}\mathrm{d}x\int_{0}^{\infty}\mathrm{d}t\ \mathrm{e}^{\mathrm{i}qx-st}f(x,t), \tag{3.6}$$

with the following properties:

$$T\left(\frac{\partial^n f}{\partial t^n}\right) = s^n\tilde{f} \tag{3.7}$$

$$T\left(\frac{\partial^n f}{\partial x^n}\right) = (-\mathrm{i}q)^n\tilde{f}. \tag{3.8}$$

Thus, by applying transformation (3.6) together with the properties (3.7, 3.8) to Eq. (3.5) we get:

$$\begin{aligned}
&s\tilde{G}(q,s) - D(-\mathrm{i}q)^2\tilde{G}(q,s) + \frac{1}{\tau}\tilde{G}(q,s) = \frac{1}{\tau} \quad \Longrightarrow \\
&\tilde{G}(q,s) = \frac{1}{\tau s + D\tau q^2 + 1}.
\end{aligned} \tag{3.9}$$

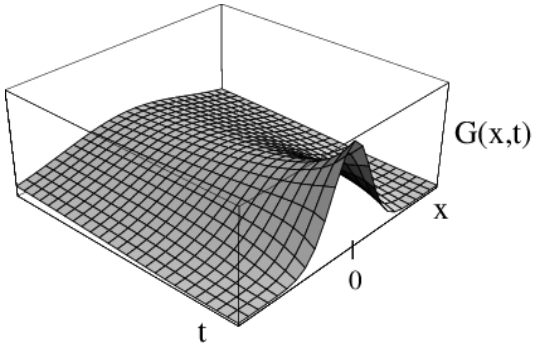

Figure 3.1: Three-dimensional plot of the Green function, Eq. (3.10). The oscillator located in the origin feels the influence of the other oscillators in its neighborhood (nonlocality), and also of their state at previous times (inertiality).

Now it is sufficient to back transform (3.9) to the (x,t)-space to obtain the searched Green function:

$$\begin{aligned} G(x,t) &= \frac{1}{4\pi \mathrm{i}^2}\int_{-\infty}^{\infty}\mathrm{d}q\int_{-\mathrm{i}\infty}^{\mathrm{i}\infty}\mathrm{d}s\ \mathrm{e}^{-\mathrm{i}qx+st}\tilde{G}(q,s) \\ &= \frac{\exp\left(-\frac{x^2}{4Dt}-\frac{t}{\tau}\right)}{2\tau\sqrt{\pi Dt}}. \end{aligned} \tag{3.10}$$

Eq. (3.10) together with Eq. (3.3) gives the integral expression of the nonlocal interaction in our system. It has to be stressed that in this general case the finiteness of τ, which we have called inertiality, gives rise to a *temporal nonlocality*: this essentially means that z adjusts to the variation of η with a certain *inertia*, within a time scale defined by τ, which can be in general large with respect to the characteristic time scale of η. The space-time nonlocality of the coupling is made clear by the three-dimensional plot of the kernel function of Eq. (3.10) shown in Fig. 3.1.

3.2 Birhythmicity

As a first step, we shall consider the problem of a single oscillator: Neglecting all the spatial couplings, we are left with an ordinary differential equation describing a nonlinear harmonic oscillator coupled to an inertial variable:

$$\dot{\eta} = (1+\mathrm{i}\omega)\eta-(1+\mathrm{i}\alpha)|\eta|^2\eta+K(z-\eta) \tag{3.11}$$

$$\tau\dot{z} = \eta-z. \tag{3.12}$$

For this system, an explicit solution can be found which shall be sought in the form:

$$\eta(t) = \rho e^{-\mathrm{i}\gamma t}. \tag{3.13}$$

In order to obtain the explicit expression for the frequency γ and the amplitude ρ of the oscillations, we first solve Eq. 3.12, obtaining:

$$\begin{aligned} z(t) &= \frac{1}{\tau}\int_0^t dt' e^{-\frac{t-t'}{\tau}}\eta(t') \\ &= \frac{1}{1-\mathrm{i}\tau\gamma}\rho e^{-\mathrm{i}\gamma t}, \end{aligned} \tag{3.14}$$

which means that z follows η oscillating with the same frequency but with different amplitude and with a constant phase shift of $\arctan\gamma\tau$ with respect to it.

Using these expressions system (3.11)-(3.12) reduces to:

$$-\mathrm{i}\gamma = \left[1 - \frac{K\tau^2\gamma^2}{1+\tau^2\gamma^2}\right] + \mathrm{i}\left[\omega + \frac{K\tau\gamma}{1+\tau^2\gamma^2}\right] - (1+\mathrm{i}\alpha)\rho^2, \tag{3.15}$$

which can be split into real and imaginary part to get two equations in the two variables γ and ρ. From the real part, we obtain the expression of the oscillation amplitude ρ of η as a function of the frequency:

$$\rho^2 = 1 - \frac{K\tau^2\gamma^2}{1+\tau^2\gamma^2}, \tag{3.16}$$

while the respective amplitude of z (which we will call r) reads:

$$r = \frac{\rho}{\sqrt{1+\tau^2\gamma^2}}. \tag{3.17}$$

Now substituting Eq. (3.16) into the real part of Eq. (3.15) we get a closed equation for the frequency, which can be written as:

$$A_3\gamma^3 + A_2\gamma^2 + A_1\gamma + A_0 = 0, \tag{3.18}$$

where the coefficients are given by:

$$\begin{aligned} A_3 &= \tau^2 \\ A_2 &= \tau^2(\omega - \alpha + \alpha K) \\ A_1 &= 1 + \tau K \\ A_0 &= \omega - \alpha. \end{aligned}$$

Eq. (3.18) may have either one or three real roots. In the latter case, the three real roots correspond to three possible modes of uniform oscillations with frequencies $\gamma_{1,2,3}$, such that

$\gamma_1 < \gamma_2 < \gamma_3$. It can be checked that oscillations with the middle frequency γ_2 are always unstable. In contrast to this, oscillations with frequencies γ_1 and γ_3 are possible for the single oscillator (although they might be unstable with respect to nonuniform perturbations when diffusion is also taken into account, as it will be discussed later). When the oscillator possesses these two different oscillatory regimes, we are in the presence of a birhythmic system (see Sec. 2.2).

The condition for the existence of birhythmicity can be analytically calculated, in particular from the classical theory of cubic equations we know that the following condition needs to be satisfied:

$$\frac{Q^2}{4} + \frac{P^3}{27} < 0, \tag{3.19}$$

where:

$$P = -\frac{\tilde{A}_2^2}{3} + \tilde{A}_1 \tag{3.20}$$

$$Q = \frac{2\tilde{A}_2^3}{27} - \frac{\tilde{A}_2\tilde{A}_1}{3} + \tilde{A}_0, \tag{3.21}$$

with $\tilde{A}_i = A_i/A_3$.

Inequality (3.19) is a condition on the system parameters: it defines parameter regions where birhythmicity is found. Such domains in the parameter spaces (τ, K) and (α, K) are shown in Fig. 3.2. In particular, from Fig. 3.2(a) it can be noticed that birhythmicity is only found when both coupling strength K and inertiality τ are large enough.

3.2.1 Bifurcation diagrams

Solutions of Eq. (3.18) together with the respective amplitudes are plotted in Fig. 3.3.

Fig. 3.3(a) displays the different solution branches obtained through a horizontal cross-section of Fig. 3.2(a). When τ vanishes, birhythmicity is not present. Around $\tau = 6$ two new limit cycles, one stable and one unstable, appear through a saddle-node bifurcation and remain present at larger values of the parameter. The corresponding amplitudes and frequencies seem to saturate approaching constant values as the inertiality is further increased.

Fig. 3.3(b) shows the solutions through a vertical cross-section of Fig. 3.2(b), thus varying K while letting all other parameters constant. Here birhythmicity is found for $K > 0.4$. With increasing K, the frequency of the new stable limit cycle grows in modulus, while its amplitude lowers, i.e. oscillations become faster and smaller. Then, as K reaches unity, the amplitude of this limit cycle vanishes: it shrinks to the origin and stabilizes the unstable fixed

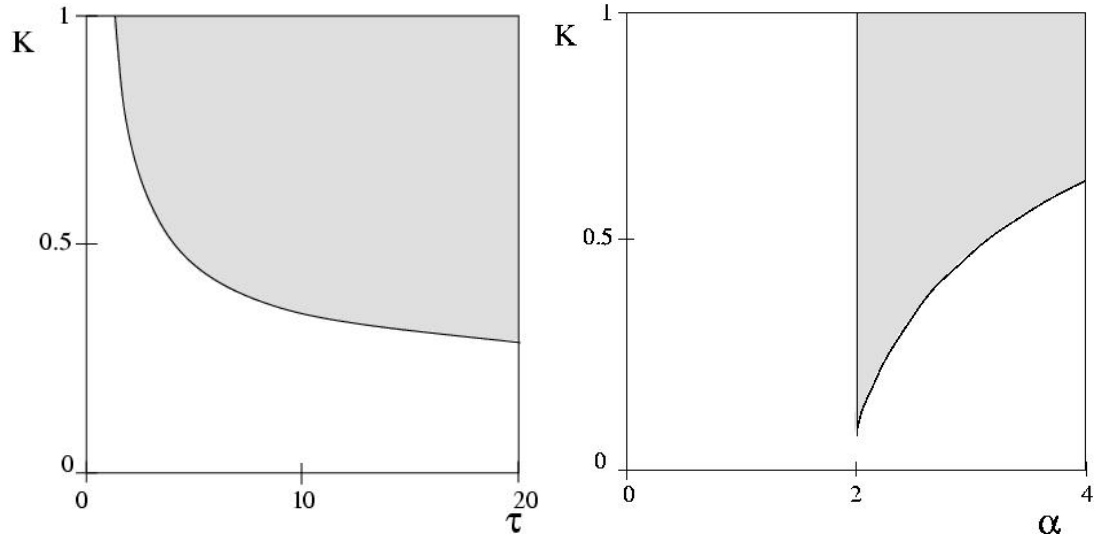

(a) (b)

Figure 3.2: Birhythmicity regions (gray) for the model (3.1)-(3.2) in the parameter planes (τ, K) and (α, K). The fixed parameters are $\tau = 10$ in the first diagram and $\omega = 2, \alpha = 2.5$ in the second diagram. The boundaries of the displayed regions do not depend on the parameters β and l of the model.

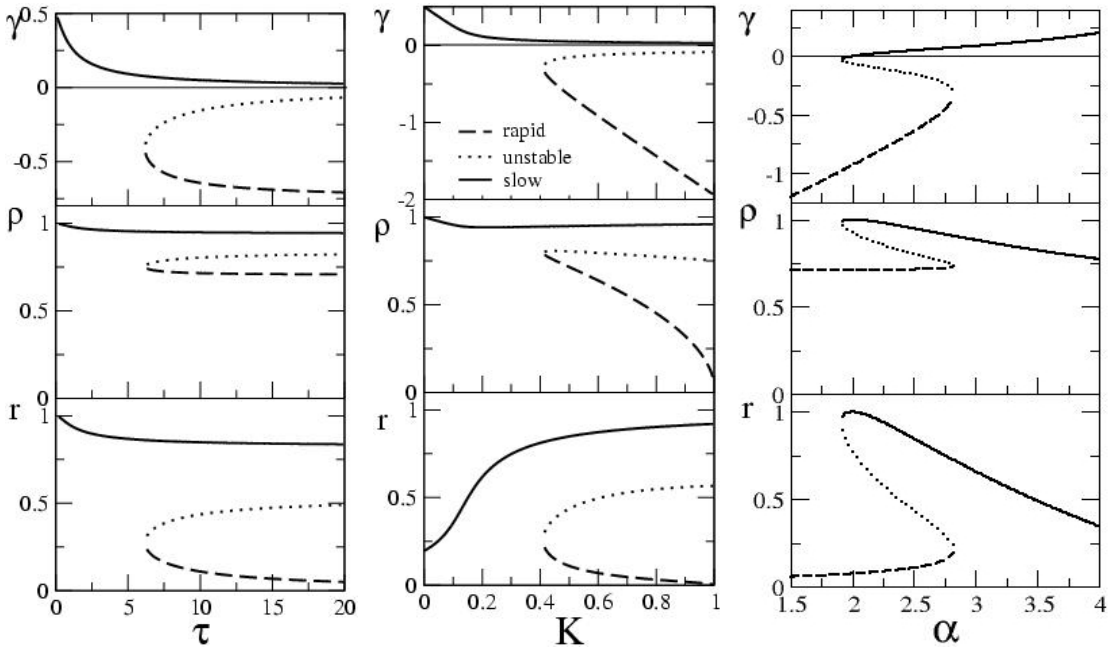

(a) (b) (c)

Figure 3.3: Bifurcation diagrams. Frequencies γ of uniform oscillations, together with the respective amplitudes $\rho = |\eta|$ and $r = |z|$ as functions of K, α and τ for slow (bold line), rapid (dashed) and absolutely unstable (dotted) uniform oscillation modes. The parameters are (a) $\omega = 2, \alpha = 2.5, K = 0.5$. (b) $\omega = 2, \alpha = 2.5, \tau = 10$ (c) $\omega = 2, K = 0.5, \tau = 10$.

point $\eta = 0$. The other limit cycle is still present and its amplitude and frequency do not undergo significant variations. The state where one stable limit cycle and one stable fixed point are simultaneously present is usually referred to as *hard excitation*.

Finally, from Fig. 3.3(c) we can see that the two stable limit cycles coexist within the interval $2 < \alpha < 2.8$. Two saddle-node points are found at the edges of the birhythmic interval.

The two limit cycles have different characteristics. Note that at $K = 0$ only one oscillating mode is present, and in this limit the system is reduced to the standard CGLE. Thus, we can expect that the branch starting at $K = 0$ (i.e. the upper one in the bifurcation diagrams of Fig. 3.3(a), 3.3(b), and 3.3(c)) would have the strongest similarities to the CGLE, even though for finite K it would be affected by the coupling to the second field. This branch is characterized by a large amplitude of the field η, which never gets significantly smaller than 1. The corresponding frequency is quite small, starting from 0.5 at $K = 0$ and slowly decreasing as K increases. Therefore, we will refer to this first attractor as to the *slow* limit cycle.

In contrast to this, the limit cycle of the lower branch has a smaller amplitude, and it shrinks as K is raised, eventually vanishing at $K = 1$. Its frequency varies significantly, but it always has a larger absolute value than the previous one and the opposite sign, so that the two oscillatory modes are always counter rotating with respect to each other. This limit cycle will therefore be called the *rapid* limit cycle. A remarkable feature of the rapid limit cycle is that the amplitude r of the field z is very small, so small that one could in first approximation neglect it in the term $K(z - \eta)$. In this case, Eq.(3.11) would be decoupled from (3.12) and just read:

$$\dot{\eta} = (1 - K + \mathrm{i}\omega)\eta - (1 + i\alpha)|\eta|^2\eta. \tag{3.22}$$

This system simply describes a Hopf bifurcation: By taking $-K$ as the control parameter, the bifurcation point is located at $K = 1$, the oscillation amplitude increases as the square root ($\rho = \sqrt{1 - K}$), whereas the oscillation frequency changes linearly ($\gamma = -\omega + \alpha - \alpha K$). These amplitude and frequency correspond to the the branch of the rapid oscillations in Fig. 3.3(b): We can state that the rapid mode in our birhythmic system arises from the terms contained in Eq. (3.22).

Thus, depending on the initial conditions, the system can choose one of the two oscillatory modes: the slow mode with entrainment of z, or the rapid mode where z does not manage to follow the oscillations and drops close to zero.

3.3 Phase dynamics

In the previous section, we have only considered the problem of a single oscillator, and have clarified how birhythmicity arises in that system. Now we want to get back to the extended system (3.1)-(3.2) and consider the effect of spatial coupling between the oscillators. The question is under what conditions a stable limit cycle can become unstable because of the effect of spatial modulations.

Analytical calculations are going to be presented for the phase dynamics approximation of the system. The concept of phase oscillator has been introduced in Sec. 2.1: as stated there, this description only holds for simple oscillators that do not leave the close vicinity of a limit cycle. In the present case, two different limit cycles are present, so that phase description is only suitable if all of the oscillators of the medium are moving close to one of the two possible attractors.

In other words, in the following calculations we assume that the considered systems is *almost* homogeneous: all of the oscillators are close to one of the two stable limit cycles and only smooth and weak modulations of the phase are present.

For the present purpose, it is convenient to describe the system by means of the following variables: ρ (amplitude of η), r (amplitude of z), ψ (phase difference between η and z), and Θ (sum of the phases of η and z). For what has been told before, one has to keep in mind that, through the entire system, oscillation amplitudes have to be close to one of the two stable branches shown in Fig. 3.3.

In terms of these variables, system (3.1)-(3.2) reads:

$$\dot{\rho} = \rho - \rho^3 + Kr\cos\psi - K\rho + \rho\left(-\frac{\nabla\Theta^2}{4} + \frac{1}{2}\beta\nabla^2\Theta\right) \tag{3.23a}$$

$$\dot{r} = \frac{\rho}{\tau}\cos\psi - \frac{r}{\tau} - \frac{l^2}{4\tau}r\nabla\Theta^2 \tag{3.23b}$$

$$\dot{\psi} = -\omega + \alpha\rho^2 - \left(\frac{kr}{\rho} + \frac{\rho}{\tau r}\right)\sin\psi + \frac{\beta}{4}\nabla\Theta^2 + \frac{1}{2}\left(1 - \frac{l^2}{\tau}\right)\nabla^2\Theta \tag{3.23c}$$

$$\dot{\Theta} = -\omega + \alpha\rho^2 - \left(\frac{kr}{\rho} - \frac{\rho}{\tau r}\right)\sin\psi + \frac{\beta}{4}\nabla\Theta^2 + \frac{1}{2}\left(1 + \frac{l^2}{\tau}\right)\nabla^2\Theta. \tag{3.23d}$$

Now, let ρ_0 and r_0 be the amplitudes of the stable limit cycle close to which the oscillators are, and ψ_0 the respective phase difference (whose value is fixed for a given limit cycle). Then the significant variable is the phase sum Θ, telling at which point of the cycle every single oscillator is.

In an almost homogeneous state, Θ is slightly modulated in space, and therefore ρ, r and ψ would only weakly deviate from their equilibrium values, and quickly relax back to the stationary point. They can be considered as fast-relaxing variables.

Thus, we can introduce small perturbations $\rho = \rho_0 + \delta\rho$, $r = r_0 + \delta r$, $\psi = \psi_0 + \delta\psi$, and linearize the equations with respect to such perturbations.

The linearized evolution equation for the phase Θ is:

$$\begin{aligned}\dot{\Theta} &= -\omega + \alpha\rho_0^2 - \left(\frac{Kr_0}{\rho_0} - \frac{\rho_0}{\tau r_0}\right)\sin\psi_0 + \delta\rho\left[2\alpha\rho_0 + \left(\frac{Kr_0}{\rho_0^2} + \frac{1}{\tau r_0}\right)\sin\psi_0\right] \\ &+ \delta r\left(-\frac{K}{\rho_0} - \frac{\rho_0}{\tau r_0^2}\right)\sin\psi_0 + \delta\psi\left(-\frac{Kr_0}{\rho_0} + \frac{\rho_0}{\tau r_0}\right)\cos\psi_0 \\ &+ \frac{\beta}{4}\nabla\Theta^2 + \frac{1}{2}\left(1 + \frac{l^2}{\tau}\right)\nabla^2\Theta. \end{aligned} \tag{3.24}$$

The fast variables $\delta\rho, \delta r, \delta\psi$ can be eliminated in the adiabatic approximation, then, substituting the result into Eq. (3.24), we are left with a closed evolution equation for the phase variable Θ.

This equation has the form:

$$\dot{\Theta} = C_0 + C_1(\nabla\Theta)^2 + C_2\nabla^2\Theta. \tag{3.25}$$

In the hope not to bore the reader with long calculations, the complete derivation of the coefficients of the phase dynamics equation is omitted here and given in Appendix A.

It is important to stress that since Eq. (3.25) is only valid to describe the evolution of weak and smooth perturbations, it assumes that the wavenumber of the considered modulation is small. For this reason, the equation does not contain any explicit dependence on the wave number of the perturbation: It can be considered to hold in the limit of a vanishing wavenumber.

Thus we can evaluate the linear stability of uniform oscillations for large wavelength perturbations estimating the sign of C_2: If $C_2 > 0$ uniform oscillations are stable (Benjamin-Feir stable regime), if $C_2 < 0$ uniform oscillations are unstable (Benjamin-Feir unstable regime), as it is well known from the general theory of diffusional processes.

The dependence of C_2 on different parameters is plotted in Fig. 3.4. The two different branches refer to the two different limit cycles: The upper one to the slow limit cycle, the lower one to the rapid limit cycle. In Fig. 3.4(c), the upper curves correspond to the slow mode for larger values of the parameter l.

Several observations can be made:

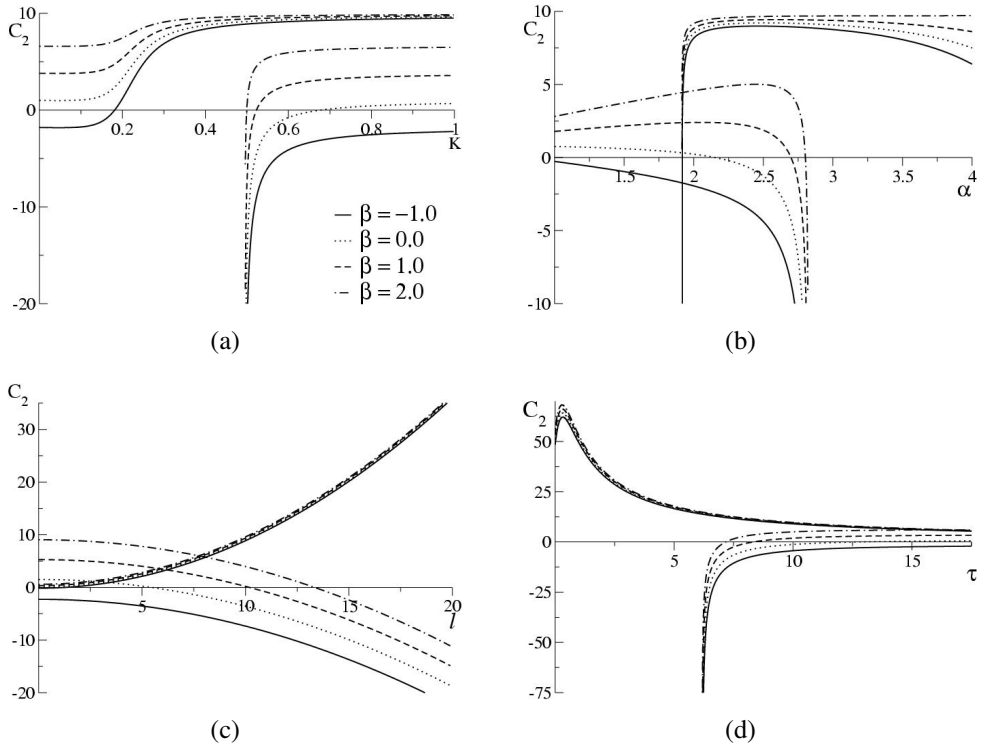

Figure 3.4: The coefficient C_2 of the phase dynamics equations as functions of K, α, l and τ for several different values of the parameter β. The upper branches in (a,b,d) and for the larger values of l in (c) correspond to slow oscillations, the lower branches are for the rapid oscillations. The oscillations are unstable if $C_2 < 0$. The parameters are (a) $\alpha = 2.5$, $l = 10$, $\tau = 10$, (b) $K = 0.5, l = 10, \tau = 10$, (c) $\alpha = 2.5$, $K = 0.5$, $\tau = 10$, (d) $\alpha = 2.5$, $K = 0.5$, $l = 10$; for all curves $\omega = 2$.

- A stronger coupling favors stability of the uniform oscillations. Even the Benjamin-Feir unstable system can become stable through the nonlocal coupling (see upper straight line of Fig. 3.4(a)).

- The fast oscillations (lower branch) are in general less stable than the slow oscillations. This is due to a much weaker effect of the nonlocal coupling on this limit cycle than on the slow one. As we have previously stated, in the small amplitude limit cycle the amplitude of the nonlocal field z is very small, this means that the nonlocal coupling is in this case not able to get synchronization into the system.

- Close to the bifurcation points the two limit cycles have different stability properties, in particular the fast oscillations can get strongly unstable, while the slow oscillations are stable (see Fig. 3.4(a) around $K = 0.4$, and Fig. 3.4(b) around $\alpha = 2.8$). As this parameter region is of particular interest, it has been investigated in numerical simulations.

- A larger diffusional length of the nonlocal field favors modulational instability of rapid uniform oscillations, while it tends to stabilize slow oscillations (see Fig 3.4(c)).

An example where the two limit cycles have different stability properties with respect to weak phase modulations is shown in Fig. 3.5. The two spatio-temporal plots show the results of two numerical simulations with the same parameters. The two simulations differ in the initial condition. In Fig. 3.5(a) all the oscillators of the system were put in the close proximity of the slow limit cycle, while in Fig. 3.5(b) they were located close to the rapid limit cycle. In both cases, the initial condition was almost uniform, and the same type of perturbation was applied, that is, a superposition of waves with small amplitude and long wavelength. Uniform slow oscillations are stable: the system goes to a uniform state and the perturbation decays. On the contrary, rapid oscillations are unstable: the initial perturbation develops in a spatial modulation of the phases.

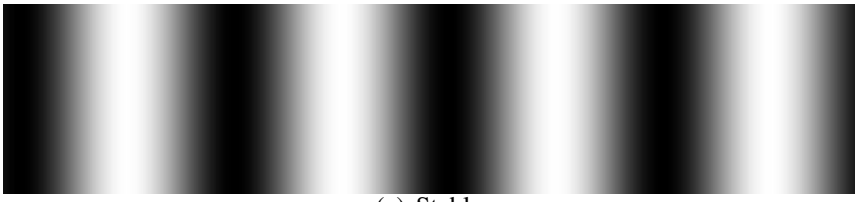

(a) Stable

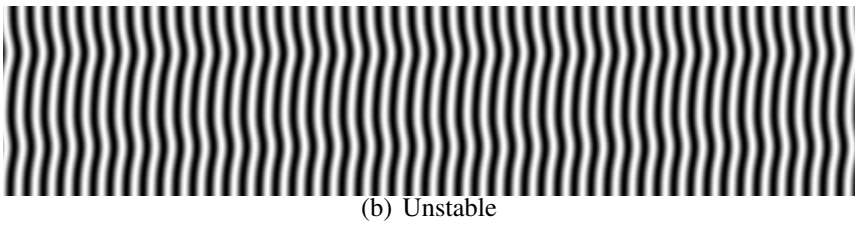

(b) Unstable

Figure 3.5: Numerical simulations of the almost homogeneous system. The parameters are like in Fig. 3.4(c) with $\beta = 1.0$, $l = 15$. We show space-time plots (space is vertical axis, time horizontal axis) of the real part of η. Graycode: brighter (darker) regions correspond to lower (higher) values. The initial condition for 3.5(a) is an almost homogeneous distribution close to the slow limit cycle (upper branch in Fig.3.4(c)), and for 3.5(b) close to the rapid limit cycle (lower branch in Fig.3.4(c)).

3.4 Numerical results

The analytical results about birhythmicity only refer to the single oscillator dynamics, or equivalently to the strictly uniform system. On the other hand, the phase dynamics holds in the cases where the oscillation amplitude does not change significantly in the pattern. Numerically, we can investigate the behaviour of the system even far from these limits, when the couplings affect the dynamics and when amplitude defects are present as well.

For numerical integration of these equations, the fourth-order Runge-Kutta algorithm has been used. The diffusional term was integrated through a first-order finite difference method. The mesh size for space discretization and the time step have been chosen to optimize the computational time for each parameter choice. Since the diffusion length and the diffusion constant of the oscillatory field have both been chosen to be equal to unity, Δx varied between 0.3 and 0.5, while Δt could vary between $(\Delta x)^2/5$ and $(\Delta x)^2/2$. Both one- and two-dimensional systems were investigated. In general, in the pattern we are going to show, no-flux boundary conditions were employed. The space-time plots illustrating the results of numerical simulations make use of a gray code where white encodes smaller values and black larger values. In general, in each figure the contrast has been adjusted independently.

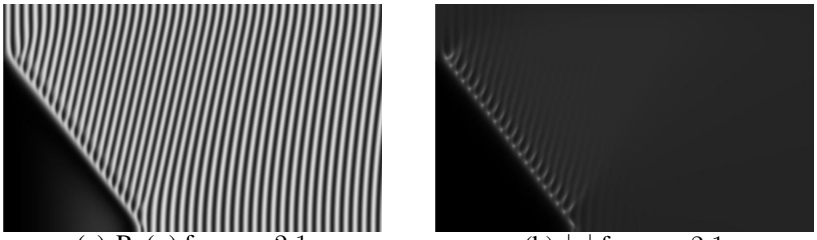

(a) Re(η) for $\alpha = 2.1$ (b) $|\eta|$ for $\alpha = 2.1$

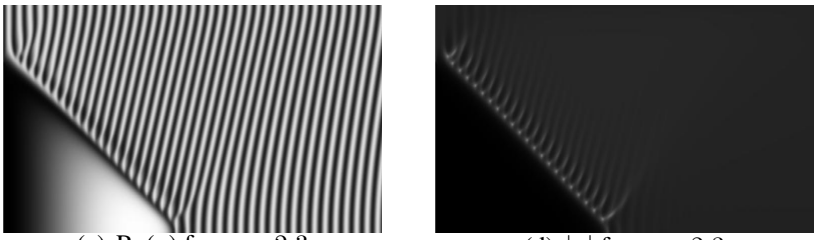

(c) Re(η) for $\alpha = 2.3$ (d) $|\eta|$ for $\alpha = 2.3$

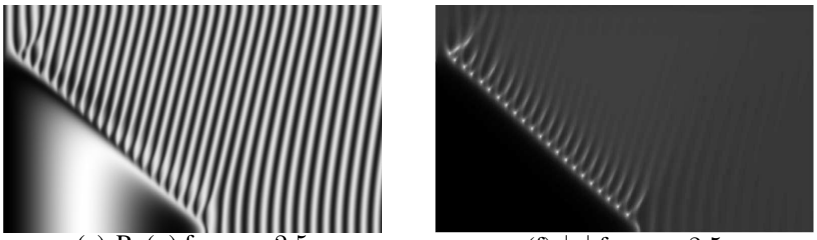

(e) Re(η) for $\alpha = 2.5$ (f) $|\eta|$ for $\alpha = 2.5$

Figure 3.6: Front propagation in the birhythmic system. Graycode as in Fig. 3.5. Space is the vertical axis, time the horizontal axis. Parameters: $\omega = 2.0,\ \beta = 1.0,\ K = 0.5,\ \tau = 10,\ l = 10$. In all of the three cases shown, front motion is linear with constant velocity. The velocity decreases as the frequency difference between the two oscillation modes diminishes.

3.4.1 Front propagation

We already know that the perfectly homogeneous system is able to show two types of oscillations. Now we want to split our system into two parts, each of them being initially uniform. One part is set to be located on the rapid limit cycle, while the other is started on the slow limit cycle. In the considered cases, both types of oscillations are stable towards smooth spatial modulations. A front separates the two domains. If the parameters are far enough from the edges of the birhythmic region where stability properties of the limit cycles may become delicate, the motion of the front is linear, as shown in Fig. 3.6.

The front always travels towards the slow oscillating region, in such a way that the system ends up with uniform oscillations of the rapid mode. The front is characterized by a periodical appearance of amplitude defects occurring when the phase difference between the two oscillatory regions equals 2π. In Figs. 3.6(b), 3.6(d), and 3.6(f), these events, known as

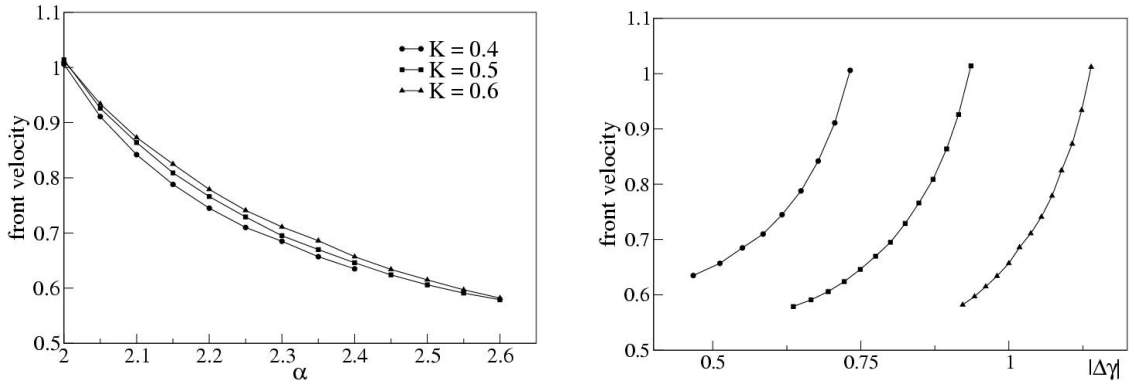

(a) (b)

Figure 3.7: Front velocity as functions of the parameter α and difference $\Delta\gamma$ of oscillation frequencies in the two modes in the birhythmic regime. The fixed parameters are $\omega = 2, \beta = 1, l = 10$, and $\tau = 10$.

phase slips, are visible as white spots on the traveling interface.

The velocity of the front propagation depends on the parameters of the system. In particular, the larger the frequency difference $\Delta\gamma$ between the two oscillations, the faster the propagation. In Fig. 3.7(a) the propagation velocity is plotted as a function of the nonlinear frequency shift α, while in Fig. 3.7(b) its dependence on the frequency difference $\Delta\gamma$ is shown.

3.4.2 One-dimensional patterns

As follows from the stability analysis of uniform oscillatory states, rapid oscillations are unstable with respect to phase modulations near the birhythmicity boundary and complex spatio-temporal regimes can be expected there.

We performed a series of numerical simulations in the interval $2.55 < \alpha < 2.8$, simultaneously varying β between -1 and 2.5, in order to get a table of the different patterns shown by the system. In this region, a high sensitivity of the system on parameters variation is present, so that significantly different patterns, from uniform oscillations to turbulence, are observed. All the patterns shown were obtained starting from completely random initial conditions.

The results are summarized in Fig. 3.8 and 3.9. The solid line in Fig. 3.8 is the stability boundary ($C_2 = 0$) of rapid oscillations according to the phase dynamics approximation: they are unstable below this line. Slow oscillations are always stable in the considered region. This

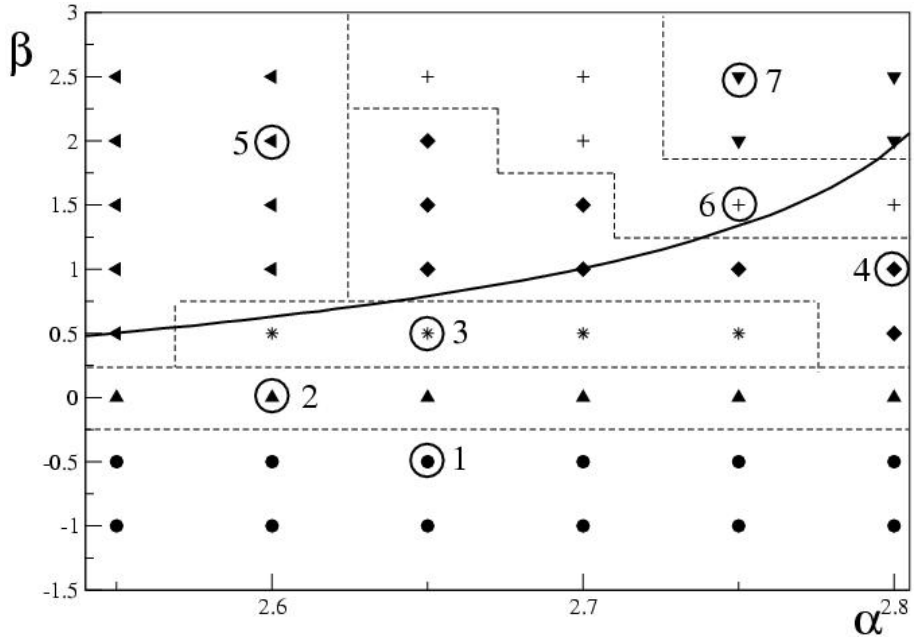

Figure 3.8: Schematic phase diagram. Numerical simulations of the one-dimensional model were performed at the values of α and β indicated by symbols in this diagram. Depending on the observed properties of patterns, the diagram is divided into regions 1 to 7. The circles indicate the values of these parameters used to produce a typical pattern for the corresponding region, displayed in Fig. 3.9. The solid line shows the stability boundary of rapid uniform oscillations, given by the condition $C_2 = 0$. Other parameters are $\omega = 2, K = 0.5, l = 10$, and $\tau = 10$.

stability boundary can serve as a reference to compare numerical results with the analytical calculations. However, as we have already stressed, the stability analysis was performed in the phase approximation of the system, that does not hold for all of the patterns shown in the present simulations. In particular, when amplitude defects are present, or jumps from one to the other limit cycle are observed, phase description clearly breaks down. In that case, the calculated stability condition only provides a partial information. For instance, it can be used to give an explanation of the dynamics of the system far from the defects.

The one-dimensional simulations were all performed for a system of total length 200 and for a total time of at least 500 to 3000 time units. However, in order to make the appearance of each different pattern as clear as possible, only selected portions of the entire simulation are shown in Fig. 3.9.

- Pattern 1: Here the stability analysis of the phase dynamics predicts Benjamin-Feir instability. Numerically, the regime of fully-developed turbulence appears. The oscil-

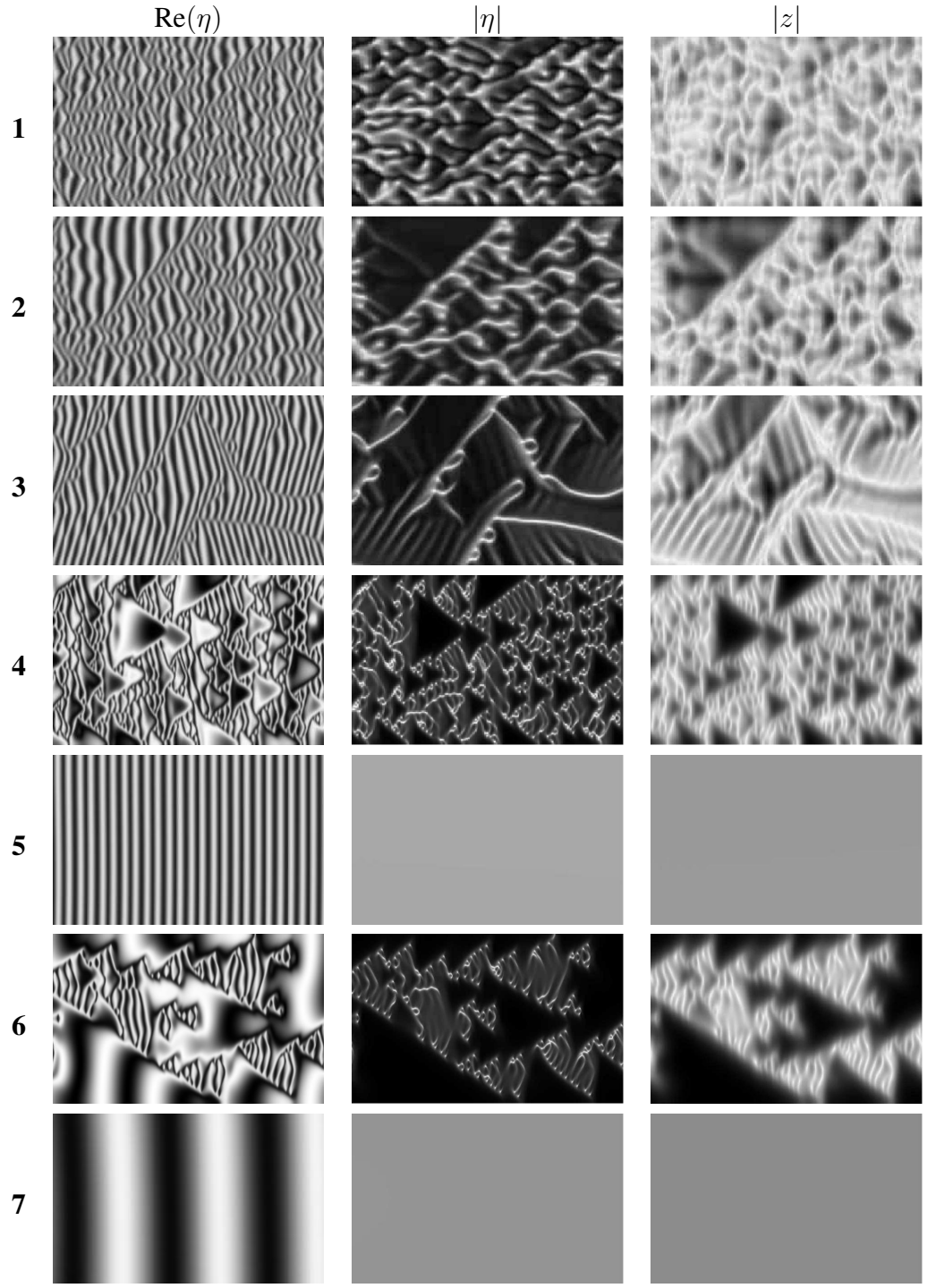

Figure 3.9: Spatio-Temporal diagrams displaying evolution of Re(η), $\rho = |\eta|$ and $r = |z|$ in typical patterns observed in the regions 1-6 for the one-dimensional system. Space is the vertical axis, time the horizontal axis. Graycode as in Fig. 3.5. The respective parameter values are given in Fig. 3.8. Graycode as in Fig. 3.5. The displayed space and time intervals are (1) $L = 100$, $T = 166$, (2) $L = 100$, $T = 166$, (3) $L = 100$, $T = 250$, (4) $L = 200$, $T = 500$, (5) $L = 100$, $T = 250$, (6) $L = 200$, $T = 500$, and (7) $L = 200$, $T = 250$.

lations have small amplitude, and a large number of defects is present.

- Pattern 2: Increasing β, we observed the emergence of groups of synchronized oscillators which become able to reach the rapid limit cycle and perform harmonical oscillations for several periods. When this occurs, amplitude defects disappear, as it can be seen in the dark region in the space-time plot for $|\eta|$.

- Pattern 3: In this rather small parameters region, frequency and amplitude of the oscillations correspond almost everywhere to those of the rapid limit cycle. However, the system does not get complete synchronization. Lines of amplitude defects travelling through the system act as wave sources, emitting waves phase-shifted by π in the two directions.

- Pattern 4: In this case a new type of turbulence is observed. This pattern is characterized by a background of rapid and chaotic oscillations, with small amplitude and numerous amplitude defects. On this highly desynchronized background *bursts of synchronization* emerge. These bursts consist of large groups of elements which suddenly start to oscillate altogether with large amplitude and small frequency corresponding to the stable slow limit cycle. However they cannot keep synchronized for a long time: after less than one oscillation period turbulence overwhelms again.
  It was observed from Fig. 3.3(b) and 3.3(c) that in the rapid limit cycle the amplitude of the nonlocal field is very small, almost vanishing, while in the slow limit cycle it gets a larger value, comparable to the amplitude of η. In the case of this pattern, it can be clearly seen that, in the synchronization bursts, $|z|$ is much larger than in the turbulent background. This means that, when the nonlocal coupling is more effective due to the large modulus of z, the oscillators can organize themselves in large groups performing a collective motion. On the contrary, when the nonlocal field is too weak and diffusion is the only effective coupling, no long-range synchronization can be obtained.

- Pattern 5: When the rapid limit cycle gets stable, the system goes to a uniformly oscillating state of the rapid type.

- Pattern 6: Here, the patterns can be described as exhibiting *bursts of desynchronization* on the background of slow uniform oscillations. Inside such bursts, the coupling field z is strongly decreased in amplitude and only short-range diffusive coupling among the oscillators is effective.

- Pattern 7: Closer to the bifurcation point where the rapid limit cycle disappears by merging with the unstable one via a saddle-node bifurcation, slow uniform oscillations are preferred.

In order to make more clear the relationship between the one-dimensional patterns and the analytical findings about birhythmicity, we show a few snapshots of the phase portrait of η in the case of pattern 6. In Fig. 3.10 each oscillator is represented as a single point in the complex plain. The two circles indicate the two stable limit cycles. In such a representation, the information about the spatial distribution of the oscillators is lost, but the motion performed by the oscillators between the two attractors is shown better.

Clearly, the distribution of the oscillators is mainly organized in the proximity of the two coexisting attractors. The oscillators sitting on the rapid limit cycle with the smaller amplitude belong to the desynchronization bursts. The elements running through the slow and large limit cycle form the synchronized background. The points located in the vicinity of the origin $\eta = 0$ correspond to amplitude defects generated at the border between spatial regions with different oscillation frequencies (bright dots in the spatio-temporal plot of $|\eta|$ for pattern 6 in Fig. 3.9). Such defects are not present at all times, and the respective points are not, for example, seen in the phase portraits at $t = 16.7$ and $t = 281.7$: In these cases the front between the two domains is smooth.

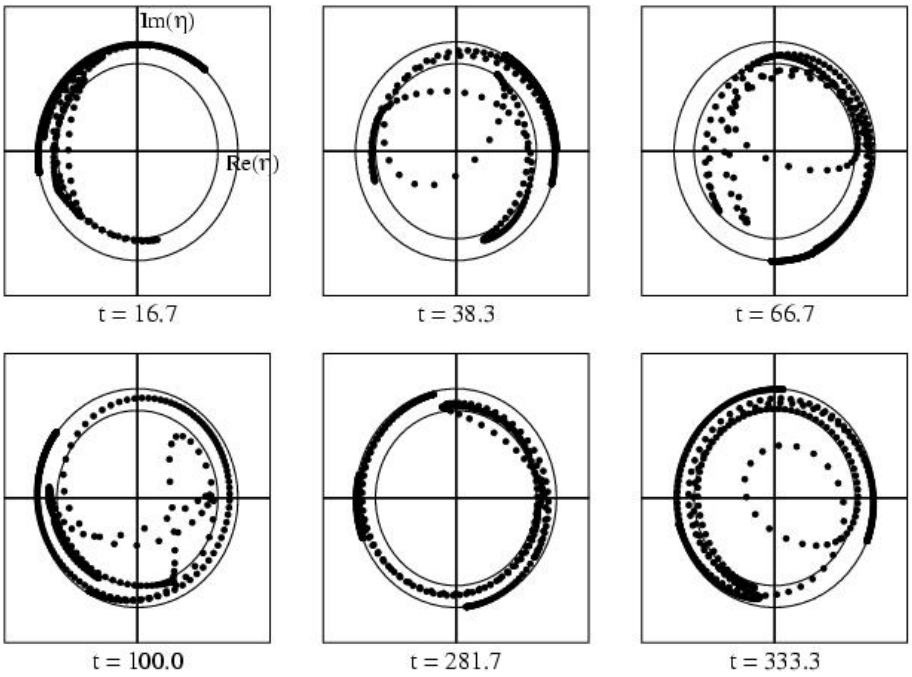

Figure 3.10: Selected snapshots of the phase portraits for the pattern 6 in Fig. 3.9. The circles show two different limits cycles in the birhythmic system.

3.4.3 Two-dimensional patterns

Two dimensional simulations have been performed as well, to investigate the behavior of the system located on a surface.

Fig. 3.11 displays a system at the same parameters as for the pattern 3 in Fig. 3.9. The space-time diagrams in the right panels show the pattern development along a horizontal cross section. The lines of amplitude defects observed in the one-dimensional pattern give rise to spiral tips in the two-dimensional case. After a transient where the tips move through the medium, a stable configuration of rotating spirals is reached.

Figure 3.12 shows two-dimensional patterns corresponding to synchronization bursts (pattern 4 in Fig. 3.9). One of such bursts can for example be seen in the left central part of the snapshots (left panels). There, the field η is approximately uniform, there are no amplitude defects and the magnitude of z is rather large as well, whereas in the rest of the medium amplitude turbulence with several spiral tips appears. The space-time diagrams (right panels) reveal that the synchronized regions with slow oscillations have only relatively short lifetimes. They are promptly replaced by irregular rapid oscillations, although they appear again and again in the course of time, giving rise to the same kind of structures observed in the one-dimensional system.

A behavior, which can be described as bursts of desynchronization, was found in our two-dimensional simulations even outside of the birhythmicity region, where only slow uniform oscillations are possible (Fig. 3.13 and 3.14). We started here with the initial condition, which is commonly used to generate rotating spirals (see Ref. [37]): real and imaginary part have a constant gradient, ranging from -1 to 1 in orthogonal directions. Thus they are both equal to zero in the center of the medium where a single amplitude defect is established. Initially a spiral wave is indeed formed, but the central core of this spiral is rotating with a different frequency than the outer part of it. This gives rise to a pattern where a circular line of amplitude defects periodically appears. This structure gets unstable after a few periods (Fig. 3.13) and the center of the spiral is now occupied by a small turbulent region where fast oscillations are observed. The development of this instability results in complete destruction of the spiral. The small turbulent core expands and splits into several domains which travel through the medium, shrinking and expanding. Typical snapshots of spatial distributions of $\mathrm{Re}(\eta)$, $|\eta|$ and $|z|$ in this pattern are displayed in the left panels in Fig. 3.14. Inside the domains, the coupling field z is reduced in magnitude and these small spatial regions are filled with irregular rapid variations of the complex field η. Thus, they can be classified

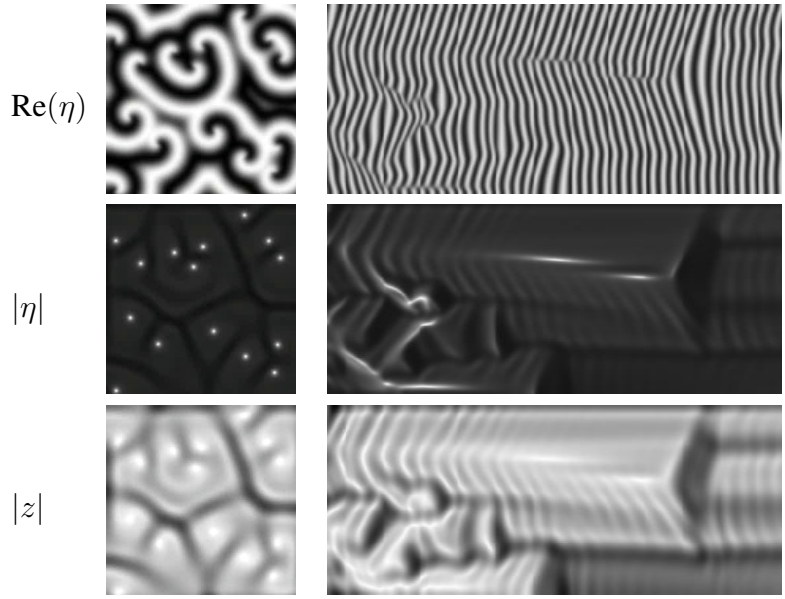

Figure 3.11: Multiple spiral waves in a two-dimensional system of size 120×120; the same parameter values as for the pattern 3 in Fig. 3.9. The right panels are space-time plots showing evolution of the pattern along one horizontal cross section; the displayed time interval is $T = 480$. Space is the vertical axis, time the horizontal axis. Graycode as in Fig. 3.5.

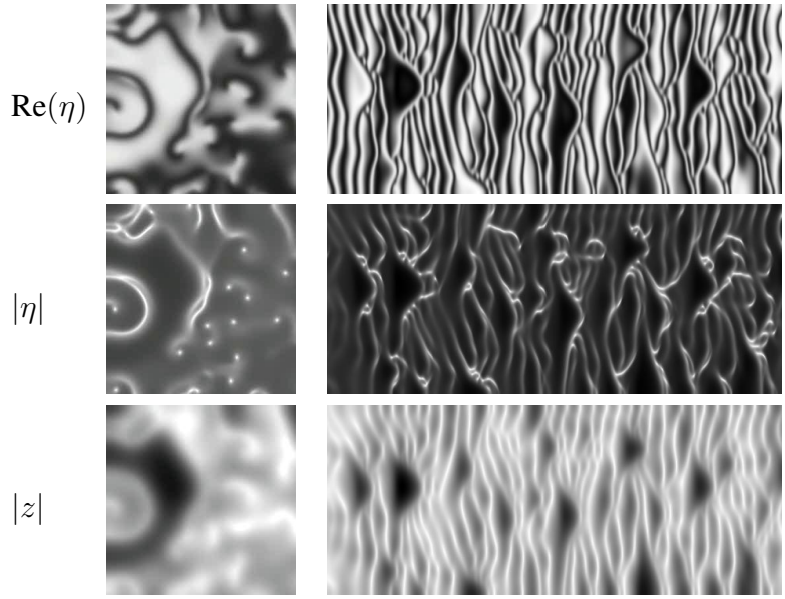

Figure 3.12: Bursts of synchronization in a two-dimensional system of size 120×120; the same parameter values as for the pattern 4 in Fig. 3.9. The right panels are space-time plots showing evolution of the pattern along one horizontal cross-section; $T = 480$. Space is the vertical axis, time the horizontal axis. Graycode as in Fig. 3.5.

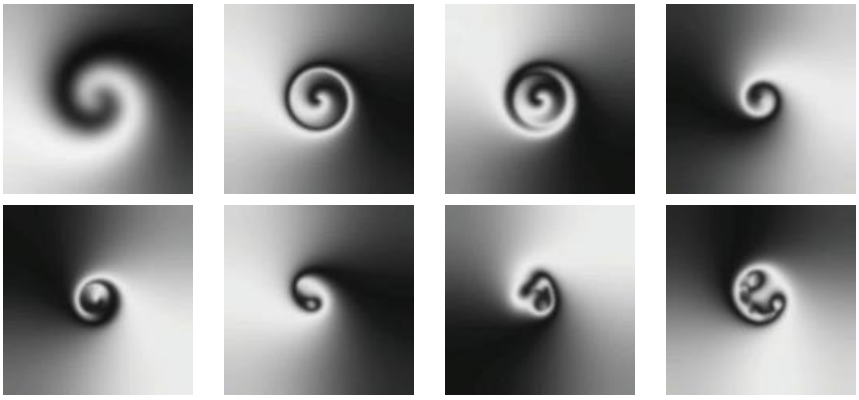

Figure 3.13: Instability of a rotating spiral. Simulation for a two-dimensional system of size 120×120 with parameters $\omega = 2, \alpha = 3, \beta = 1, K = 0.4, l = 10,$ and $\tau = 10$. Graycode as in Fig. 3.5. Subsequent snapshots of the field Re(η) at times T = 2.8, 10.0, 15.2, 37.2, 96.8, 119.6, 130.0, and 139.2 are presented.

as desynchronization bursts. The space-time diagrams through one horizontal cross section of the medium (right panels in Fig. 3.14) confirm the similarity with pattern 7 of the one-dimensional case. The edges of these structures are marked by the appearance of amplitude defects where $|\eta|$ is close to zero.

It is worth to mention that, by removing diffusion of the oscillatory field (the Laplacian term in equation (3.1)), we observed spiral waves with phase-randomized cores. This pattern has been described in the Introduction (see Sec. 2.3.3, Fig. 2.14) and was actually found in a system where only nonlocal coupling is present. Thus, the inclusion of diffusive coupling has a strong effect on pattern formation in the system. Though patterns resembling spiral waves with phase-randomized core are indeed initially developing in the diffusively coupled case, they are unstable and, after a transient, lead to the development of intermittent spatio-temporal regimes with desynchronization bursts.

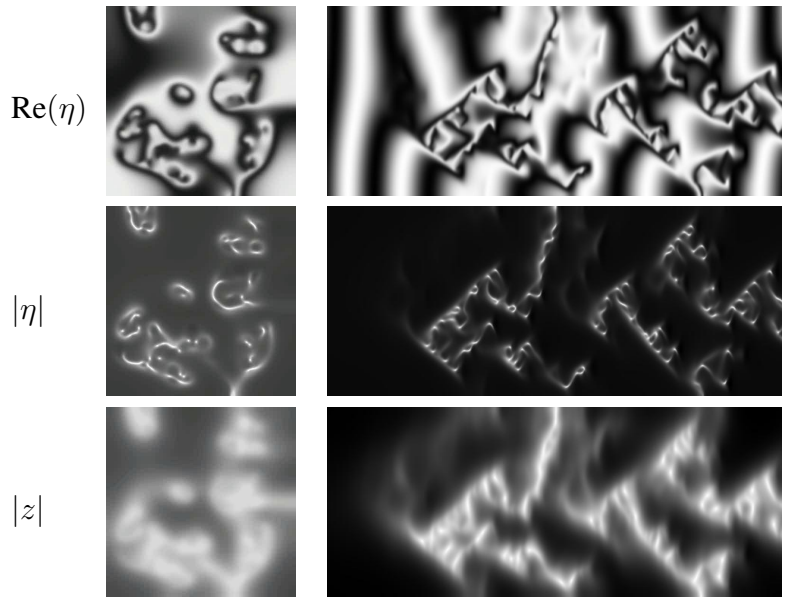

Figure 3.14: Bursts of desynchronization in a two-dimensional system of size 120×120; continuation of the simulation presented in Fig. 3.13. The parameters are $\omega = 2, \alpha = 3, \beta = 1, K = 0.4, l = 10$, and $\tau = 10$. The right panels are space-time plots showing evolution of the pattern along one horizontal cross-section; $T = 720$. Space is the vertical axis, time the horizontal axis. Graycode as in Fig. 3.5.

Chapter 4

Biological oscillators

4.1 Classical biological oscillators

In the previous Chapter, we have presented a general and abstract model for an oscillatory system with nonlocal coupling. Below, we want to consider an example of oscillations occurring in living cells, which play an especially interesting role in the domain of out-of-equilibrium systems. A single living cell has an extremely complex structure consisting of a large number of distinct objects (see Fig 4.1), where a wealth of chemical reactions take place. Almost all of these reactions are catalyzed by specific biocatalysts, which are proteins called enzymes. The way this intense chemical activity proceeds is a beautiful example of self-organization: The functioning of this highly complex system has to be efficiently regulated despite the very large number of individual processes involved and of the uncontrolled variation of external conditions like, e.g., the temperature. The mechanisms through which self-organization is successfully achieved are correspondingly complex and are the result of evolution. Because of the intrinsic complexity of these phenomena, the description and the modeling of biological systems has to be carried on different levels in parallel, ranging from the extremely detailed and realistic modeling of single reaction-pathways, up to abstract models aimed to the identification of general features of regulatory mechanisms operating in different systems.

In the case of oscillatory chemical reactions, the task of the scientist often consists in the designing of appropriate systems, which can be suited to display interesting behaviors. On the contrary, when approaching living systems, an impressive variety of complex processes is immediately at disposal, and the challenge becomes finding the key features among the extremely large number of steps involved. These complex processes often involve self-sustained oscillations which have been observed in many different biological contexts. How-

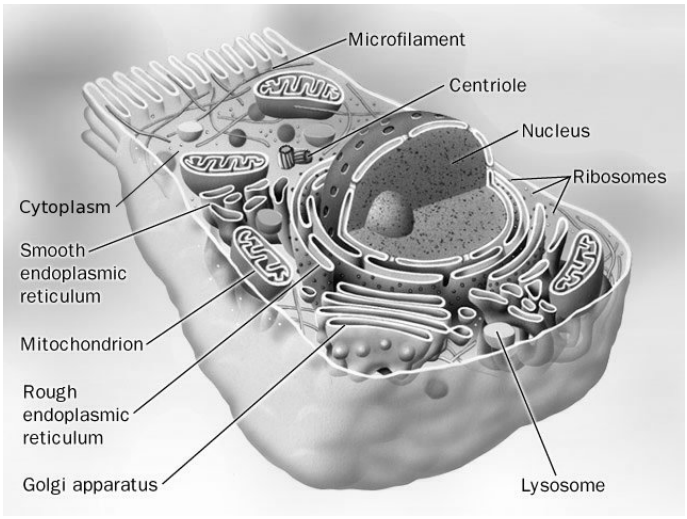

Figure 4.1: Schematic view of an eukaryotic cell. After [152].

ever, the question often remains open, whether these oscillations do play a functional role and what is the advantage resulting from their presence.

The known oscillatory processes in biology cover a vast range of time scales and their variety becomes even broader if we also include spatio-temporal pattern formation [12, 13, 23, 153]. In the following, a brief summary of some of the most studied cases is given.

4.1.1 Circadian rhythm

This term is used to indicate the presence of a periodic behavior in the physiological functioning of many living organisms [12, 13, 23]. The period of these oscillations is very close to the duration of a day and involves many measurable quantities describing the state of the organism: In human beings, for instance, it is observed in body temperature variations, enzyme activity, and hormonal level and it is related to the sleep-awake periodicity, thus regulating also neuronal activity and nutrition. Although this periodicity is -as intuition suggests- related to environment adaption, it turns out that it is preserved with a remarkably good precision also under modified environmental conditions, like, e.g., in subjects exposed to constant light or darkness. However, the circadian rhythm can also be entrained by external forcing of modified light-darkness cycles or phase-shifted when exposed to light pulses. Concerning the modeling of this phenomenon, it has to be stressed that the mechanism can be considerably different for the different living beings in which it has been studied, ranging from unicellular organisms to mammalians, going through fungi and flies. Some of the most

recent models have a high degree of complexity and involve up to 16 differential equations. However, it seems to be accepted that the central mechanism causing oscillations is represented by a negative feedback exerted by a protein on the expression of its corresponding gene. Experiments have shown that circadian rhythm arises from synchronization of cellular clocks in the brain [24].

4.1.2 Ca^{++} oscillations

Oscillations of the cytosolic concentration of Ca^{++} ions are used as a communication tool within a cell and between living cells [12,28,30]. In fact, Ca^{++} is called a second messenger: Simple oscillations and more complex spatio-temporal patterns of calcium concentration are used to transmit information which is essential for the regulation of several primary cellular activities like fertilization, differentiation, electric neural activity, cell death and many others. The characteristic time scales and wavelengths of these patterns vary in a wide range. Calcium ions can pass through the cell membrane via ion channels which are organized in clusters having a typical extension of the order of tens of nanometers. Thus, stochastic processes on this length scale may need to be considered, such as the binding and detaching of Ca^{++} ions to and from single channels. On the other hand, waves of calcium concentration are also observed at an intercellular level, having a characteristic length of tens of micrometers. Similarly, time periodicity ranges from fractions of a second for individual calcium sparks up to tens of hours for regulation of cell division.

4.1.3 Glycolytic oscillations

Glycolysis [12, 15–19] is an important step of metabolism of living cells. It is a sequence of 10 biochemical reactions, whose net effect is the production of two ATP molecules (detailed reaction path is shown in Fig.4.2). In this way, the cell stores the energy taken from glucose (received through nutrition) in ATP, from which it can be successively extracted for usage. More than 40 years ago, it has been observed that self-sustained oscillations can be present in such a reaction. In particular, the concentration of NADH (product of the fourth reaction step) can be monitored through fluorescence. It has been experimentally determined that the regulating step responsible for emergence of oscillations is the third one, catalyzed by the enzyme phosphofructokinase (PFK). In fact, in order for sustained oscillations to be observed, it is necessary to continuously supply to a glycolytic system (like, e.g., highly concentrated yeast extracts) the substrate of one of the first four reaction steps (namely, glucose or fruc-

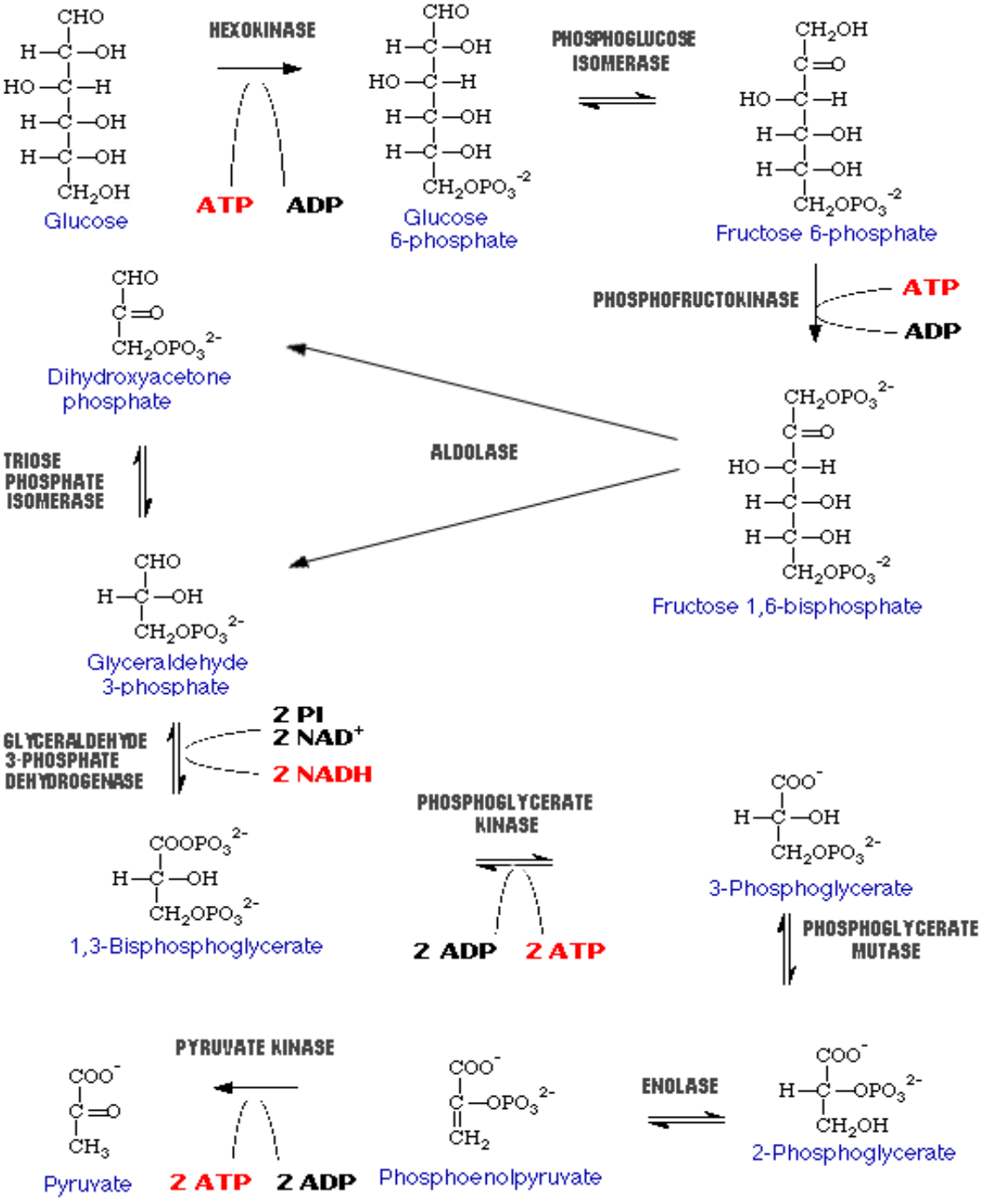

Figure 4.2: Glycolysis pathway. After [154].

tose or fructose-6-phosphate) while, for instance, supplying fructose-1,6-biphosphate does not give rise to oscillations. The role of PFK as *oscillophore* has been the subject of many investigations and there is not yet a definitive agreement on the explanation of the mechanisms through which oscillations occur. However, a large part of the scientific community agrees in that a central role in the emergence of periodic behavior is played by feedback regulation of PFK. In particular, the catalytic activity of the enzyme PFK is affected by the concentration of its own reaction product fructose-1,6-biphosphate, and in the same time its substrate ATP can also act as an inhibitor of the catalytic activity. The property of PFK of being regulated by other molecules is called allostery and is going to be explained in Sec. 4.2.1. Experimental investigations of glycolysis in an extended system provided by yeast extracts have allowed the observation of propagating waves [20, 21], thus showing that cellular metabolism is not only a self-oscillatory phenomenon, but can also give rise to spatio-temporal pattern formation. Wave propagation of glycolytic activity has also been reported in single white blood cells [155].

4.2 Self-organization at a molecular level

Calcium and glycolytic oscillations are chemical oscillations of the same type as, for instance, those occurring in the Belousov-Zhabotinsky reaction [61–66], with the important difference that they emerge in biological systems at a cellular level. However, such chemical oscillations have typical periods of the order of tens of seconds up to hours, much larger than the time scales on which individual biochemical events take place, such as for instance protein-protein interactions or enzyme-catalyzed reactions. Therefore, in the last ten years the question was raised, whether also oscillations on the time scale of such single reaction events can be observed [57, 156]. These oscillations might result from synchronization of macromolecules operating as molecular machines [53–56, 157], and would therefore represent a means of regulation of cellular activity on the smallest time scale of biological processes in living beings. In contrast to macroscopic chemical oscillations, they would require the emergence of rigid correlations between the functioning of individual enzymes. In this sense, one should think of a cell as a network of interacting molecular machines, rather than as a usual reaction-diffusion system [52, 158].

Concerning the possibility of pattern formation phenomena (such as wave propagation) on a sub-cellular micrometer length scale, it was believed that they should be excluded due to too strong mixing inside the cell (cf. Sec. 5.1). However, taking into account possible self-

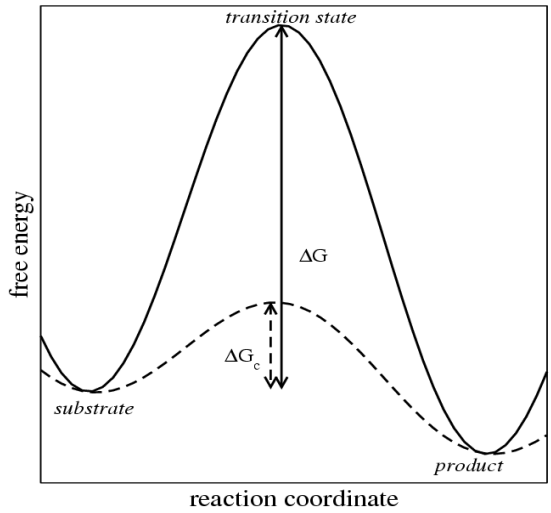

Figure 4.3: In the transition state theory, the conversion of a substrate into a product is seen as a transformation passing through an intermediate state called transition state. This state has a larger free energy than the initial substrate. Thus an energy barrier has to be overcome, whose height is referred to as activation energy (ΔG). For the spontaneous reaction (solid line) this barrier can be very high. Binding of the substrate to the enzyme provides a different reaction path (dashed line), such that the activation energy of the catalyzed reaction (ΔG_c) can be much smaller.

organization due to intermolecular correlations, it turns out that patterns on the length scale of a few microns can occur [57, 156], which can be contained within a single cell. Experimental observations of metabolic intracellular waves have been reported [155], although the generating mechanism has not yet been clarified.

From a theoretical point of view, the description of possible self-organized microscopic synchronization of molecules requires an unconventional description of biochemical reactions. In this picture, biomolecules such as enzymes, must be seen as phase oscillators. Before explaining in detail how this can be achieved, we shall recall the basic concepts of classical enzyme kinetics.

4.2.1 Classical enzyme kinetics

Almost all of the biochemical reactions occurring in living systems are only possible in the presence of catalysts [159]. This function is carried out by enzymes, which are a class of protein molecules. In the above mentioned case of glycolysis, each reaction step is catalyzed by a specific enzyme. Its task is to facilitate the transformation of a molecule (the *substrate*)

into another molecule (the *product*). The enzyme itself exits the reaction unchanged. That is, although being involved in the transformation, it returns to its native state after the reaction has been completed.

Like other proteins, enzymes are in general large molecules with complex structures. They provide a support in which the very high energy barrier, which should be overcome for the reaction to spontaneously take place, is strongly decreased. In other terms, reactions which would have such a small rate that they would in practice never occur, are made possible by enzymes. The task of an enzyme is to reduce the activation energy (see fig. 4.3). The result is an increase of the reaction rate of both the forward and the inverse reaction (that is, the reaction equilibrium is not shifted). A striking feature is that often biocatalysts bring about an increase of approximately one million of the reaction rate!

Moreover, enzymes have a high degree of specificity, essentially related to their structural specificity. Each of them generally catalyzes a unique reaction (or a few very similar reactions) and binds exclusively to its own substrates. Substrate binding can succeed only on a specific location of the enzyme molecule which is called the *active site*: A three-dimensional entity made up of several groups coming from different parts of the amino acids sequence. This site is in general rather small with respect to the overall dimension of the enzyme, meaning that, for the binding to succeed, the substrate needs to find and approach the appropriate location.

The classical model which gives in many cases a good quantitative description of the enzymatic activity is the so-called Michaelis-Menten mechanism [159, 160]. In this picture, the enzyme E combines to the substrate S to form a complex ES, which can either dissociate back to E and S or proceed to form the product P. The latter then dissociates from the enzyme. The scheme is as follows:

$$E + S \underset{k_2}{\overset{k_1}{\rightleftharpoons}} ES \overset{k_3}{\rightarrow} E + P \tag{4.1}$$

At equilibrium, the concentrations of enzyme, substrate, and enzyme-substrate complex are related through:

$$[\mathrm{ES}] = \frac{[\mathrm{E}][\mathrm{S}]}{K_M}, \tag{4.2}$$

where $K_M = \dfrac{k_2 + k_3}{k_1}$ is the Michaelis-Menten constant, which allows to calculate the reaction rate as a function of the substrate concentration. The relation is:

$$V = V_{\max} \frac{[\mathrm{S}]}{[\mathrm{S}] + K_M}, \tag{4.3}$$

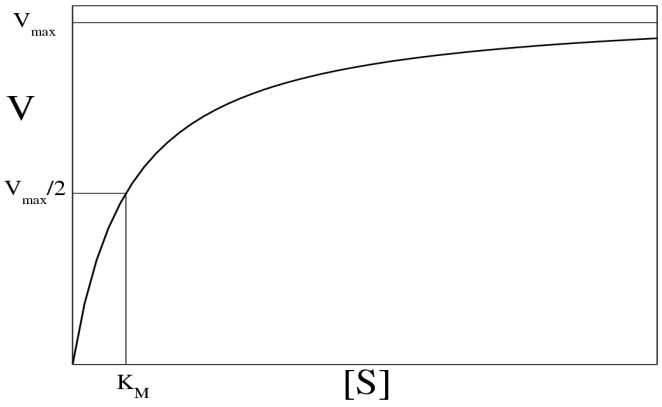

Figure 4.4: Reaction velocity vs. substrate concentration according to the Michaelis-Menten mechanism

and is plotted in Fig. 4.4. $V_{\max}$ is the maximal reaction rate asymptotically reached as $[\mathrm{S}] \rightarrow \infty$.

The curve shows a saturation effect which is experimentally observed. This is due to the fact that the reaction proceeds via formation of the ES complex, so that, keeping the enzyme concentration fixed, the rate of transformation cannot overcome the velocity reached when all of the enzymes are simultaneously engaged in catalysis. Thus, a further increase of the substrate concentration does not cause any speed-up of the reaction.

The maximal rate $V_{\max}$ reveals the *turnover number* of the enzyme, i.e. the average number of substrate molecules converted into products per unit time by a single enzyme, when the reaction is fully saturated with substrate. The inverse of the turnover number is the *turnover time*, i.e. the average time taken to convert one substrate into one product.

A rather large class of enzymes possess an additional feature called *allostery*. Allostery is a regulatory mechanism, through which the activity of the catalyst can be modulated by effector molecules, that are not necessarily involved in the reaction. Allostery provides the cell with a powerful control mechanism: The rates of the catalytic reactions can be regulated according to the varying concentrations of other species.

Allosteric regulation can occur in many different ways, so that good fitting of the experimental data requires in practice enzyme-specific modelling. However, also general models exist. Among them, the best known descriptions of allosteric interactions (the *symmetric* [161] and the *sequential* model [162]) assume the enzyme to be constituted of several subunits. The cooperation among such subunits is the cause of the regulatory effect. In-

deed, the large majority of the known allosteric enzymes are oligomers, i.e. made up of more identical subunits. However, regulatory behavior can also be observed in monomeric enzymes [163–166], and can also be explained without invoking interactions between subunits. One possible mechanism of allosteric regulation is that the effector molecule binds to the enzyme at a *regulatory* site distinct from the active site, the latter remaining reserved for the substrate. Binding of such effector molecule causes a conformational change of the enzyme [167–171]. In particular, the structure of the active site becomes modified so that its affinity for the substrate changes. If the active site becomes more suitable to bind the substrate, the effector is an *activator*, if, on the contrary, the affinity for the substrate is reduced, the effector is an *inhibitor*.

One possible consequence of allosteric regulation is that the saturation curve of the enzyme does not show the Michaelis-Menten behavior shown in Fig. 4.4, but has a different shape.

4.2.2 Conformational changes and enzyme kinetics

All of the above mentioned models for enzyme kinetics depict enzymes as molecules being able to perform transitions between a set of different states. In the Michaelis-Menten mechanism, the states are the free enzyme and the enzyme-substrate complex, while the models for allosteric regulation take additionally into account that the enzyme itself may exist in different conformational states with differential affinity for the substrate, and that fluctuations among these different structures are possible. But in all cases, an individual catalytic event is seen as an instantaneous event, i.e. a stochastic transition between distinct states, which are different from a chemical and a conformational point of view.

However, it is known that an inherent and relevant part of a turnover time is constituted by slow conformational motions taking place during the conversion of a substrate into a product. Such structural motions have a functional role, that is, they are essentially needed for the occurrence of the catalytic conversion [172]. The binding of a substrate makes the enzyme leave its equilibrium conformation and begins a sequence of conformational changes, which are necessary to achieve the catalytic conversion of the substrate into the product. Afterwards, the product can be released and the enzyme can follow another succession of structural changes, eventually getting back to the ground state. The overall sequence of transformations is thus a *conformational cycle* which brings the enzyme back to its ground state after a non-equilibrium excursion in the structural space. In some cases (such as phosphory-

lation which is ubiquitous in biochemical reaction paths), the chemical aspect of the catalytic reaction can be very simple (covalent binding of a phosphate transferred from one molecule to another), but the corresponding structural process can be extremely complex (binding of phosphate to an enzyme, which is in this case a kinase, requires important conformational adaption) [173].

Evidence of such conformational cycles is becoming available thanks to experimental techniques which allow the investigation of single molecules. Although there are still limitations to the possibility of observing dynamical conformational motions, information can be obtained from techniques such as X-ray analysis of crystal enzyme structures, [171, 174–177], fluorescence correlation spectroscopy [178–186], fluorescence resonance energy transfer [187, 188], nuclear magnetic resonance spectroscopy [189], and surface-enhanced raman spectroscopy [184, 186]. With these techniques, single-molecule experiments have been performed on a still relatively small number of species (see [51] for a short review). Theoretical modelling has shown that the experimental results can be reproduced only if slow conformational motions are properly considered [50, 51, 190]. A mathematical description of the conformational cycle can be given by describing the structural relaxation of the protein as a diffusive drift along a conformational coordinate ϕ. Such coordinate must be a quantity carrying information about the conformational state of the enzyme; it can be some characteristic length featuring the distance between functional subunits of the molecule, or the rotation angle of a monomer with respect to the main body, or any other quantity to be established for the specific molecule considered. In the simplest case, its evolution equation can be given in the form a Langevin equation [50, 157]:

$$\frac{\mathrm{d}\phi}{\mathrm{d}t} = v + \eta(t), \tag{4.4}$$

where v is a constant drift velocity and $\eta(t)$ is a stochastic time-dependent variable.

Eq. (4.4) corresponds to the definition of a phase oscillator given in Eq. (2.12) with the addition of a diffusive component which accounts for the presence of fluctuations. Thus, we have described an enzyme as a stochastic phase oscillator. As we have already stressed, such a description is only possible when the conformational cycle of the enzyme is constituted by a well-defined sequence of transformations. If the effect of the fluctuations becomes too strong, the phase description of the catalytic cycle does not hold.

Assuming that Eq. (4.4) appropriately describes one given enzyme, the question arises, whether synchronization of a population of such oscillators can occur. If the enzymes can influence each other, for example through the exchange of some regulatory molecule, it is

possible to expect the emergence of spatio-temporal correlations among their catalytic cycles.

It has been experimentally proved that a population of enzymes can be synchronized through external forcing [191–193]. The cytochrome p-450 dependent monooxygenase system is known to have light-sensitive catalytic activity. An experiment was realized, in which the concentration of the reaction products was optically monitored. In normal conditions, the concentration showed a continuous increase. This arises from equilibrium conditions of the enzyme population, that is, the catalytic cycles are uncorrelated and the overall product concentration grows at a constant rate.

Under the effect of periodic light pulses, a step-like behavior of the product concentration was observed. The phases of the catalytic cycles became synchronized by the external light forcing and the reaction products were released simultaneously by a large number of the enzymes. If the time-period of the forcing was set to be slightly smaller than the turnover time of one single catalytic cycle, the synchronization achieved its optimal value of 80%. Moreover, synchronization was found to be kept for a few cycles also after switching off the light.

A theoretical model was proposed for this system [194]. In the model, the enzyme operation is described as a cycle, consisting of a discrete sequence of states. One of these states is assumed to be light dependent (i.e. transition rate to the following state is strongly increased in the presence of light). The finding of the model is that if the number of states equals the number of intermediate chemical states experienced by the enzyme-substrate complex (8 for the considered reaction), the experimentally observed synchronization is not reproduced. It is necessary to assume a larger number of discrete states (40-60) in order to recover the 80% synchronization of the enzyme system. Thus, the synchronization of enzyme cycles is only explained if one takes into account the presence of physical (conformational) substates passed by the enzyme during the catalytic process.

The above-mentioned arguments strongly suggest that also spontaneous synchronization of enzymatic molecular cycles can occur. The theoretical studies [52–57, 156–158, 195, 196] have given general indications about the possible mechanisms that could give rise to this phenomenon.

Chapter 5

Spatio-temporal self-organization of molecular cycles

5.1 The system

5.1.1 Reaction mechanism and enzyme dynamics

As we have already mentioned in Sec. 4.2.2, a series of theoretical studies has investigated the possibility of synchronization of the conformational cycles of enzyme molecules. Here we want to provide an extension of previously studied systems [53, 55]. In those works, the considered reaction was assumed to occur in a very small volume where diffusion of the molecules could guarantee complete mixing. Under such conditions, a wandering particle can be assumed to have "forgotten" its initial position within a time interval much shorter than any other time scale involved in the system, so that in practice the spatial distribution of the particles inside the system can be assumed to be uniform and only variations of the average concentrations need to be considered. In this case, self-organization manifests itself as a purely temporal phenomenon.

In the present study, we want to overcome the constraint on the reaction volume size, and extend the analysis to larger systems. This means that we want also to take into account the emergence of spatio-temporal patterns due to the non-homogeneous distribution of the diffusing molecules over large distances.

In the present section, we recall the features of the system presented in [53–55] by including the new characteristics which are peculiar to the present case.

The reaction system we want to consider is constituted by an array of enzymes. The positions of the enzymes are assumed to be fixed. This can be realized experimentally, for instance, by attaching the molecules to a glass through a biotin molecule [183]. Thus, we

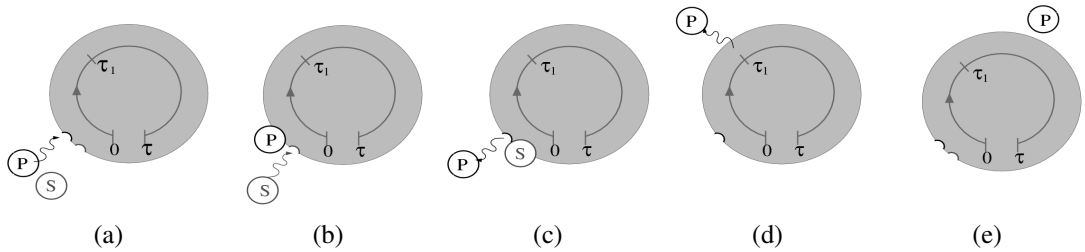

Figure 5.1: Reaction mechanism. (a) A regulatory product molecule attaches to the regulatory site of the enzyme. (b) The probability of binding a substrate is enhanced, although the substrate can also bind in the absence of a regulatory product (not shown). (c) The substrate binds, and the regulatory product, if any, detaches. (d) After transformation of the substrate into a product, the latter is released. (e) The product molecule diffuses and decays if it does not bind to another enzyme.

have a two-dimensional surface on which the enzymes stick. They are immersed in a liquid (e.g., water) where other molecules can freely diffuse. The other molecules of concern are the substrates and the products of the reaction catalyzed by the enzyme:

$$E + S \longrightarrow ES \longrightarrow E + P, \tag{5.1}$$

that is, a substrate molecule S is converted into a product molecule P via formation of an enzyme-substrate complex. Moreover, the enzymes are assumed to be allosterically activated by the product molecules (see Sec. 4.2.1): The enzyme has a binding site for the substrate (called *active site*) and a distinct binding site for the product molecule (*regulatory site*) which can carry out regulatory function by improving the catalytic activity of the enzyme itself. That is, an enzyme which has a product molecule attached to its regulatory site has a higher probability to catch a substrate and start conformational changes. This mechanism generates positive feedback in the system: the higher the concentration of product molecules, the more the enzymes are activated. The reaction mechanism is depicted in Fig. 5.1. Furthermore, we assume that:

- Once an enzyme-regulatory product complex has formed, it might also break apart without having started the conformational cycle;
- Freely diffusing product molecules, which are not bound to the regulatory site of an enzyme, decay with a given average life-time;
- Substrate molecules are continuously supplied to the system and are present in abundance.

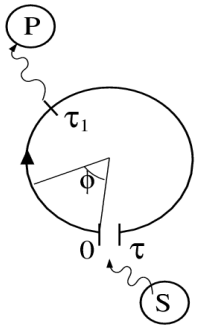

Figure 5.2: Schematic view of an enzyme operating as a phase oscillator. Once the substrate is attached to the active site, the conformational state begins to change, and its instantaneous state is indicated by the value of the phase ϕ. After a time τ_1, the product is released. After a time τ, the cycle has been completed, the phase reaches the value of 2π and the enzyme is back to the ground state, where it waits until a new substrate molecule binds.

An important assumption concerns the operating mode of the enzyme. We assume that the catalytic process occurs through a series of conformational changes taking place in the protein, and that these changes are not random rearrangements of its structure, but rather follow a well-defined sequence (cf. Sec. 4.2.1 and Sec. 4.2.2). Under these assumptions, the enzyme operation can be seen as a cycle of conformational changes, which are started by the binding of the substrate to the active site. After this first step has succeeded, a series of physical transformations starts, which allow the enzyme to achieve the catalytic conversion of the substrate into the product. As we have noted, in this case one can approximately describe an enzyme as a phase oscillator (see Fig. 5.2): The catalytic cycle is viewed as the motion along a conformational coordinate which can be seen as the phase within the loop. How the conformational coordinate can be defined for a real enzyme is not a matter for the present work, we shall just mention that it must be a quantity carrying information about the conformational state of the enzyme. In what concerns the reaction, it is characterized by the following rates:

- β: attachment rate of a product molecule to the regulatory site of the enzyme ($E + P \xrightarrow{\beta} EP$);
- κ: dissociation rate of a regulatory product-enzyme complex, ($EP \xrightarrow{\kappa} E + P$);
- α_0: rate of cycle initiation for an enzyme in absence of a regulatory product molecule;
- α_1: rate of cycle initiation for an enzyme with an attached regulatory product molecule (allosteric product-activation of the enzyme corresponds to the condition $\alpha_1 \gg \alpha_0$);
- γ: decay rate of free product molecules.

5.1.2 Characteristic length and time scales

The conditions under which the system is able to show synchronization are closely related to the relationship between different time and length scales characterizing the occurring processes. They have been discussed, with specific attention to the reaction in a small volume with complete mixing, in references [55, 156, 195, 196]. Here we recall these arguments and provide their extension to the non-homogeneous case.

Let us consider a three-dimensional reaction volume. The Fokker-Planck equation for the probability p to find a diffusing particle at time t in position $\mathbf{x}$ is:

$$\frac{\partial p(\mathbf{x},t)}{\partial t} = D\frac{\partial^2 p(\mathbf{x},t)}{\partial x^2} \tag{5.2}$$

which, with initial condition $p(\mathbf{x},0) = \delta(\mathbf{x})$, has the solution:

$$p(\mathbf{x},t) = \frac{e^{-\frac{\mathbf{x}^2}{4Dt}}}{(4\pi Dt)^{\frac{3}{2}}}. \tag{5.3}$$

One consequence of Eq. (5.3) is that, if we consider a spherical volume of radius L, a characteristic time scale:

$$t_{\text{mix}} = \frac{L^2}{D} \tag{5.4}$$

can be defined, which represents the *mixing time*. This is the typical time interval after which a particle can be found with approximately equal probability in any point of the system, regardless of its initial position.

The diffusing particles have then to meet their targets. In the present case, a freely diffusing product molecule must find one of the enzymes. We assume that each appropriate collision event causes the formation of a chemical bond, i.e. that whenever a product molecule hits an enzyme at its regulatory site, it sticks to it. The relevant time scale carrying information about the collisions is the *traffic time*, i.e. the average time interval needed for a diffusing particle to find a particular target. It is given by:

$$t_{\text{traffic}} = \frac{L^3}{DR}. \tag{5.5}$$

Here R is the sum of the radii of the diffusing particle and the regulatory site, assumed to be much smaller than L. We can also introduce the *transit time*, defined as the average time interval after which a diffusing particle first finds *any* of the N targets, randomly distributed inside a volume. This is given by:

$$t_{\text{transit}} = \frac{t_{\text{traffic}}}{N} = \frac{L^3}{DRN}. \tag{5.6}$$

The transit time can be seen as the average waiting time for the occurrence of a collision event. It can also be used to calculate another important quantity: the *correlation length*, the average length along which a product molecule travels between two successive collisions:

$$L_{\text{corr}} = \sqrt{t_{\text{transit}} D} = \sqrt{\frac{L^3}{NR}} = \frac{1}{\sqrt{cR}}, \tag{5.7}$$

where $c = L^3/N$ is the concentration of the target molecules.

This quantity plays a key role in our system: It gives the typical length scale on which the product-mediated interaction between the enzymes occurs. For this reason, it must be compared with the average distance L_{diff} that one free diffusing product molecule can cover within its life-time after having been released until it decays. If γ is the decay rate of product molecules (so that $t_{\text{life}} = \gamma^{-1}$ is the average life-time), we have:

$$L_{\text{diff}} = \sqrt{\frac{D}{\gamma}}. \tag{5.8}$$

The feedback mechanism due to product activation of the enzymes will be able to introduce a communication mechanism among the different enzymes only if:

$$L_{\text{corr}} < L_{\text{diff}}. \tag{5.9}$$

The meaning of condition (5.9) is that a regulatory molecule released from one enzyme must, in average, be able to meet at least one target enzyme before decaying, for the interaction among the enzymes to be effective. Note that this is equivalent to the inequality for the time scales:

$$t_{\text{transit}} < t_{\text{life}}. \tag{5.10}$$

Condition (5.9) is translated into a condition on the concentration of enzymes by substituting Eqs. (5.7) and (5.8):

$$\frac{1}{\sqrt{Rc}} < \sqrt{\frac{D}{\gamma}}. \tag{5.11}$$

Thus, if the enzyme concentration is larger than the critical value:

$$c^* = \frac{\gamma}{RD} \tag{5.12}$$

product-mediated interactions between the enzymes are possible.

Now let us estimate typical orders of magnitude of the mentioned quantities. The diffusion constant of molecules in water is about $D = 10^{-5}\text{cm}^2\text{s}^{-1}$. Choosing the decay rate of

product molecules as $\gamma = 10^3 s^{-1}$, corresponding to an average life-time of approximately 1 ms, we find for the diffusion length the value:

$$L_{\text{diff}} = 1\mu\text{m}. \tag{5.13}$$

From this, we can estimate the typical mixing time, taking into account that it increases quadratically with the linear dimension of the system (Eq. (5.4)). It takes, for example, the value $t_{\text{mix}} = 10^{-5}$ s for a system of length about 0.1 μm, and increases up to 0.1 s if the length is 10μm, where the two extremes both lie within the range of possible dimensions of a living cell.

Regulatory sites of enzymes are formed by a group of atoms, and their characteristic linear size is about $R = 10^{-7}$ cm. We assume that the product molecule is small as compared to the regulatory site of the enzyme. Thus, the critical enzyme concentration turns out to be:

$$c^* = 10^{15}\text{cm}^{-3} \simeq 1\mu\text{M}. \tag{5.14}$$

This concentration[1] corresponds to an average distance l^* between the enzymes in the reaction volume given by:

$$l^* = \left(\frac{1}{c^*}\right)^{\frac{1}{3}} = 0.1\mu\text{m}. \tag{5.15}$$

In our ideal experiment the enzymes are assumed to be immobilized on a two-dimensional glass surface, while regulatory molecules and substrates are diffusing in the volume. The estimates for this situation can be obtained as follows. Let us consider diffusion of product molecules in the three-dimensional reaction volume. After being released from one enzyme at the glass surface, the product molecule performs diffusive motion in the liquid, and the average distance it can cover before undergoing decay is equal to the diffusion length. Thus, the effective linear dimension in the direction perpendicular to the glass surface is L_{diff}, since product molecules which have traveled farther away would not be able to bind to an enzyme before they decay.

Suppose that c_2 is the two-dimensional concentration of enzymes immobilized on the surface. Then, we can introduce an effective three-dimensional concentration c of enzymes in this system as:

$$c = \frac{N}{L^2 L_{\text{diff}}} = \frac{c_2}{L_{\text{diff}}}. \tag{5.16}$$

[1]This high concentration is in agreement with known physiological concentrations of enzymes in living cells. In Ref. [17] the concentrations of many glycolytic enzymes were found to be higher than 10^{-5} M.

where L the is side-length of the square glass. Note that L_{diff} plays the role of the effective depth of the reaction volume. Thus, the critical two-dimensional concentration of c_2^* of immobilized enzymes is:

$$c_2^* = c^* L_{\text{diff}} \tag{5.17}$$

and the critical distance l^* between two neighboring enzymes is:

$$l_2^* = \left(\frac{1}{c_2^*}\right)^{\frac{1}{2}}. \tag{5.18}$$

Now, we have a system of enzymes, communicating with each other via diffusing product molecules with a regulatory function. As we have already mentioned, the enzymes of our concern carry out their catalytic activity by following a sequence of conformational changes, and they can therefore be considered as molecular machines. The question is, under which conditions the communication among these machines can give rise to pattern formation, such as the propagation of waves of product concentration.

This phenomenon can arise from synchronization among catalytic cycles of the enzymes, i.e. through synchronization of their phases. Such synchronization is possible if interactions among the molecular oscillations are efficient. The life-time t_{life} of a regulatory product molecule must be large enough, so that it can find a target before it decays (cf. condition (5.10)). On the other hand, t_{life} cannot also be very long. Indeed, if it is much longer than the time τ of an individual molecular turnover cycle, product molecules would be accumulated over many subsequent cycles. In this way, they would not be able to carry any information about the moment when they were released, and this would prevent self-organization.

Thus, the necessary conditions for the emergence of spatio-temporal patterns due to product-mediated enzyme correlations are:

$$t_{\text{transit}} < t_{\text{life}} < \tau \tag{5.19}$$

where τ stands for the average turnover time, i.e. the time taken for the enzyme to perform one catalytic cycle.

5.2 Mean-field equations

The system we have described can be modeled by partial differential equations (PDE's), by using concentrations of chemical species as the dynamical variables. A model in terms

of PDE's corresponds to the mean-field approximation, which is valid only if the system satisfies certain conditions.

The principal assumption of the mean-field approximation is that statistical fluctuations are small and that the system can be completely described by its local averages. For the considered system, this means that the number of regulatory product molecules within the correlation radius is large. This condition implies $L_{\text{diff}} \gg L_{\text{corr}}$, or, equivalently, $\tau_{\text{life}} \gg \tau_{\text{transit}}$. Additionally, we will assume that the turnover cycles of all enzymes have fixed duration τ and that each enzyme releases a product at a fixed time τ_1 after the cycle was initiated. Assuming those times to be fixed, we are neglecting intramolecular fluctuations.

Once an enzyme has bound a substrate, it immediately begins the conformational cycle where the enzyme-substrate complex undergoes a sequence of required transformations. In this way, the substrate is converted into a product, and, after a time τ_1 from the cycle initiation, the product detaches from the active site and is released into the solution. Enzymes which have not bound a substrate and are therefore not "inside" their cycle are in the *ground state*.

Since fluctuations are neglected in this description, the system is completely determined by local values of the three quantities n_0, n_1 and m. Here, n_0 is the concentration of enzymes in the ground state without a regulatory molecule attached, n_1 is the concentration of enzymes in the ground state with a regulatory molecule attached, and m is the concentration of free product molecules. In the notations used in Eq. (5.1), n_1 is the concentration of EP, n_0 is the concentration of E, m_0 is the concentration of P.

As we have already mentioned, the substrate concentration does not appear as a dynamical variable, since we assume that substrate molecules are constantly supplied to the system and are present in abundance. Their concentration is thus constant and be considered as being implicitly present in the parameters α_0 and α_1.

The mean-field equations for our system read:

$$\frac{\partial n_1}{\partial t}(x,t) = \beta m(x,t) n_0(x,t) - \kappa n_1(x,t) - \alpha_1 n_1(x,t) \tag{5.20a}$$

$$\begin{aligned}\frac{\partial n_0}{\partial t}(x,t) = &- \beta m(x,t) n_0(x,t) + \kappa n_1(x,t) - \alpha_0 n_0(x,t) \\ &+ \alpha_0 n_0(x,t-\tau) + \alpha_1 n_1(x,t-\tau)\end{aligned} \tag{5.20b}$$

$$\begin{aligned}\frac{\partial m}{\partial t}(x,t) = &- \beta m(x,t) n_0(x,t) + \kappa n_1(x,t) + \alpha_1 n_1(x,t) - \gamma m(x,t) \\ &+ \alpha_1 n_1(x,t-\tau_1) + \alpha_0 n_0(x,t-\tau_1) + D\nabla^2 m(x,t)\end{aligned} \tag{5.20c}$$

Let us go through the equations and describe the different terms.

Binding of a product to a regulatory site: This event has probability rate β. The number of such events is proportional to the concentration m of P and to the concentration n_0 of E. Each event increases the concentration of EP complexes while it decreases the concentration of free P and of E;

Dissociation of a product from a regulatory site: It has probability per unit time κ. The number of such events is proportional to the concentration n_1 of EP complexes. The concentrations of both free P and E are raised as a consequence, while the concentration of EP is lowered;

Binding of a substrate to an active site: This event occurs with different probability depending on whether an enzyme has a regulatory product bound to it or not. In the first case, the probability per unit time is α_1, in the second case is α_0 ($\alpha_1 \gg \alpha_0$). Whenever binding takes place, the enzyme-substrate complex starts its conformational cycle. Therefore, the number of enzymes in the ground state is decreased. When an EP complex binds a substrate, its regulatory product is instantaneously released as the cycle is started. Therefore, the number of free product molecules increases;

Release of a product after the reaction has occurred: During the catalytic cycle, product release takes place. This happens after a time τ_1 from cycle beginning. Thus, the concentration of free product molecules is increased proportionally to the concentration of enzyme molecules which have bound a substrate a time τ_1 before. This gives rise to the delayed terms with the delay equal to τ_1;

Product decay: It takes place through the usual first order kinetics, with the probability rate γ;

Return of an enzyme to the ground state: All enzymes (both in the form E and EP) which have entered the cycle at time τ before, return to the ground state without regulatory product attached (as we mentioned above, it gets detached as the cycle begins). The delay terms with the delay τ, equal to the total cycle duration, are thus present in the equation for the concentration n_0;

Diffusion of product molecules: While enzymes are immobilized, small product molecules can perform diffusive motion through the liquid. This is represented by a Laplacian term with diffusion constant D.

The main feature of this system of PDE's is the presence of terms with delay. They arise from the non-Markovian reaction mechanism due to the finite duration of the conformational cycle. Such memory effects are not included in the standard kinetic description of chemical reactions, where catalysis events are seen as being instantaneous.

5.3 Bifurcation analysis

5.3.1 Fixed points

First of all, we want to find the uniform steady state of system (5.20). This is given by the conditions:

$$\frac{\partial n_1}{\partial t}(x,t) = 0 \tag{5.21a}$$

$$\frac{\partial n_0}{\partial t}(x,t) = 0 \tag{5.21b}$$

$$\frac{\partial m}{\partial t}(x,t) = 0. \tag{5.21c}$$

Note that constant values of the the dynamic variables of the mean-field model correspond to stationary average values in a real system with intrinsic statistical fluctuations. That is, fixed points of the mean field equations occur in the classical desynchronized state where correlations between the cycles of individual enzymes are absent.

In order to calculate the steady state solutions, we shall start from the conserved quantity representing the total concentration of enzymes n_t. This is the sum of the enzymes in the ground state both with and without regulatory product attached (respectively, n_1 and n_0) and of the enzymes which are at present performing the conformational cycle. At a given time t, the latter quantity is given by the time integral of the enzymes which have started the cycle in the previous τ interval, i.e.:

$$n_t = n_0(t) + n_1(t) + \int_{t-\tau}^{t} \alpha_0 n_0(t')\mathrm{d}t' + \int_{t-\tau}^{t} \alpha_1 n_1(t')\mathrm{d}t'. \tag{5.22}$$

By calling $\bar{n}_0$ and $\bar{n}_1$ the stationary concentrations, we get

$$n_t = \bar{n}_0 + \bar{n}_1 + \alpha_0\tau\bar{n}_0 + \alpha_1\tau\bar{n}_1. \tag{5.23}$$

By combining this equation with Eq. (5.21b), we obtain:

$$\bar{n}_1 = \frac{n_t\beta\bar{m}}{(1+\alpha_0\tau)(\kappa+\alpha_1) + \beta\bar{m}(1+\alpha_1\tau)} \tag{5.24}$$

$$\bar{n}_0 = \frac{n_t}{1+\alpha_0\tau}\left[1 - \frac{\beta\bar{m}(1+\alpha_1\tau)}{(1+\alpha_0\tau)(\kappa+\alpha_1) + \beta\bar{m}(1+\alpha_1\tau)}\right]. \tag{5.25}$$

To determine $\bar{m}$, we make use of Eqs. (5.21c), (5.24), and (5.25), and we get a second-order equation:

$$\bar{m}^2 + \frac{\bar{m}}{1+\alpha_1\tau}\left[\frac{(1+\alpha_0\tau)(\kappa+\alpha_1)}{\beta} - \frac{n_t\alpha_1}{\gamma}\right] - \frac{n_t\alpha_0(\kappa+\alpha_1)}{\gamma\beta(1+\alpha_1\tau)} = 0, \tag{5.26}$$

which has two solutions, one positive and one negative. Since $\bar{m}$ is a concentration, only the positive solution is physically meaningful.

5.3.2 Uniform oscillations in a small volume

Now we want to investigate the stability of the calculated stationary solution. This can be done through the linear stability analysis of the system, by considering small perturbations to the stationary concentrations. In the present section, we derive the results for the completely mixed case, holding when the reaction takes place in a small volume and uniform concentrations can be assumed.

We shall consider the temporal evolution of homogeneous perturbations to the stationary state $m(t) = \bar{m} + \delta m(t)$, $n_0(x,t) = \bar{n}_0 + \delta n_0(t)$, $n_1(t) = \bar{n}_1 + \delta n_1(t)$. We can seek the solution of these linear differential equations with delays in the form:

$$\delta n_1(t) = Ae^{\lambda t} \tag{5.27a}$$

$$\delta n_0(t) = Be^{\lambda t} \tag{5.27b}$$

$$\delta m(t) = Ce^{\lambda t}, \tag{5.27c}$$

where λ can take complex values.

By substituting these expressions into Eqs. (5.20) and keeping only the first-order terms, we derive the linear system:

$$\begin{pmatrix} \dot{\delta n_1} \\ \dot{\delta n_0} \\ \dot{\delta m} \end{pmatrix} = \hat{L}(\lambda) \begin{pmatrix} \delta n_1 \\ \delta n_0 \\ \delta m \end{pmatrix}, \tag{5.28}$$

where:

$$\hat{L}(\lambda) = \begin{pmatrix} -\kappa-\alpha_1 & \beta\bar{m} & \beta\bar{n}_0 \\ \kappa+\alpha_1 e^{-\lambda\tau} & -\beta\bar{m}-\alpha_0(1-e^{-\lambda\tau}) & -\beta\bar{n}_0 \\ \kappa+\alpha_1 e^{-\lambda\tau_1} & -\beta\bar{m}+\alpha_0 e^{-\lambda\tau_1} & -\gamma-\beta\bar{n}_0 \end{pmatrix}, \tag{5.29}$$

Thus we obtain the following equations for the coefficients A, B, and C:

$$\lambda \begin{pmatrix} A \\ B \\ C \end{pmatrix} = \hat{L}(\lambda) \begin{pmatrix} A \\ B \\ C \end{pmatrix} \tag{5.30}$$

that have a nontrivial solution provided that:

$$|\hat{L}(\lambda) - \lambda \hat{I}| \equiv P(\lambda) = 0. \tag{5.31}$$

Since the coefficients of the matrix $\hat{L}(\lambda)$ contain exponential dependence on λ due to the delay terms, Eq. (5.31) is a quasi-polynomial equation. It contains a very large number of terms, and it is therefore not convenient to write it in an explicit form. All the linear stability analysis calculations were done with the help of the software Mathematica.

The solutions of such an equation constitute a set of infinite size. That is, a parametric family of eigenvalues

$$\lambda_n = \mu_n + \mathrm{i}\omega_n \qquad \text{with } n = 1, 2, 3, \ldots \tag{5.32}$$

exists, which satisfy (5.31).

Real parts μ_n of λ_n represent the exponential growth-rates of the considered perturbations, as follows from Eq. (5.27). That is, the stationary state becomes unstable, only if at least one μ_n is non negative. In that case, any small perturbation to the steady-state concentrations gives rise to oscillations with a characteristic frequency ω_n. The possible frequencies labeled by n constitute a discrete spectrum, i.e. a set of values, each of them lying close to one of the harmonics of the turnover frequency:

$$\omega_n \simeq \frac{2\pi n}{\tau}. \tag{5.33}$$

Thus, oscillations with frequency ω_n grow starting with a perturbed uniform state, when μ_n is larger than zero.

Let us first consider the case with $n = 1$. When μ_1 is positive, uniform oscillations of the product concentration with frequency approximately equal to $2\pi/\tau$ can emerge. In such oscillations, the maxima are due to synchronized product release from the enzymes, then product decay causes a drop in the concentration, until a new maximum occurs and so on. In this case, the oscillations are found to have a period which is slightly larger than the cycle duration τ. This means that the maxima occur once for each catalytic cycle, and that a certain waiting time is spent by the enzymes in the ground state until a new substrate binds.

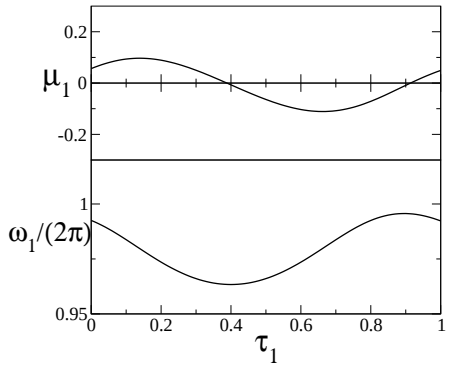

(a) Growth-rate of the one-group mode

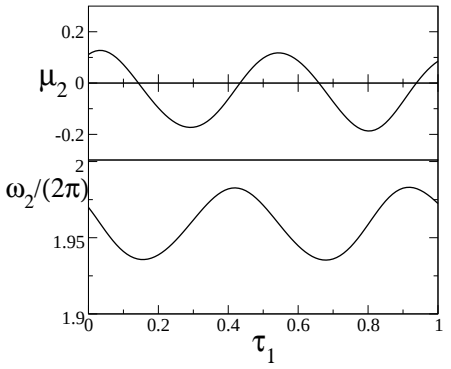

(b) Growth-rate of the two-groups mode

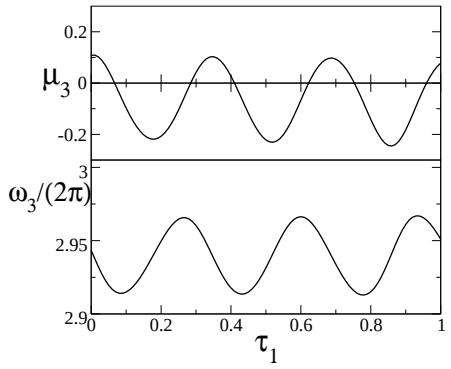

(c) Growth-rate of the three-groups mode

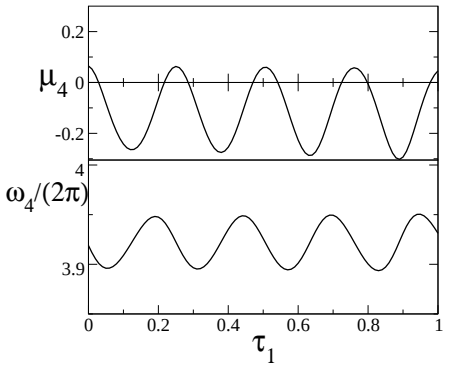

(d) Growth-rate of the four-groups mode

Figure 5.3: Plots of the coefficients $\mu_{1,2,3,4}$ and of the corresponding frequencies $\omega_{1,2,3,4}$ as functions of the parameter τ_1, at $\beta = 5$. Other parameters are $n_t = 100, \alpha_0 = 1, \alpha_1 = 1000, \kappa = 10, \gamma = 10$. See App. B for the explanation of the parameters. The stationary state is unstable and oscillations of one, two, three, or four groups can develop when, respectively, μ_1, μ_2, μ_3, or μ_4 are larger than zero.

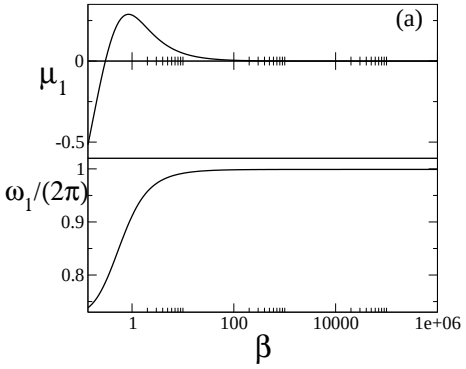

(a) Growth-rate of the one-group mode

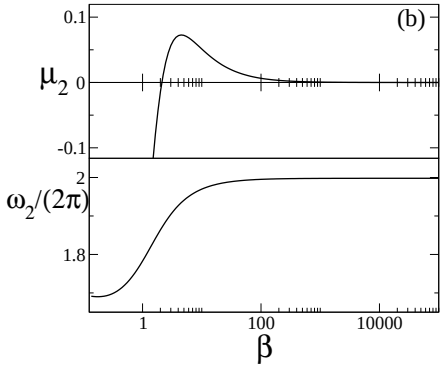

(b) Growth-rate of the two-groups mode

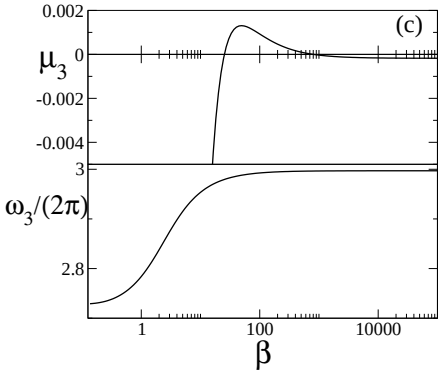

(c) Growth-rate of the three-groups mode

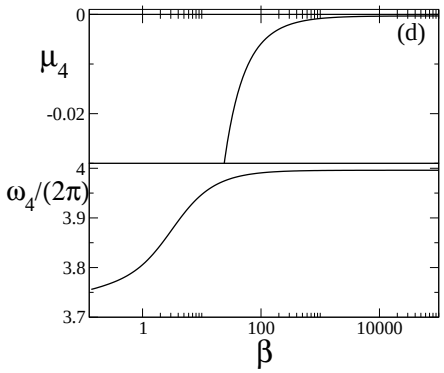

(d) Growth-rate of the four-groups mode

Figure 5.4: Plot of the coefficients $\mu_{1,2,3,4}$ and of the corresponding frequencies $\omega_{1,2,3,4}$ as functions of the parameter β, at $\tau_1 = 0.1$. Other parameters as in Fig. 5.3. For large values of β, also μ_1 and μ_2 become negative, but the scale of the plots does not allow good visualization in this region.

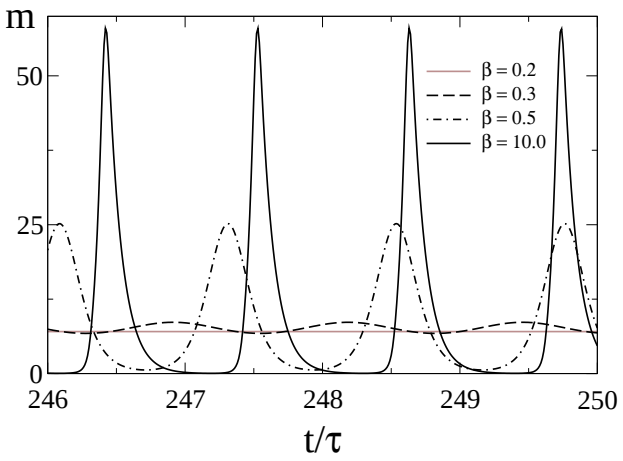

Figure 5.5: Temporal evolution of the product concentration under complete mixing. with $\tau_1 = 0.1$, at different values of β. Other parameters as in Fig. 5.3. At $\beta = 0.2$ the steady state is stable (no oscillations). With increasing β oscillations appear. For smaller values of β they are harmonic and have small amplitude, but for larger values of the parameter they become sharper. Moreover, the frequency increases with increasing β and approaches the value $\frac{2\pi}{\tau}$ corresponding to the appearance of exactly one maximum per turnover cycle.

However, more complicated situations may arise. Oscillations with larger frequency (modes with $n > 1$ in Eq. (5.33)) can develop. If $n = 2$, the enzymes are split into two groups. Inside each group they are synchronized and therefore release the products simultaneously. The two groups are phase-shifted with respect to each other, which means that the temporal distance between two maxima approximately equals $\tau/2$. Similarly, the emergence of oscillations with even larger frequencies can be explained with the formation of larger numbers of groups.

In Fig. 5.3 we show μ_n for n = 1, 2, 3, and 4, and the corresponding frequencies ω_n as functions of the parameter τ_1, all other rates being fixed. Oscillations are possible only within specific ranges of τ_1, periodically occurring with different periodicity depending on the number of groups.

In Fig. 5.4 the dependence of μ_n and ω_n on β at fixed τ_1 is plotted. We see that μ_1, μ_2, and μ_3 are positive in an interval of the parameter β, specifying the intensity of allosteric regulation. μ_4 remains always negative, so that for the considered parameters, four-group oscillations are not possible.

Let us consider Fig. 5.4(a). For very low attachment rate of the products to the regulatory

site, synchronization is not possible due to low efficiency of the interaction through allosteric activation. At larger β, synchronization takes place. Integrating the nonlinear evolution Eqs. (5.20), we find that, close to the bifurcation point, the oscillations are harmonic and have a small amplitude, which is typical for a supercritical Hopf bifurcation. With increasing β, the maxima become sharper (see Fig. 5.5). This behavior can be explained.

Increasing β enhances synchronization and also reduces the waiting time for a product molecule to bind to the regulatory site of an enzyme. Thus, as β becomes very large, the enzymes operate completely simultaneously and the released products are immediately captured after release: This gives rise to very steep spikes. Moreover, the waiting time in the ground state tends to sink, due to very efficient allosteric activation, thus the oscillation period becomes exactly equal to the cycle duration. For very large β, the products are so quickly catched, that oscillations can no longer be observed. This explains the upper boundary in the interval of β where oscillations exist.

Next we want to construct two-dimensional bifurcation diagrams, to identify regions in the parameter space where synchronization oscillations are observed. To find the bifurcation boundaries, we solve numerically Eq. (5.31) with the condition $\mu_n = 0$.

We consider the plane (τ_1, β), with all the other parameters fixed (Fig. 5.6). The intervals with positive μ_n in Fig. 5.3 and 5.4 become closed regions in the two-dimensional space, shown in the upper plot of Fig. 5.6. One-group oscillations thus exist within the domain bordered by the continuous line, two-group oscillations exist within the domains with dashed edges, and three-groups oscillations within the domains with dotted edges. Oscillations with more than three groups are also possible, but the domains are not shown here in order to keep the diagram clear.

In the lower plot of Fig. 5.6 the frequencies of the oscillations at the boundaries are shown. The lower frequency always corresponds to the smaller value of β, since, as we have already mentioned, for weak β the waiting time is longer and the oscillations are slower.

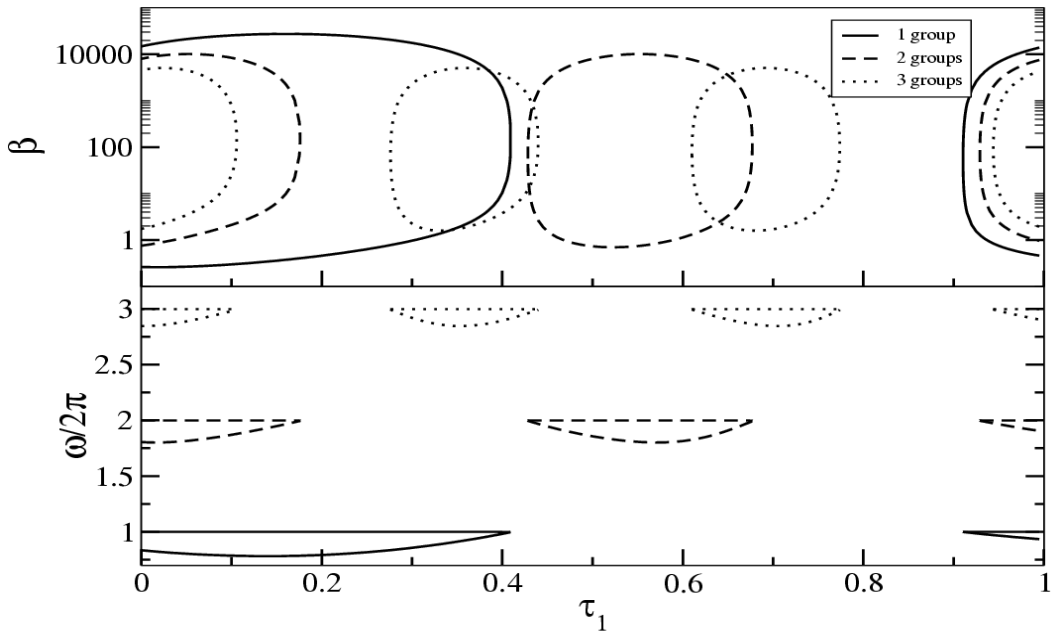

Figure 5.6: Bifurcation diagram. Parameters as in Fig. 5.3. In the upper plot, the lines form the boundaries of the parameter region where oscillations with 1, 2, or 3 groups may set according to the linear stability analysis. In the lower plot, the frequencies of the oscillations at the boundaries are shown; the lower frequency always refers to the lower β value.

5.3.3 Wave bifurcation

In the case of an extended system without complete mixing, spatial inhomogeneities must be considered. Evolution of non-uniform perturbations is affected by the diffusion term in the equations, which was neglected in the previous bifurcation analysis.

To account for the possibility that the stationary state becomes unstable through spatially nonuniform perturbations, we must consider perturbations of the type $m(x,t) = \bar{m} + \delta m(x,t)$, $n_0(x,t) = \bar{n}_0 + \delta n_0(x,t)$, $n_1(x,t) = \bar{n}_1 + \delta n_1(x,t)$. After linearization, we look for the solutions in the form of plane waves:

$$\delta n_1(x,t) = Ae^{\lambda t + \mathrm{i}qx} \tag{5.34a}$$

$$\delta n_0(x,t) = Be^{\lambda t + \mathrm{i}qx} \tag{5.34b}$$

$$\delta m(x,t) = Ce^{\lambda t + \mathrm{i}qx}. \tag{5.34c}$$

We can proceed as in the previous case and find that the matrix of the linear system is:

$$\hat{L}(\lambda,q) = \begin{pmatrix} -\kappa - \alpha_1 & \beta\bar{m} & \beta\bar{n}_0 \\ \kappa + \alpha_1 e^{-\lambda\tau} & -\beta\bar{m} - \alpha_0(1 - e^{-\lambda\tau}) & -\beta\bar{n}_0 \\ \kappa + \alpha_1 e^{-\lambda\tau_1} & -\beta\bar{m} + \alpha_0 e^{-\lambda\tau_1} & -\gamma - \beta\bar{n}_0 - Dq^2 \end{pmatrix}, \tag{5.35}$$

where the explicit dependence on the wavenumber q becomes clear. The extended-system version of Eq. (5.31) is:

$$|\hat{L}(\lambda,q) - \lambda\hat{I}| \equiv P(\lambda,q) = 0. \tag{5.36}$$

In Eq. (5.36), spatial effects are included through the term $-Dq^2$, where the wavenumber q should be considered as an additional variable. Thus, if we want to find the roots of Eq. (5.36) with the condition $\mu_n = 0$ to locate the bifurcation point, we must take into account that the minimal β, at which the stationary solution looses its stability, depends on the wavenumber of the considered perturbation. It might happen that, while uniform perturbations are still decaying, concentration waves with a finite wavenumber can already grow into the system. In this case, a *wave bifurcation* is present.

The appearance of a wave bifurcation can be made clear by the dispersion curves showing the dependence of the coefficient μ_n on the wavenumber q of the perturbation. In Fig. 5.7, two examples are shown. In each subfigure the dependence $\mu_1(q)$ for two different values of the parameter β is plotted. In 5.7(a), the first bifurcating mode has $q = 0$, which means that uniform oscillations appear at the bifurcation point. This is the usual Hopf bifurcation. If β

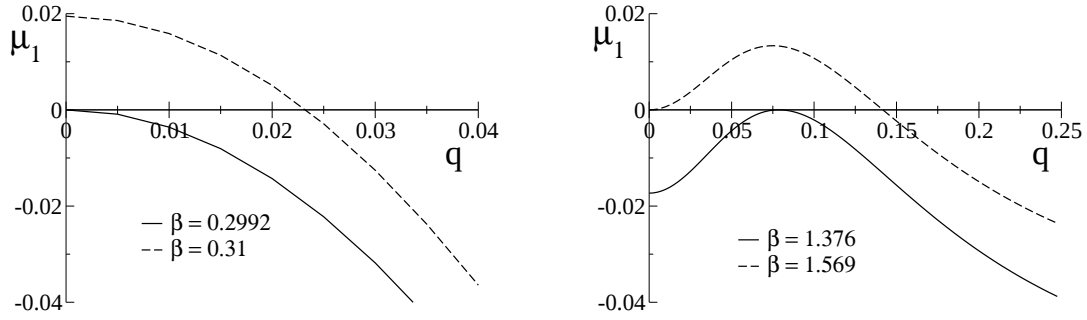

(a) Hopf bifurcation

(b) Wave bifurcation

Figure 5.7: Dispersion curves showing the dependence of μ_1 on the wavenumber q for (a) $\tau_1 = 0.1$ and (b) $\tau_1 = 0.34$ at different values of β. Other parameters are $n_t = 100, \alpha_0 = 1, \alpha_1 = 1000, \kappa = 10, \gamma = 10, D = 1000$. See App. B for the explanation of the parameters.

is further raised, the range of the wavenumbers for which the eigenvalue has positive real part widens, and patterns with different wavelengths become possible. In Fig. 5.7(b), the real part μ_1 of the eigenvalue λ_1 first crosses the zero-axis at a non-vanishing wavenumber. This means that, very close to this bifurcation point, patterns with a well defined wavelength are expected to occur. All other oscillating modes, including uniform oscillations ($q = 0$), are decaying. When the control parameter β is further increased, the interval of wavenumbers with growing amplitudes broadens and a point eventually comes, at which uniform oscillations begin to grow too. This point corresponds to the Hopf bifurcation of the completely mixed system with the same parameters.

From these considerations, it is clear that a wave bifurcation occurs when two conditions are simultaneously satisfied:

$$\begin{cases} \mu_n(q^*) = 0 \\ \left.\dfrac{\partial \mu_n(q)}{\partial q}\right|_{q* \neq 0} = 0. \end{cases} \tag{5.37}$$

Eqs. (5.37) also determine the wavenumber q^* of the unstable mode.

As another example of how the presence of diffusion can modify the stability properties of the system, we show in Fig. 5.8 the dependence of the coefficient μ_1 on the decay rate γ. We see that μ_1 is negative for very small γ, that is, oscillations cannot arise when decay of product molecules is very slow. The minimal γ, required for oscillations to set on, can be strongly affected by the presence of product diffusion, as the difference between Fig. 5.8(a) and Fig. 5.8(b) indicates. However, it must be stressed that in this example, the wavenumber

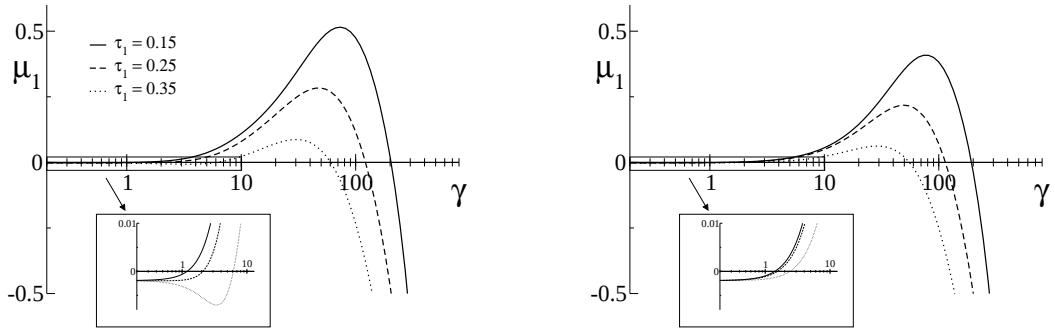

(a) Homogeneous system ($q = 0$) (b) Non-homogeneous system ($q = 0.1$)

Figure 5.8: μ_1 vs. γ with and without diffusion, with $\beta = 5.0$, at different values of τ_1. Other parameters as in Fig. 5.7. In both cases, μ_1 is positive only within a bounded interval. But in the second case, the edges of the interval are modified: oscillations with the given wavenumber can emerge at a smaller γ than in the previous case and also disappear earlier.

q is fixed, that is, we only get informations about the possibility of observing patterns with a specific wavelength. Thus, even if μ_1 is negative for this given value, it might be positive for other choices of q.

If we want to investigate the possibility of self-organization in the spatially extended system, the wavenumber q should be treated as an independent variable. Let us consider the bifurcation diagram in the plane (τ_1, β), which was already shown for the homogeneous system in Fig. 5.6. Now, if we want to find the value of β for any given τ_1 at which μ_1 crosses the zero axis, we must take into account that μ_1 is in general a function of the wavenumber q. When $\mu_1(q)$ has a shape like in Fig. 5.7(b), we have to decrease β until the curve becomes tangent to the zero axis. This is the wave-bifurcation point, and the corresponding wavenumber indicates the characteristic length of the patterns which can be observed immediately above the bifurcation.

The results are shown in Fig. 5.9 only for the lower boundary in the case of one group oscillations. The wave bifurcation line merges in a codimension-two bifurcation point with the Hopf bifurcation. In the domain included between the dashed line (Hopf bifurcation) and the continuous line (wave bifurcation), propagation of waves with finite wave number is possible, while uniform oscillations cannot set on. This means that, in a system with complete mixing with these parameters, synchronization of the molecular cycles cannot occur. However, in an extended system allowing for non-homogeneous concentrations, self-organized patterns with finite wavelength can emerge.

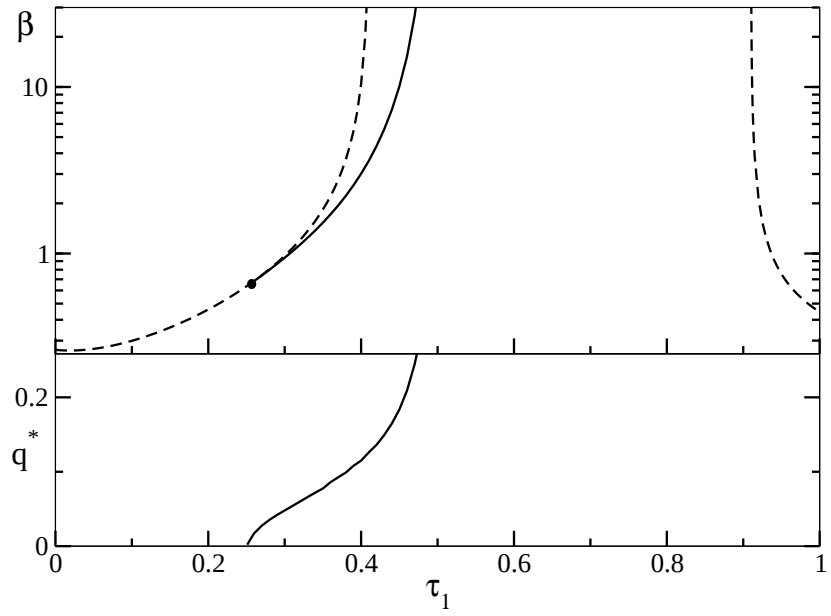

Figure 5.9: Bifurcation diagram for the system with product diffusion. Parameters as in Fig. 5.7. The Hopf bifurcation (homogeneous system) is shown as a dashed line, while the wave bifurcation is represented with a straight line. The black dot is the codimension-2 Hopf-wave bifurcation point. In the lower plot, the critical wavenumber at the bifurcation is shown. Only the bifurcation lines for the emergence of one-group oscillations are displayed.

The wave bifurcation is also found for two or more oscillating groups, that is, system (5.37) has solutions also for $n > 1$. However, these additional wave-bifurcation lines are not shown in the diagram of Fig. 5.9.

5.4 Numerical simulations

Numerical simulations were performed for both the one- and two-dimensional system. We used an explicit Euler algorithm and a first-order finite difference discretization for the Laplacian term.

As we have previously mentioned (cf. Sec. 5.1.2), the mesh size for the space discretization is $\Delta x = 0.1\mu$m. The time step for one single integration iteration is between τ/4000 and τ/1500.

In the one-dimensional simulations we have used the same parameters as for the two-dimensional case, thus assuming that the former must be seen as a special case of the latter, that is, the one-dimensional patterns are nothing but two-dimensional patterns where a completely uniform concentration profile can be assumed in one direction. This is an artifact, but one-dimensional simulations are a very useful means to investigate the self-organization properties of the system.

Due to the very rich and complex behavior of the system, we have investigated only a confined region of the parameter space.

5.4.1 One-dimensional patterns

As it can be expected from the bifurcation analysis, the spatially system has a very complex behavior. The presence of oscillatory instabilities with multiple groups together with the existence of a codimension-two Hopf-wave bifurcation, opens up the possibility of a large variety of patterns. In our numerical simulations, we have focused our attention on single-group oscillations with the period close to $2\pi/\tau$.

In the phase diagram of Fig. 5.10 we outline the domains where different kinds of one-dimensional patterns are observed. The boundaries between the different domains are hand-drawn according to the results of a set of numerical simulations on this parameter region. The simulations have been performed for systems of length of 256 or 512 (respectively, 25 and 50 diffusion lengths). Numerical integrations were performed for a total time of 2000

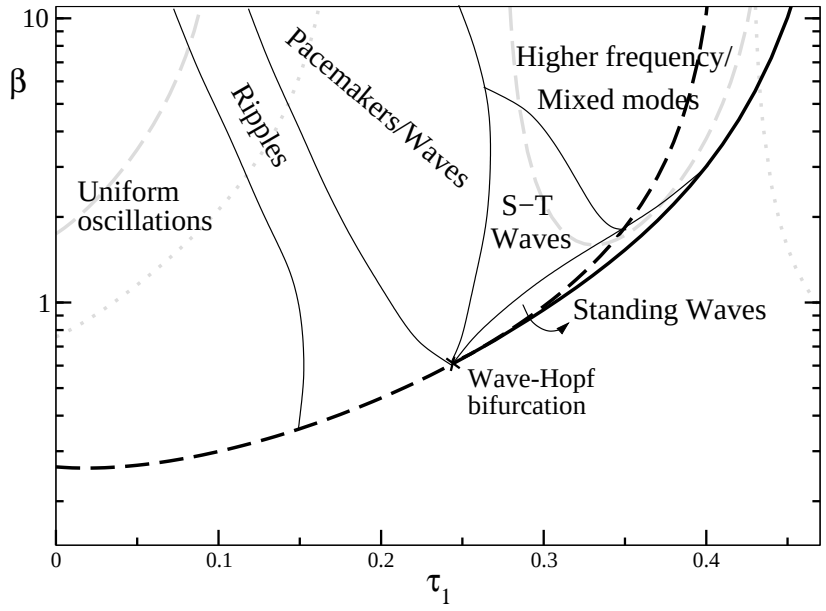

Figure 5.10: Phase diagram. Parameters as in Fig. 5.7. Existence domains of different patterns for a system of length L=256 with no-flux boundary conditions are shown. For reference, the bifurcation lines are plotted: black solid for the wave bifurcation with frequency ω_1, black dashed for the Hopf bifurcation with ω_1, gray dotted for the Hopf bifurcation with ω_2, gray dashed for the Hopf bifurcation with ω_3. The wave bifurcation for the oscillations with frequency ω_2 and ω_3 is not shown.

to 6000 turnover cycles. Here we discuss only the patterns which set into the system after discarding a transient of at least 45-50 τ.

We applied no-flux boundary conditions, although, in some cases, also simulations for the system with periodic boundary conditions were done for comparison. As initial condition, we provided the state of the system for the duration of one entire turnover cycle, due to the presence of delay terms. This was done by setting the concentrations into their stationary values except for the last time step, where a random, spatially uncorrelated perturbation was applied to the product concentration.

Space-time plots of the one-dimensional patterns are shown in Fig. 5.11.

- **Uniform oscillations**, Fig.5.11(a). Immediately above the Hopf bifurcation, small-amplitude harmonic uniform oscillations set. With increasing β, the maxima become more steep, as in the case of oscillations in the small volume.

- **Standing waves**, Fig.5.11(b). Immediately above the wave-bifurcation, standing waves with a well-defined wavelength appear. This wavelength corresponds to the critical wavenumber at the bifurcation point, which is plotted in Fig. 5.9.

- **Ripples**, Fig. 5.11(c). On the right-hand side of the uniform oscillations region, weakly space-periodically modulated oscillations are observed. We call them ripples. Their characteristic distance appears to be an intrinsic property, solely depending on the parameters, and independent, in particular, of the system size.

- **Pacemakers and waves**, Fig 5.11(d). Increasing β above the wave bifurcation, various types of waves are induced in the system. It is well known that such patterns, arising in presence of a finite-wavelength bifurcation, are highly sensitive to boundary conditions, initial conditions, and total system length [197, 198], which makes it rather difficult to trace a well defined boundary separating the existence domains. This would require a major computational effort to test (i) different initial conditions to establish the presence of multistability between different patterns, (ii) different system lengths and boundary conditions to determine which behaviours are mainly due to finite-size effects and interaction with the boundaries. The results of our simulations can be summarized as follows. For a system length of 256 Δx with no-flux boundary conditions, stationary pacemakers (see Fig. 5.11(d)) tend to emerge in the left part of the region denoted as Pacemakers/Waves. On the right part, such pacemakers become usually unstable, and a pattern which we would describe as *intermittent pacemakers*

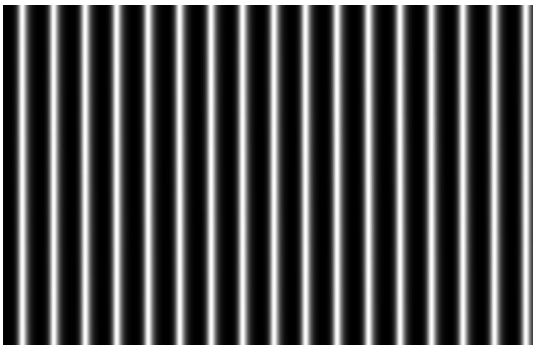

(a) Uniform oscillations $\tau_1 = 0.04, \beta = 0.4$.

(b) Standing waves $\tau_1 = 0.3, \beta = 0.95$.

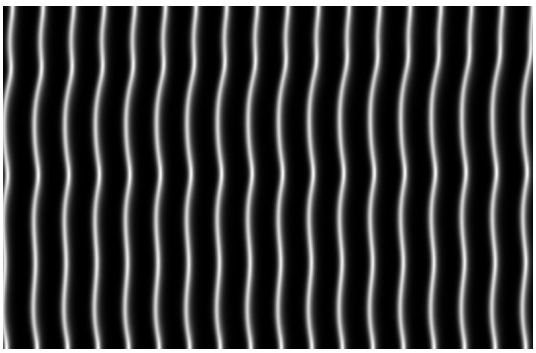

(c) Ripples $\tau_1 = 0.14, \beta = 2.6$.

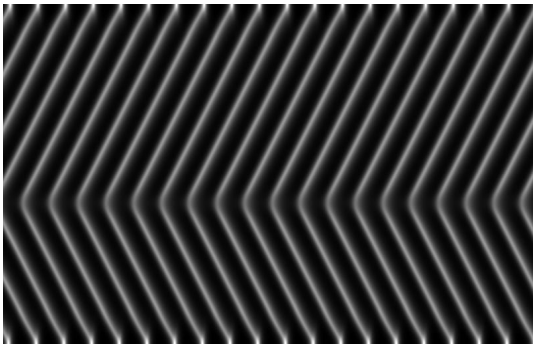

(d) Pacemaker $\tau_1 = 0.22, \beta = 6.0$.

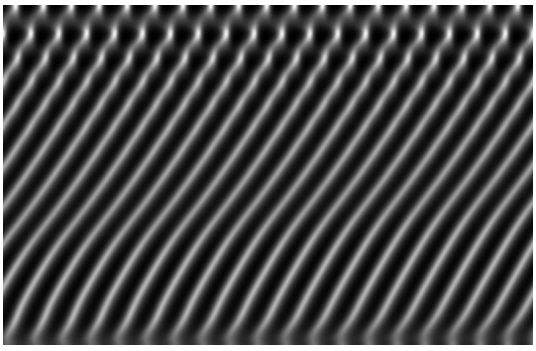

(e) Standing traveling waves $\tau_1 = 0.3, \beta = 3.8$.

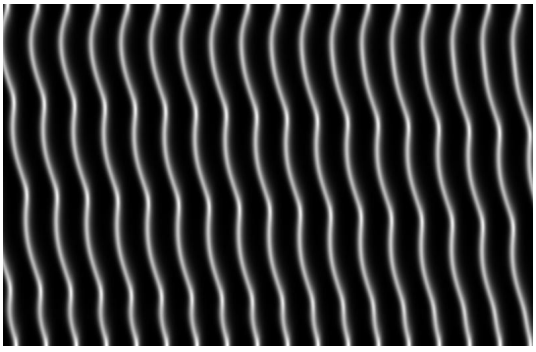

(f) Rippled waves $\tau_1 = 0.16, \beta = 3.0$.

Figure 5.11: Space-time plots of the one-dimensional patterns of products concentration. Other parameters as in Fig. 5.7. Time is the horizontal axis, space the vertical axis. Graycode: brighter (darker) regions correspond to higher (lower) product concentrations. In each plot a time interval equal to 20τ is shown, while system dimension is 512. Each pattern is a typical sample of one of the spatio-temporal behaviors listed in Fig. 5.10.

tends to set. Such pattern is shown in Fig. 5.12: (a) a pacemaker forms rather close to the boundary of the system, (b) it moves towards the boundary and collides with it, (c) it disappears and leaves a free traveling wave, (d) this wave interacts with the boundary, and (e) forms again a pacemaker. The sequence is then repeated. This behavior seems not to be a transient, because it was found to persist for a long time (at least up to 6000 τ). However, if periodic boundary conditions are applied, we never find such intermittent pacemakers. Instead, free traveling waves (without formation of any pacemaker) develop. Similarly, such intermittent pacemakers turn out to be unstable for larger systems ($L = 512$) where travelling waves set on.

- **Standing-traveling waves**, Fig. 5.11(e). This pattern consists of a superposition of a traveling wave and a standing wave, as it might be seen more clearly from the overlay of 50 instantaneous concentration profiles in Fig. 5.13: close to the right boundary the oscillation amplitude shows the modulation which is typical of standing waves. A similar pattern is reported in [197, 198] as a typical case for a system with the wave bifurcation in presence of no-flux boundary conditions.

- **Rippled waves**, Fig. 5.11(f). At the boundary between the existence domains of ripples and pacemakers, we observed rippled propagating waves.

- **Mixed modes**. When oscillations with a larger number of groups are possible, the richness and complexity of structures become even more striking. All of the above described patterns are also seen in the case of higher frequencies (ω_n with $n > 1$), and mixed patterns arising from the superposition of different oscillatory instabilities emerge as well. One typical example is given in Fig. 5.14: the one-dimensional system splits into several domains, each dominated by a different pattern: almost uniform oscillations with frequency ω_5, traveling waves and standing-traveling waves with ω_3, traveling waves with ω_1 superimposed and modulated by higher frequencies.

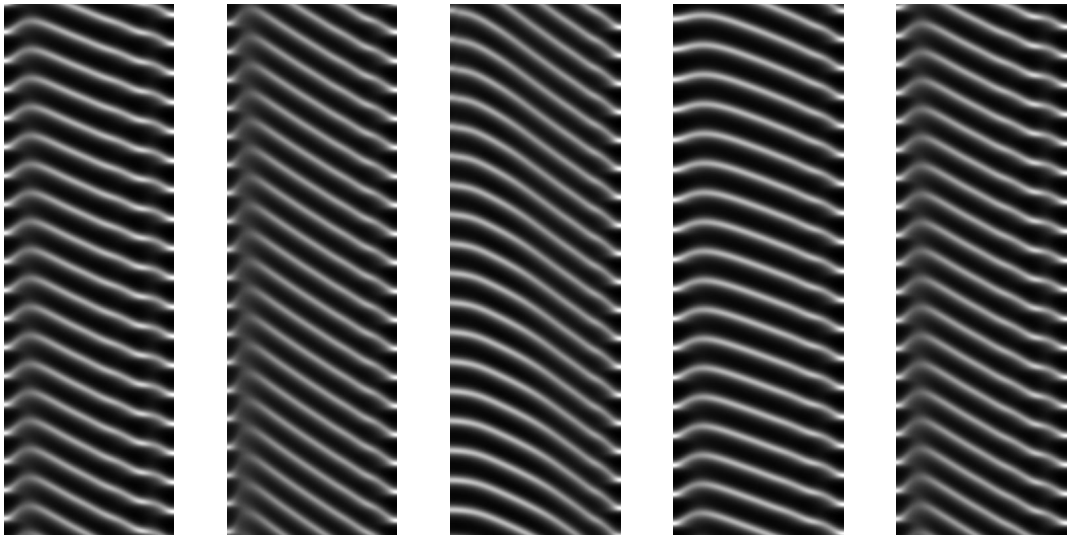

Figure 5.12: The evolution of a typical intermittent pacemaker is shown. $\tau = 0.24$, $\beta = 2.6$, other parameters as in Fig. 5.7. Space is here the horizontal axis, time the vertical axis, running from top to bottom. Graycode as in Fig. 5.11. System size is 256, each plot shows a time interval of 20 τ, and two successive plots are separated by 20 τ.

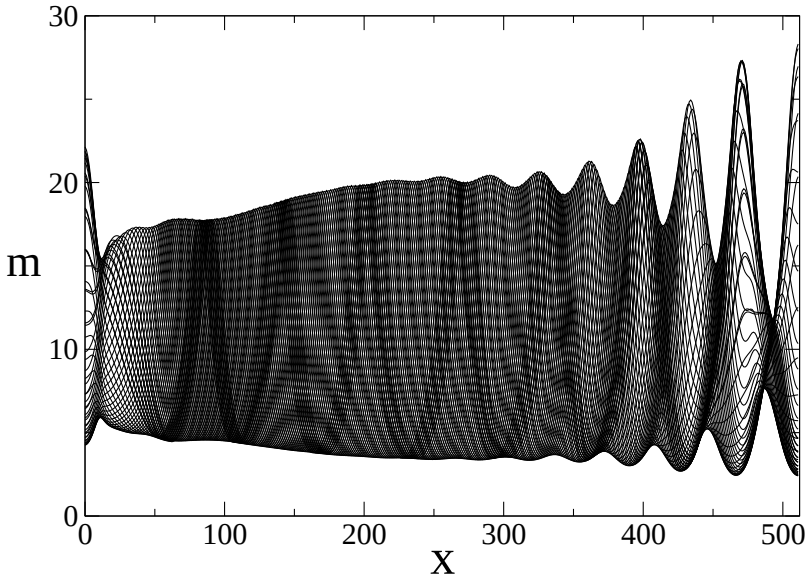

Figure 5.13: Overlay of 50 wave profiles for the stationary-traveling wave shown in Fig. 5.11(e).

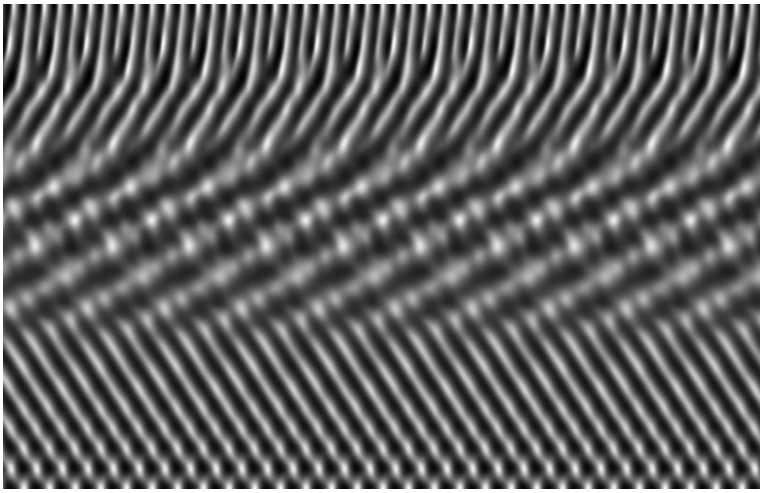

Figure 5.14: Mixed mode $\tau = 0.42, \beta = 8.0$, other parameters as in Fig. 5.7. Space is the vertical axis, time the horizontal axis. Graycode as in Fig. 5.11. System length is 512, time interval 10τ.

5.4.2 Two-dimensional patterns

We have performed simulations for the two-dimensional system with no-flux boundary conditions. Here, the choices of the diffusion length and of the system size were different from the one-dimensional case, because of restrictions due to the larger computational effort required for two-dimensional simulations. In particular, we have chosen $D = 100$ ($L_{\text{diff}} = 3$) and L = 128×128. Having decreased the diffusion constant while keeping the concentration fixed, the diffusion length is only slightly larger than the correlation length. All simulations were started from a random distribution of the product concentration.

For parameters above the Hopf bifurcation line, where the one-dimensional system shows uniform oscillations, a stable pattern of rotating spirals has been found. It is shown in Fig 5.15, in five successive snapshots of the product concentration. With these parameters, there is bistability between uniform oscillations and rotating spirals. The number and the rotation direction of the spirals depend on the initial conditions.

Going to the wave bifurcation region, immediately above the bifurcation line, standing waves are observed, which are shown in Fig. 5.16. For these parameters, the system displays a very long transient from the random state to a stationary pattern. This has been observed also in the one-dimensional case, where standing waves become stationary after approximately 3000 turnover cycles. In the two-dimensional case, we have run the simulation for 1400 τ, and therefore the waves are not yet completely standing, but still some traveling domains persist, which however can be expected to vanish in the long run.

For larger values of β, target patterns appear, which are the two-dimensional counterpart of the one-dimensional pacemakers. However, even starting from different realizations of the random initial conditions, such target patterns are always found to coexist with rotating spirals. The waves sent by the spirals eventually destroy the pacemakers. We have never found stable two-dimensional pacemakers. In Fig 5.17 (a)-(e) we show the transient pattern where pacemakers and spirals are simultaneously present. To highlight the different appearance of the spiral core with respect to the pacemaker core, one-dimensional space-time plots are also shown (Fig. 5.17 (f),(g)), displaying the temporal evolution along a cross section passing through such cores. Moreover, overlays of several waves profiles (Fig. 5.17 (h),(i)) through the same line are shown, from which the local oscillation amplitude can be seen. The spiral core is characterized by a vanishing oscillation amplitude, where the product concentration remains constant. On the contrary, the pacemaker core only shows a slight reduction of the oscillation amplitude within a distance which is of the order of the diffusion length. In both

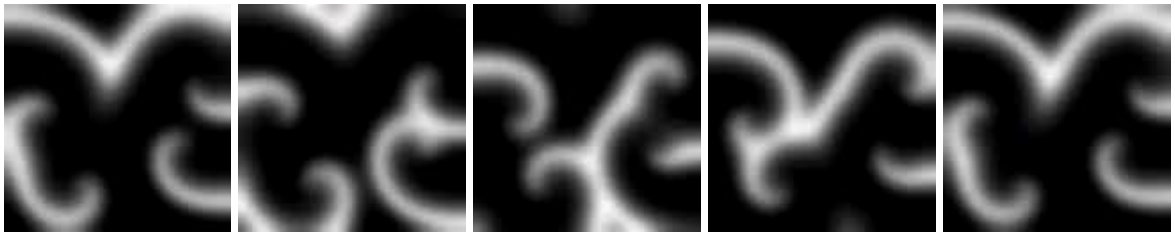

(a) (b) (c) (d) (e)

Figure 5.15: Snapshots of the two-dimensional system for $D = 100$, $\tau_1 = 0.1$, and $\beta = 0.5$. Other parameters as in Fig. 5.7. Graycode as in Fig. 5.11. A stable pattern of four rotating spirals is found. The five snapshots are equally separated in time within a total time interval of $1.17\ \tau$.

cases, an evident increase of the oscillation amplitude is seen where two waves travelling from opposite directions meet, as well as in the collision with the zero-flux boundaries.

In the proximity of the codimension-2 Hopf-wave bifurcation, more irregular patterns can be observed. In Fig. 5.18 two sequences of the evolution of one system in that parameter region are shown. After the initial transient, an irregular spiral is formed (Fig. 5.18 (a)-(e)). The wavelength of the emitted wave is not isotropic, but is shorter in the direction toward the right-bottom corner. Moreover, the core of the spiral is not point-like as in Figs. 5.15 and 5.17, but is an extended domain where the oscillation amplitude does not vanish. This spiral is not stable. Through interaction with the boundaries it is destroyed and gives rise to three coexisting irregular pacemakers (Fig. 5.18 (f)-(j)). This system does not reach any stationary pattern within 1600τ. Irregular pacemakers and spirals are continuously formed and destroyed through interaction with other structures or with the boundaries.

For slightly different parameters, but still very close to the Hopf-wave bifurcation, turbulence is found. The pattern is shown in Fig. 5.19. From the snapshots (Fig. 5.19(a)-(e)) it can be seen that the spatial structure of the product concentration does not show any apparent regularity. However, the pattern is approximately temporally periodical, as the space-time plot in Fig. 5.19(f) across the central horizontal line shows.

The two-dimensional system shows a very rich spatio-temporal behavior. Many different stationary patterns as well as long transients have been observed. Moreover, multistability between different structures arising from different initial conditions usually occurs. This makes it very difficult to classify the patterns within a small number of typologies as we have done for the one-dimensional system. For this reason, we have given only an overview of some of the most characteristic spatio-temporal behaviors encountered in our numerical simulations.

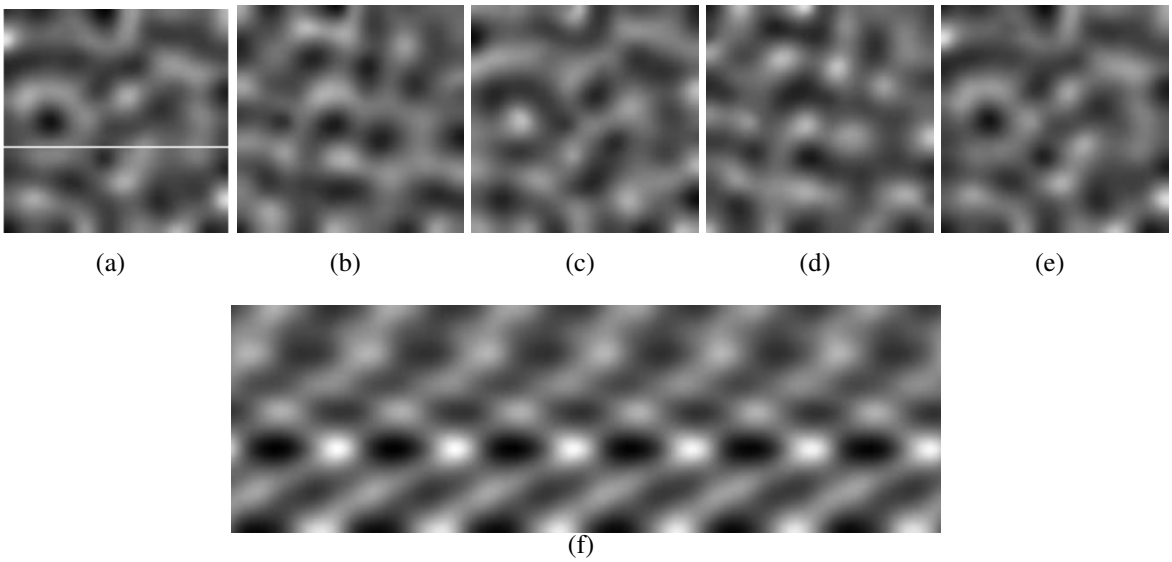

Figure 5.16: (a)-(e)Snapshots of the two-dimensional standing waves for $D = 100$, $\tau_1 = 0.34$, and $\beta = 1.42$. Other parameters as in Fig. 5.7. The five snapshots are equally separated in time within a total time interval of $1.27\ \tau$. (f) One-dimensional space-time plot along a horizontal cross-section (white line in (a)). Space is the vertical coordinate, time the horizontal coordinate. The total time interval is 6.7τ. Graycode as in Fig. 5.11.

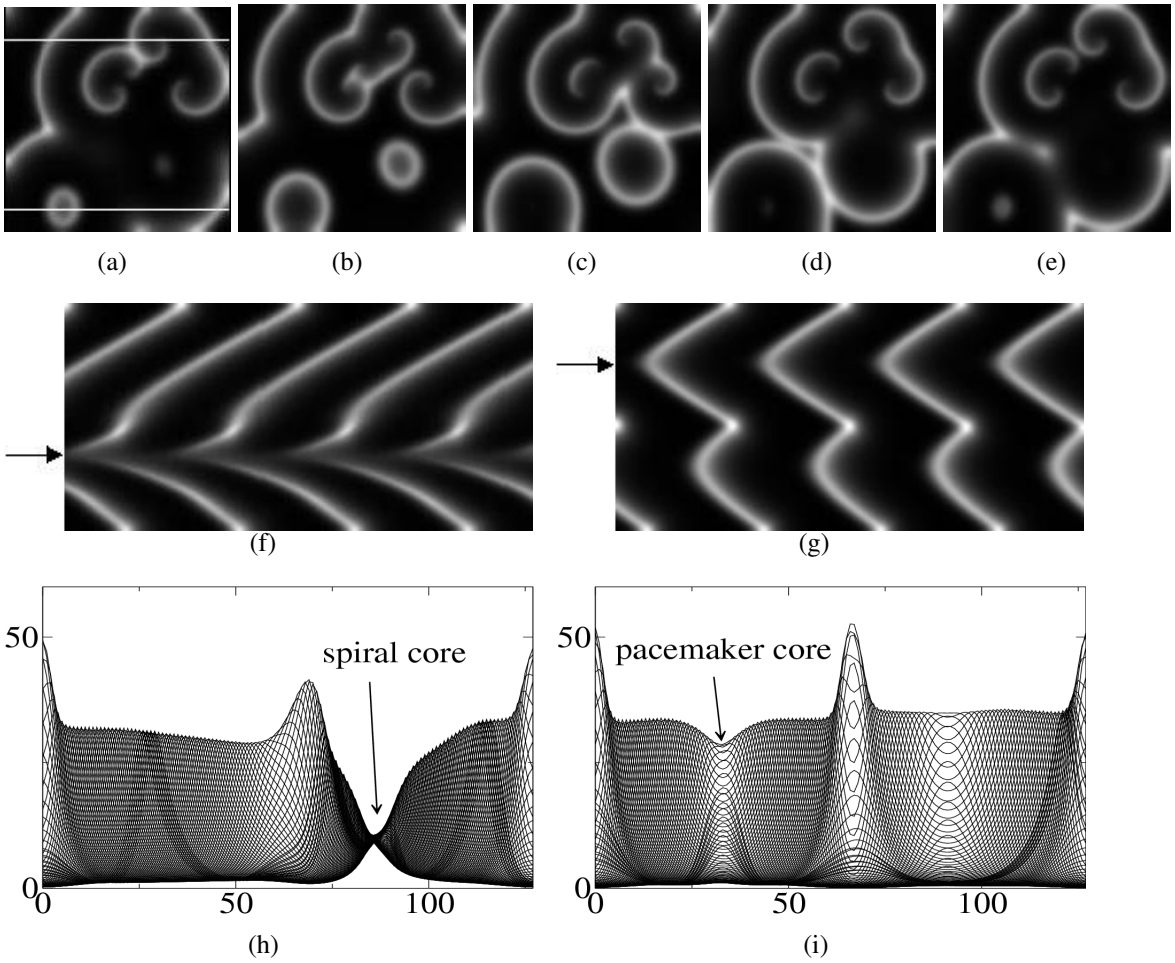

Figure 5.17: Coexisting spirals and pacemakers for $D = 100,\ \tau_1 = 0.34, \beta = 3.0$. Other parameters as in Fig. 5.7. Graycode as in Fig. 5.11. (a)-(e) Five snapshots of the product concentration. The snapshots are equally separated in time within a total time-interval of 0.93 τ. (f) One-dimensional space-time plot through the upper white line drawn in (a), showing the behavior of the spiral core (indicated by the arrow). (g) One-dimensional space-time plot through the lower white line drawn in (a), showing the behavior of the pacemaker core (indicated by the arrow). Space is the vertical coordinate, time the horizontal coordinate. (h)-(i) Overlay of wave profiles at different times.

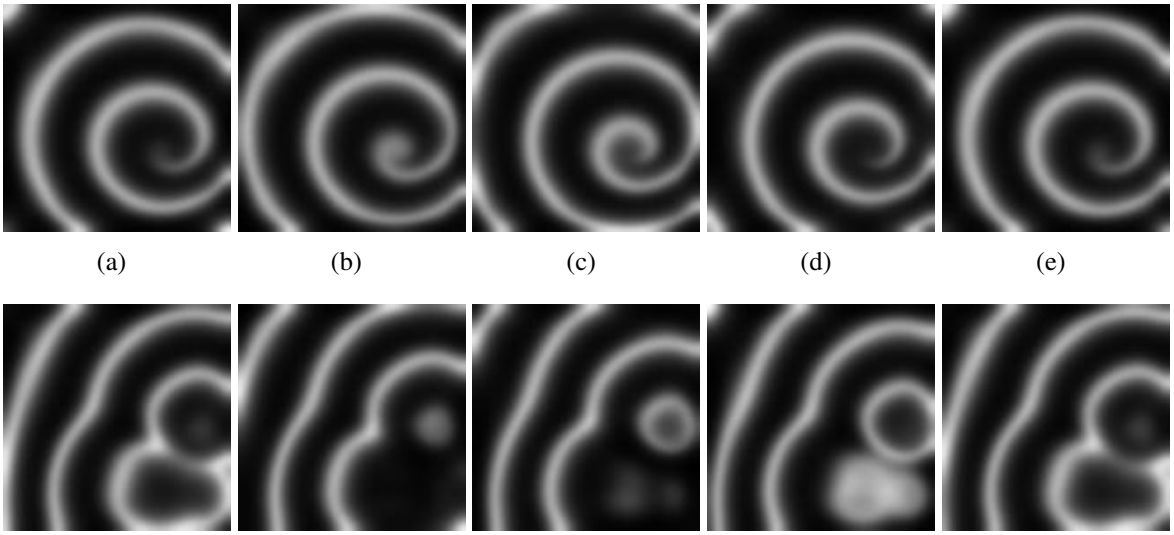

(a) (b) (c) (d) (e)

(f) (g) (h) (i) (j)

Figure 5.18: System with for $D = 100$, $\tau_1 = 0.2$, and $\beta = 1.0$. Other parameters as in Fig. 5.7. Graycode as in Fig. 5.11. (a)-(e) Five snapshots equally separated in time within a total time interval of $1.2\ \tau$. (f)-(j) Five later snapshots within a total time interval of $1.2\ \tau$.

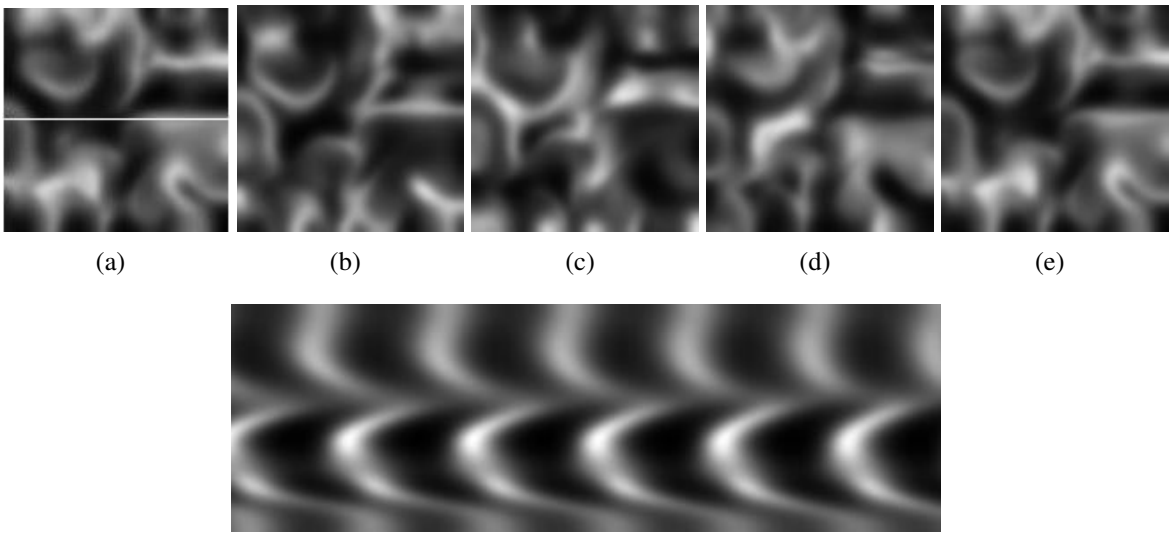

(a) (b) (c) (d) (e)

(f)

Figure 5.19: System with $D = 100$, $\tau_1 = 0.25$, $\beta = 1.0$. Other parameters as in Fig. 5.7. Graycode as in Fig. 5.11. (a)-(e) Five snapshots equally separated in time. Total time 1.2τ. (f) One-dimensional space-time plot along a horizontal cross-section (white line in (a)). Space: vertical coordinate, time: horizontal coordinate. Total time 6.7τ.

Chapter 6

Conclusions

In this thesis, we have investigated the spatio-temporal behavior of systems of interacting oscillators. We have proposed a model where an active oscillatory field described by the complex Ginzburg-Landau equation is interacting through both a local and a nonlocal coupling. The local coupling is due to the presence of diffusion in the dynamics of the oscillators, while the nonlocal coupling is carried out by a second complex field. This additional component has passive dynamics, it is linearly coupled to the oscillatory species, and it is diffusive. Nonlocality arises from the fact that the diffusion constant of the second component is much larger than the other one. Moreover, the nonlocal field is assumed to be inertial, i.e. its relaxation time is large as compared to the kinetics of the oscillators.

We have started with the analysis of the single element dynamics, thus neglecting the spatial couplings due to the diffusional terms. We have shown that, provided that the interaction between the two components is strong enough and that the passive field is inertial enough, the system can display birhythmicity: It has two distinct stable limit cycles which can be reached starting from different initial conditions. A third, unstable limit cycle separates the basins of attraction.

At the boundaries of the parameter region where birhythmicity exists, one stable limit cycle disappears by merging with the unstable one through a saddle-node bifurcation. When they coexist, the two limit cycles are found to have strongly different features. We have called them the *slow* and the *rapid* limit cycle respectively. The slow limit cycle has the oscillation amplitude close to unity for both the active and the passive fields. On the contrary, in the rapid mode, the oscillation amplitude of the active component is much smaller than unity, and it is even almost vanishing for the passive field.

This is found to have an important effect when spatial couplings are taken into account.

We have calculated the linear stability conditions for the extended system in the phase dynamics approximation which holds when the system is found in an almost homogeneous state. This analysis allows to investigate the stability properties of uniform oscillations towards weak spatial perturbations. The results have shown that the rapid oscillations can become unstable due to spatial inhomogeneities even when the slow oscillations remain stable. This is due to the fact that, in the rapid mode, the nonlocal inertial field is not able to follow the fast dynamics of the oscillatory component.

Numerical simulations were performed to investigate the spatio-temporal behavior of the system. In the parameter regions where the two limit cycles are both diffusionally stable, we have observed linear front propagation. The fronts travel from the system region where rapid oscillations are established, and invade the domain entrained by slow oscillations. The interface between the two differently oscillating domains is characterized by periodic emergence of amplitude defects, i.e. phaseless points where the oscillation amplitude vanishes. The front velocity increases as the frequency difference between the two modes rises. Additionally, simulations have been performed in the parameter domain close to the stability boundary of rapid oscillations when the slow oscillations are stable. We have observed two different types of intermittent turbulence. In the pattern that we have called *bursts of synchronization*, a rapidly oscillating and turbulent background is intermittently ripped by the emergence of synchronized domains. They consist of large groups of elements which suddenly reach the large-amplitude slow limit cycle and oscillate synchronously for less than one period. Then the rapidly oscillating and turbulent background overwhelms again. This pattern occurs when the rapid oscillations are unstable. Slightly above their stability boundary, another pattern is found, which we have called *bursts of desynchronization*. In this case, the background oscillates slowly and synchronously, and rapidly oscillating domains intermittently emerge which have a more turbulent appearance.

This work was aimed to provide new information on the not yet extensively investigated domain of nonlocally coupled systems. In particular, we think that the presence of a diffusional coupling besides the nonlocal interaction renders our model suitable to the description of experimental systems where diffusion is present, thus facilitating the comparison between experimental and theoretical investigations. Furthermore, our model is an interesting example of a birhythmic system where spatio-temporal pattern formation can be investigated. Indeed, most of the known models displaying birhythmicity were only investigated in the spatially homogeneous case, while in the present case we have provided evidence that spatial couplings can give rise to novel turbulent patterns. The number of experimental studies

on birhythmic systems is still very small, and we believe that this theoretical study could provide a new thrust in this direction.

Then, another system of interacting oscillators is presented. In this case, single active units are individual enzyme molecules. The enzymes are supposed to be immobilized on a two-dimensional surface and immersed in a liquid. Substrate and product molecules of the biochemical reaction catalyzed by the enzymes are freely diffusing through the liquid. The enzymes are allosteric: Their catalytic efficiency can be affected by the presence of other molecules bound on a specific regulatory site of the enzyme itself. In the present case, the regulatory function is carried out by the same product molecule resulting from the catalytic reaction. Thus, a product released by one enzyme can reach another enzyme through diffusion and bind to it, provided that the enzyme concentration is large enough. Namely, the average distance between two enzymes must be smaller than the distance a product molecule can travel before decay. Once the product has bound to another enzyme, the latter has an enhanced probability of catalyzing a new reaction event. The product molecules are thus the means through which the enzymes interact with each other.

We assume that a single enzyme can be described as a phase oscillator. That is, we consider enzymes which carry out their catalytic activity by performing a relaxational motion in the conformational space. While not operating, they are found in a stable equilibrium conformation. Binding of a substrate molecule triggers a structural modification of the catalyst, driving it to an out-of-equilibrium state. Then, the physical conformation of the enzyme-substrate complex undergoes a sequence of changes which lead to the release of the product molecule resulting from chemical transformation of the substrate. After that, the enzyme returns to the ground state. Thus, the condition of the enzyme can be described by a conformational coordinate with a circular motion starting from the equilibrium state and getting back to it after an excursion through different states.

In our system, all processes occur on a time scale which is smaller than or comparable to the duration of an individual catalytic event. Therefore, the system cannot be described in the framework of the classical chemical kinetics which assumes a single reaction event to be instantaneous. In the present case, spatio-temporal self-organization on a molecular level can take place.

The mathematical description of the system in the mean-field approximation is a set of three partial differential equations with time delay. The delay terms convey the presence of a memory effect which is due to finite duration of the catalytic cycle. This means that individ-

ual molecular processes come into play and can be involved in self-organization phenomena. In previous works, it was shown that synchronization of the enzyme cycles can occur in a small reaction volume, because of the global coupling due to products diffusion. When the enzyme population operates in such a synchronous mode, rigid correlations between conformational states of individual molecules are established. Oscillations of the product concentration can be observed, whose period is close to the duration of one catalytic cycle. Moreover, clustering is observed. The enzymes can split into several groups, the cycles are synchronized within each group, while different groups are phase-shifted with respect to each other.

In this work, we have extended this result to the case of a larger reaction volume. Assuming that the system is wider than the diffusion length of the product molecules, the enzymes can synchronize non-uniformly, giving rise to spatially organized patterns. The linear stability analysis of the spatially extended system has revealed the existence of a wave bifurcation. When such a bifurcation occurs, patterns with a well-defined wavelength emerge also when uniform oscillations are not capable to entrain the system.

We have investigated the system by means of numerical simulations, finding a rich variety of patterns: Uniform oscillations, ripples, traveling waves, pacemakers, standing waves, standing-traveling waves, mixed-mode oscillations have been seen in the one-dimensional system. Some of such patterns were also observed in the two-dimensional system where additionally spiral waves are formed.

We believe that experimental investigations on a system of interacting proteins aimed to the highlighting of synchronization phenomena would turn out to be of great interest. It would give indications on possibly new self-organization mechanisms within living cells. Indeed, in our theoretical study we have shown that synchronization and pattern formation phenomena can occur for concentrations and time and length scales which are of the order of known physiological values for living cells. Stochastic simulations performed in our group show that fluctuations due to system discreteness and intrinsic noise do not prevent synchronization and pattern formation to occur. Thus, we can expect a real system under appropriate conditions to show self-organization despite the unavoidable stochastic effects neglected in our mean-field approximation.

In conclusion, we have analyzed the properties of systems of coupled oscillators with local and nonlocal interactions, by focusing on the emergence of different collective behaviours, ranging from uniform oscillations to coherent structures and turbulence. These

findings can provide further motivation for investigations of self-organization in chemical reactions and biological systems.

Appendix

A Coefficients of the phase dynamics approximation

The calculations shown in this Appendix were performed with the help of the software Mathematica.

Starting from system (3.23) we linearize the first three equations around the values ρ_0, r_0, ψ_0 of the uniform oscillations. The system that we obtain can be written as

$$\dot{\delta\rho} = a_1\delta\rho + b_1\delta r + c_1\delta\psi + d_1\nabla\Theta^2 + e_1\nabla^2\Theta \tag{A.1a}$$

$$\dot{\delta r} = a_2\delta\rho + b_2\delta r + c_2\delta\psi + d_2\nabla\Theta^2 \tag{A.1b}$$

$$\dot{\delta\psi} = a_3\delta\rho + b_3\delta r + c_3\delta\psi + d_3\nabla\Theta^2 + e_3\nabla^2\Theta \tag{A.1c}$$

$$\dot{\Theta} = a_4\delta\rho + b_4\delta r + c_4\delta\psi + d_4\nabla\Theta^2 + e_4\nabla^2\Theta + f_4 \tag{A.1d}$$

where the coefficients are given in the following table

$$\begin{array}{ll}
a_1 = 1 - 3\rho_0^2 - K & a_3 = 2\alpha\rho_0 + \left[\frac{Kr_0}{\rho_0^2} - r_0\frac{1}{\tau}\right]\sin(\psi_0) \\
b_1 = K\cos(\psi_0) & b_3 = \sin(\psi_0)\left[-\frac{K}{\rho_0} + \frac{\rho_0}{\tau r_0^2}\right] \\
c_1 = -Kr_0\sin(\psi_0) & c_3 = \cos(\psi_0)\left[-K\frac{r_0}{\rho_0} + \frac{\rho_0}{\tau r_0}\right] \\
d_1 = -\frac{\rho_0}{4} & d_3 = -l^2\frac{r_0}{4\tau} \\
e_1 = \frac{1}{2}\rho_0\beta & e_3 = \frac{1}{2}\left(1 - \frac{l^2}{\tau}\right) \\
a_2 = \frac{1}{\tau}\cos(\psi_0) & a_4 = 2\alpha\rho_0 + \left[K\frac{r_0}{\rho_0^2} + \frac{1}{\tau\rho_0}\right]\sin(\psi_0) \\
b_2 = -\frac{1}{\tau} & b_4 = \sin(\psi_0)\left[-\frac{K}{\rho_0} - \frac{\rho_0}{\tau r_0^2}\right] \\
c_2 = -\frac{\rho_0}{\tau}\sin(\psi_0) & c_4 = \cos(\psi_0)\left[-K\frac{r_0}{\rho_0} + \frac{\rho_0}{\tau r_0}\right] \\
d_2 = -l^2\frac{r_0}{4\tau} & d_4 = \frac{\beta}{4} \\
e_2 = 0 & e_4 = \frac{1}{2}\left(1 + \frac{l^2}{\tau}\right) \\
f_4 = -\omega + \alpha\rho_0^2 + \left[-K\frac{r_0}{R_0} + \frac{\rho_0}{\tau r_0}\right]\sin(\psi_0) &
\end{array}$$

Now, since we are in the approximation where ρ, r, ψ adjust adiabatically to Θ, we can

assume $\dot{\delta\rho} = \dot{\delta r} = \dot{\delta\psi} = 0$, so that we get from (A.1d)

$$\begin{aligned}
\delta\rho &= \frac{b_3c_2d_1 - b_2c_3d_1 - b_3c_1d_2 + b_1c_3d_2 + b_2c_1d_3 - b_1c_2d_3}{-a_3b_2c_1 + a_2b_3c_1 + a_3b_1c_2 - a_1b_3c_2 + a_2b_1c_3 - a_1b_2c_3}\nabla\Theta^2 \\
&\quad + \frac{b_3c_2e_1 - b_2c_3e_1 + b_2c_1e_3 - b_1c_2e_3}{-a_3b_2c_1 + a_2b_3c_1 + a_3b_1c_2 - a_1b_3c_2 + a_2b_1c_3 - a_1b_2c_3}\nabla^2\Theta \qquad \text{(A.2)} \\
\delta r &= \frac{a_3c_2d_1 - a_2c_3d_1 - a_3c_1d_2 + a_1c_3d_2 + a_2c_1d_3 - a_1c_2d_3}{a_3b_2c_1 - a_2b_3c_1 - a_3b_1c_2 + a_1b_3c_2 + a_2b_1c_3 - a_1b_2c_3}\nabla\Theta^2 \\
&\quad + \frac{a_3c_2e_1 - a_2c_3e_1 + a_2c_1e_3 - a_1c_2e_3}{a_3b_2c_1 - a_2b_3c_1 - a_3b_1c_2 + a_1b_3c_2 + a_2b_1c_3 - a_1b_2c_3}\nabla^2\Theta \qquad \text{(A.3)} \\
\delta\psi &= \frac{a_3b_2d_1 - a_2b_3d_1 - a_3b_1d_2 + a_1b_3d_2 + a_2b_1d_3 - a_1b_2d_3}{-a_3b_2c_1 + a_2b_3c_1 + a_3b_1c_2 - a_1b_3c_2 - a_2b_1c_3 + a_1b_2c_3}\nabla\Theta^2 \\
&\quad + \frac{a_3b_2e_1 - a_2b_3e_1 + a_2b_1e_3 - a_1b_2e_3}{-a_3b_2c_1 + a_2b_3c_1 + a_3b_1c_2 - a_1b_3c_2 - a_2b_1c_3 + a_1b_2c_3}\nabla^2\Theta. \qquad \text{(A.4)}
\end{aligned}$$

These expressions can be put into the equation for Θ to get

$$\dot{\Theta} = C_0 + C_1(\nabla\Theta)^2 + C_2\nabla^2\Theta \qquad \text{(A.5)}$$

where

$$\begin{aligned}
C_0 &= f_4 \qquad \text{(A.6)} \\
C_1 &= d_4 + [c_4(a_3b_2d_1 - a_2b_3d_1 - a_3b_1d_2 + a_1b_3d_2 + a_2b_1d_3 - a_1b_2d_3) \\
&\quad - b_4(a_3c_2d_1 - a_2c_3d_1 - a_3c_1d_2 + a_1c_3d_2 + a_2c_1d_3 - a_1c_2d_3) \\
&\quad + a_4(b_3c_2d_1 - b_2c_3d_1 - b_3c_1d_2 + b_1c_3d_2 + b_2c_1d_3 - b_1c_2d_3)]\,/ \\
&\quad (-a_3b_2c_1 + a_2b_3c_1 + a_3b_1c_2 - a_1b_3c_2 - a_2b_1c_3 + a_1b_2c_3) \qquad \text{(A.7)} \\
C_2 &= e_4 + [c_4(a_3b_2e_1 - a_2b_3e_1 + a_2b_1e_3 - a_1b_2e_3) \\
&\quad - b_4(a_3c_2e_1 - a_2c_3e_1 + a_2c_1e_3 - a_1c_2e_3) \\
&\quad + a_4(b_3c_2e_1 - b_2c_3e_1 + b_2c_1e_3 - b_1c_2e_3)]\,/ \\
&\quad (-a_3b_2c_1 + a_2b_3c_1 + a_3b_1c_2 - a_1b_3c_2 - a_2b_1c_3 + a_1b_2c_3) \qquad \text{(A.8)}
\end{aligned}$$

B Rates of the enzyme mean-field model

For the calculations and the numerical simulations on the enzyme mean-field model, we choose an enzyme concentration ten times larger than the critical concentration estimated in Sec. 5.1.2. Thus we have:

$$c = 10^{16}/\text{cm}^3 \tag{B.9}$$

which gives for the renormalized two-dimensional concentration:

$$c_2 = 10^{12}/\text{cm}^2. \tag{B.10}$$

The corresponding correlation length is

$$L_{\text{corr}} = 0.3\mu\text{m}, \tag{B.11}$$

and represents the smallest length scale involved in the system.

For the average duration of a single catalytic cycle, we take the value $\tau = 10$ ms, thus assuming our enzyme to be rather slow, but still within the range of experimentally known values [159, 172].

All parameters values are given as pure numbers, which must be considered as referred to the following units:

- **Unit length** is $\Delta x = 0.1\mu\text{m} = \dfrac{L_{\text{corr}}}{3}$, which is also used as mesh size in the numerical calculations,
- **Unit time** is $\tau = 10$ ms, i.e. the duration of one catalytic cycle.

Many of the parameters are kept constant all over the numerical simulations, therefore we indicate their values here. If not otherwise stated, we have used:

- $D = 10^{-5}$ cm^2/s = $10^{-5}(10^5\Delta x)^2/100\tau = 1000$
- $n_t = 10^{12}$ cm^{-2} = 100
- $\alpha_0 = 100$ s$^{-1} = 1$
- $\alpha_1 = 10^5$ s$^{-1} = 1000$
- $\kappa = 10^3$ s$^{-1} = 10$
- $\gamma = 10^3$ s$^{-1} = 10$

In general, β and τ_1 are used as control paramaters.

Bibliography

[1] G. Nicolis, I. Prigogine, *Self-Organization in Nonequilibrium Systems*, Wiley, New York, 1977.

[2] E. Schrödinger, *What is Life?*, Cambridge University Press, 1944.

[3] R. Kapral, K. Showalter (editors), *Chemical Waves and Patterns*, Kluwer Academic Publishers, Dordecht, 1995.

[4] M.C. Cross, P.C. Hohenberg, *Pattern-formation outside of equilibrium*, Rev. Mod. Phys. **65** (1993), 851–1112.

[5] K. Krischer, *Nonlinear dynamics in electrochemical systems*, Advances in Electrochemical Science and Engineering (R.C. Alkire, D.M. Kolb, editors), vol. 32, Wiley-VCH, 2003, pp. 89–208.

[6] D. Walgraef, *Spatio-temporal Pattern Formation*, Springer, New York, 1997.

[7] E. Bodenschatz, W. Pesch, G. Ahlers, *Recent developments in Rayleigh-Bénard convection*, Ann. Rev. Fluid. Mech. **32** (2000), 709.

[8] E. Schöll, *Nonlinear Spatio-Temporal Dynamics and Chaos in Semiconductors*, Cambridge University Press, Cambridge, 2001.

[9] H.M. Jaeger, S.R. Nagel, R.P. Behringer, *Granular solids, liquids and gases*, Rev. Mod. Phys. **68** (1996), 1259.

[10] F.T. Arecchi, S. Boccaletti, P.L. Ramazza, *Pattern formation and competition in nonlinear optics*, Phys. Rep. **318** (1999), 1.

[11] S. Residori, *Patterns, fronts, and structures in a liquid-crystal-light-valve with optical feedback*, Phys. Rep. **416** (2005), 201–272.

[12] A. Goldbeter, *Biochemical Oscillations and Cellular Rhythms*, Cambridge University Press, 1996.

[13] A.T. Winfree, *The Geometry of Biological Time*, Springer, New York, 2001.

[14] J.D. Murray, *Mathematical Biology*, Springer, Berlin, 1989.

[15] J. Higgins, *A chemical mechanism for oscillation of glycolytic intermediates in yeast cells*, PNAS **51** (1964), no. 6, 989–994.

[16] E.E. Sel'kov, *Self-organization in glycolysis. 1.A simple kinetic model*, European J. Biochem. **4** (1968), 79–86.

[17] B. Hess, A. Boiteux, J.Krüger, *Cooperation of glycolytic enzymes*, Adv. Enzyme Regul. **7** (1969), 149–167.

[18] S. Danø, F. Hynne, S. De Monte, F. d'Ovidio, P.G. Sørensen, H.Westerhoff, *Synchronization of glycolytic oscillations in a yeast cell population*, Faraday Discuss. **120** (2001), 261–276.

[19] M.F. Madsen, S. Danø, P.G. Sørensen, *On the mechanism of glycolytic oscillation in yeast*, FEBS Journal **272** (2005), 2648–2660.

[20] T. Mair, S.C. Müller, *Traveling NADH and proton waves during oscillatory glycolysis* in vitro, J. Biolog. Chem. **271** (1996), 627–630.

[21] S.C. Müller, T. Mair, O. Steinbock, *Traveling waves in yeast extract and in cultures of* Dictyostelium discoideum, Biophys. Chem. **72** (1998), 37–47.

[22] J.J. Tyson, C.I. Hong, C.D. Thron, B. Novak, *A simple model of circadian rhythms based on dimerization and proteolysis of PER and TIM*, Biophysical Journal **77** (1999), 2411.

[23] A. Goldbeter, *Computational approaches to cellular rhythms*, Nature **420** (2002), 238.

[24] S. Yamaguchi, H. Isejima, T. Matsuo, R. Okura, K. Yagita, M. Kobayashi, H. Okamura, *Synchronization of cellular clocks in the superchiasmatic nucleus*, Science **302** (2003), 1408.

[25] A.T. Winfree, *Electrical turbulence in 3-dimensional heart-muscle*, Science **266** (1994), 1003.

[26] A.T. Winfree, *Heart muscle as a reaction-diffusion medium: The roles of electric potential diffusion, activation front curvature, and anisotropy*, Int. J. Bif. Chaos **7** (1997), 487.

[27] H. Levine E. Ben-Jacob, I. Cohen, *Cooperative self-organization of microorganisms*, Adv. Phys. **49** (2000), 395–554.

[28] M. Falcke, *Reading the patterns in living cells. The physics of Ca^{+}+ signalling*, Advances in Physics **53** (2004), 255–440.

[29] J. Lechleiter, S. Girard, E. Peralta, D. Clapham, *Spiral calcium wave propagation and annihilation in* Xenopus laevis *Oocytes*, Science **252** (1991), 123–126.

[30] M. J. Berridge, M.D. Bootman, P. Lipp, *Calcium–a life and death signal*, Nature **395** (1998), 645–648.

[31] H.R. Petty, *Dynamic chemical instabilities in living cells may provide a novel route in drug development*, ChemBioChem **5** (2004), 1359–1364.

[32] P.A. Tass, *Effective desynchronization by means of double-pulse phase resetting*, Europhys. Lett. **53** (2001), 15–21.

[33] P.A. Tass, *Effective desynchronization with a stimulation technique based on soft phase resetting*, Europhys. Lett. **57** (2002), 164–170.

[34] H. Haken, *Synergetics. An Introduction*, Springer, Berlin, 1978.

[35] A.T. Winfree, *Biological rhythms and the behavior of populations of coupled oscillators*, J. Theor. Biol. **16** (1967), 15–42.

[36] Y. Kuramoto, *Self-entrainment of a population of coupled non-linear oscillators*, International Symposium on Mathematical Problems in Theoretical Physics (H. Araki, editor), Lecture Notes in Physics, vol. 39, Springer, New York, 1975, p. 420.

[37] Y. Kuramoto, *Chemical Oscillations, Waves and Turbulence*, Springer, New York, 1984.

[38] A.S. Mikhailov, S.C. Manrubia, D.H. Zanette, *Emergence of Dynamical Order: Synchronization Phenomena in Complex Systems*, World Scientific, Singapore, 2004.

[39] A. S. Mikhailov, A.Yu. Loskutov, *Foundations of Synergetics I: Distributed Active Systems*, Springer, Berlin, 1994.

[40] A. S. Mikhailov and A.Yu. Loskutov, *Foundations of Synergetics II: Chaos and Noise*, Springer, Berlin, 1996.

[41] A. Pikovsky, M. Rosenblum, J. Kurths, *Synchronization. A Universal Concept in Nonlinear Sciences*, Cambridge University Press, 2001.

[42] S. H. Strogatz, *From Kuramoto to Crawford: exploring the onset of synchronization in populations of coupled oscillators*, Physica D **143** (2000), 1.

[43] Y. Kuramoto, *Scaling behavior of turbulent oscillators with non-local interaction*, Prog. of Theor. Phys. **94** (1995), 321–330.

[44] Y. Kuramoto, H. Nakao, *Origin of power-law spatial correlations in distributed oscillators and maps with nonlocal coupling*, Phys. Rev. Lett. **76** (1996), 4352–4355.

[45] Y. Kuramoto, D. Battogtokh, H. Nakao, *Multiaffine chemical turbulence*, Phys. Rev. Lett. **81** (1998), 3543–3546.

[46] Y. Kuramoto, *Reduction methods applied to nonlocally coupled oscillator systems*, Nonlinear Dynamics and Chaos: Where do we go from here? (S.J. Hogan, A. Champneys, A.R. Krauskopf, M. di Bernardo, R.E. Wilson, H.M. Osinga, M.E. Homer, editors), Institute of Physics, Bristol, 2002, pp. 800–819.

[47] D. Tanaka, Y. Kuramoto, *Complex Ginzburg-Landau equation with nonlocal coupling*, Phys. Rev. E **68** (2003), 026219.

[48] S. Shima, Y. Kuramoto, *Rotating spiral waves with phase-randomized core in nonlocally coupled oscillators*, Phys. Rev. E **69** (2004), 036213.

[49] D.M. Abrams, S.H. Strogatz, *Chimera states for coupled oscillators*, Phys. Rev. Lett. **93** (2004), 174102.

[50] H.P. Lerch, A.S Mikhailov, B. Hess, *Conformational-relaxation models of single-enzyme kinetics*, PNAS **99** (2002), 15410.

[51] H.P. Lerch, R. Rigler, A.S. Mikhailov, *Functional conformational motions in the turnover cycle of cholesterol oxidase*, PNAS **102** (2005), 10807.

[52] P. Stange, D. Zanette, A.S. Mikhailov, B.Hess, *Self-organizing molecular networks*, Biophys. Chem. **79** (1999), 233.

[53] P. Stange, A.S. Mikhailov, B. Hess, *Mutual synchronization of molecular turnover cycles in allosteric enzymes*, J. Phys. Chem. **102** (1998), 6273.

[54] P. Stange and A.S. Mikhailov and B. Hess, *Mutual synchronization of molecular turnover cycles in allosteric enzymes II. Product inhibition*, J. Phys. Chem. **103** (1999), 6111.

[55] P. Stange, *Theoretische Untersuchungen der mikroskopischen Synchronisation von molekularen Enzymzyklen*, Ph.D. thesis, Otto-von-Guericke-Universität Magdeburg, 2001.

[56] H. Lerch, P. Stange, A.S. Mikhailov, B. Hess, *Mutual synchronization of molecular turnover cycles in allosteric enzymes III. Intramolecular cooperativity*, J. Phys. Chem. **106** (2002), 3237–3247.

[57] B. Hess, A.S. Mikhailov, *Self-organization in living cells*, Science **264** (1994), 223.

[58] O. Decroly, A. Goldbeter, *Birhythmicity, chaos and other patterns of temporal self-organization in a multiply regulated biochemical system*, Proc. Natl. Acad. Sci. USA **79** (1982), 6917–6921.

[59] M. Alamgir, I.R. Epstein, *Birhythmicity and compound oscillation in coupled chemical oscillators: Chlorite-Bromate-Iodide System*, J. Am. Chem. Soc. **105** (1983), 2500–2502.

[60] C.G. Hocker, I.R. Epstein, *Analysis of a four-variable model of coupled chemical oscillators*, J. Chem. Phys. **90** (89), 3071–3080.

[61] A.N. Zaikin, A.M. Zhabotinsky, *Concentration wave propagation in a two-dimensional liquid-phase self-oscillating system*, Nature **225** (1970), 535.

[62] A.T. Winfree, *Spiral waves of chemical activity*, Science **175** (1972), 634.

[63] A.T. Winfree, *The prehistory of the Belousov-Zhabotinsky oscillator*, J. Chem. Educ. **61** (1984), 661.

[64] A.M. Zhabotinsky, *A history of chemical oscillations and waves*, Chaos **1** (1991), 379.

[65] V.K. Vanag, I.R. Epstein, *Inwardly rotating spiral waves in a reaction-diffusion system*, Science **294** (2001), 835.

[66] T. Sakurai, E. Mihaliuk, F. Chirila, K. Showalter, *Design and control of wave propagation in excitable media*, Science **296** (2002), 2009.

[67] P. Lamba, J.L. Hudson, *Experimental evidence of multiple oscillatory states in a continuous reactor*, Chem. Eng. Comm. **32** (1985), 369–375.

[68] H.J. Krug, L. Pohlmann, L. Kuhnert, *Analysis of the modified complete Oregonator accounting for oxygen sensitivity and photosensitivity of Belousov-Zhabotinsky systems*, J. Phys. Chem. **94** (1990), 4862–4866.

[69] M. Stich and M. Ipsen and A.S. Mikhailov, *Self-organized stable pacemakers near the onset of birhythmicity*, Phys. Rev. Lett. **86** (2001), 4406.

[70] M. Stich, M. Ipsen, A.S. Mikhailov, *Pattern formation in birhythmic media*, Physica D **171** (2002), 19–40.

[71] M. Stich, *Target Patterns and Pacemakers in Reaction-Diffusion Systems*, Ph.D. thesis, Technische Universität Berlin, 2003.

[72] A. Einstein, *Über die von der molekularkinetischen Theorie der Wärme geforderte Bewegung von in ruhenden Flüssigkeiten suspendierten Teilchen*, Ann. Phys. **17** (1905), 549.

[73] A. Einstein, *Zur Theorie der Brownschen Bewegung*, Ann. Phys. **19** (1906), 371.

[74] M. Smoluchowski, *Zur kinetischen Theorie der Brownschen Molekularbewegung und der Suspensionen*, Ann. Phys. **20** (1906), 756.

[75] M. Smoluchowski, *Über Brownsche Molekularbewgung unter Einwirkung äußerer Kräfte und deren Zusammenhang mit der verallgemeinerten Diffusionsgleichung*, Ann. Phys. **48** (1915), 1103.

[76] A. Einstein, *Investigations on the Theory of the Brownian Movement*, Courier Dover Publications, 1956.

[77] I.S. Aranson, L. Kramer, *The world of the complex Ginzburg-Landau equation*, Rev. Mod. Phys. **74** (2002), 99–143.

[78] W. van Saarlos, P.C. Hohenberg, *Fronts, pulses, sources and sinks in generalized Ginzburg-Landau equations*, Physica D **56** (1992), 303–367.

[79] H. Chaté, P. Manneville, *Phase diagram of the two-dimensional complex Ginzburg-Landau equation*, Physica A **224** (1996), 348.

[80] M. van Hecke, *Building blocks of spatiotemporal intermittency*, Phys. Rev. Lett. **80** (1998), 1896.

[81] B.I. Shraiman, A. Pumir, W. van Saarlos, P.C. Hohenberg, H. Chaté, M. Holen, *Spatiotemporal chaos in the one-dimensional complex Ginzburg-Landau equation*, Physica D **57** (1992), 241.

[82] L. Brusch, M.G. Zimmermann, M. van Hecke, M. Bär, A. Torcini, *Modulated amplitude waves and the transition from phase to defect chaos*, Phys. Rev. Lett. **85** (2000), 86.

[83] C. Beta, *Controlling turbulence in surface chemical reactions*, Ph.D. thesis, Freie Universität Berlin, 2004.

[84] R. Imbihl, G. Ertl, *Oscillatory kinetics in heterogeneous catalysis*, Chem. Rev. **95** (1995), 697.

[85] M. Eiswirth, G. Ertl, *Kinetic oscillations in the catalytic CO oxidation on a Pt(110) surface*, Surf. Sci. **77** (1986), 90.

[86] M. Eiswirth, K. Krischer, G. Ertl, *Transition to chaos in an oscillating surface reaction*, Surf. Sci. **202** (1988), 565.

[87] K. Krischer, M. Eiswirth, G. Ertl, *Oscillatory CO oxidation on Pt(110): Modeling of temporal self-organization*, J. Chem. Phys. **96** (1992), 9161.

[88] H.H. Rotermund, W. Engel, M. Kordesch, G. Ertl, *Imaging of spatiotemporal pattern evolution during carbon-monoxide oxidation on platinum*, Nature **343** (1990), 355.

[89] H.H. Rotermund, G. Haas, R.U. Franz, R.M. Tromp, G.Ertl, *Imaging pattern formation in surface reactions from ultrahigh vacuum up to atmospheric pressures*, Science **270** (1995), 608–610.

[90] H.H. Rotermund, *Imaging pattern formation in surface reactions from ultrahigh vacuum up to atmospheric pressures*, Surface Science **386** (1997), 10–23.

[91] M. Falcke, M. Bär, H. Engel, , M. Eiswirth, *Traveling waves in the CO oxidation on Pt(110): Theory*, J. Chem. Phys. **97** (1992), 4555.

[92] M. Bär, M. Hildebrand, M. Eiswirth, M. Falcke, H. Engel, M. Neufeld, *Chemical turbulence and standing waves in a surface reaction model: The influence of global coupling and wave instabilities*, Chaos **4** (1994), 499.

[93] I.Z. Kiss, Y. Zhai, J.L. Hudson, *Emerging coherence in a population of chemical oscillators*, Science **296** (2002), 1676.

[94] D. Golomb, D. Hansel, B. Shairman, H. Sompolinsky, *Clustering in globally coupled phase oscillators*, Phys. Rev. A **45** (1992), 3516.

[95] K. Okuda, *Variety and generality of clustering in globally coupled oscillators*, Physica D **63** (1993), 424.

[96] D. Hansel, G. Mato, C. Meunier, *Clustering and slow switching in globally coupled phase oscillators*, Phys. Rev. E **48** (1993), 3470.

[97] H. Kori, Y. Kuramoto, *Slow switching in globally coupled oscillators: robustness and occurrence through delayed coupling*, Phys. Rev. E **63** (2001), 046214.

[98] V.K. Vanag, L. Yang, M. Dolnik, A.M. Zhabotinsky, I.R. Epstein, *Oscillatory cluster patterns in a homogeneous chemical system with global feedback*, Nature **406** (2000), 389.

[99] V. Hakim, W. Rappel, *Dynamics of the globally coupled complex Ginzburg-Landau equation*, Phys. Rev. A **46** (1992), 7347.

[100] N. Nakagawa, Y. Kuramoto, *Collective chaos in a population of globally coupled oscillators*, Prog. Theor. Phys. **89** (1993), 313.

[101] A.S. Pikovsky, J. Kurths, M.G. Rosenblum, *Synchronization in a population of globally coupled chaotic oscillators*, Europhys. Lett. **34** (1996), 165.

[102] D.H. Zanette, A.S. Mikhailov, *Condensation in globally coupled populations of chaotic dynamical systems*, Phys. Rev. E **57** (1998), 276.

[103] S. Boccaletti, J. Kurths, G. Osipov, D.L. Valladares, C.S. Zhou, *The synchronization of chaotic systems*, Phys. Rep. **36** (2002), 1.

[104] S. Jakubith, H.H. Rotermund, W. Engel, A. Von Oertzen, G. Ertl, *Spatiotemporal concentration patterns in a surface-reaction - Propagating and standing waves, rotating spirals, and turbulence*, Phys. Rev. Lett. **65** (1990), 3013.

[105] A. von Oertzen, H.H. Rotermund, A.S. Mikhailov, G. Ertl, *Standing wave patterns in the CO oxidation reaction on a Pt(110) surface: Experiments and Modeling*, J. Phys. Chem. B **104** (2000), 3155.

[106] K.C. Rose, D. Battogtokh, A.S. Mikhailov, R. Imbihl, W. Engel, A.M. Bradshaw, *Cellular structures in catalytic reaction with global coupling*, Phys. Rev. Lett. **76** (1996), 3582.

[107] F. Mertens, R. Imbihl, A.S. Mikhailov, *Breakdown of global coupling in oscillatory chemical reactions*, J. Chem. Phys. **99** (1993), 8668.

[108] F. Mertens and R. Imbihl and A.S. Mikhailov, *Turbulence and standing waves in oscillatory chemical reactions with global coupling*, J. Chem. Phys. **101** (1994), 9903.

[109] H. Levine, X. Zou, *Standing waves in catalysis at single-crystal surface*, Phys. Rev. Lett. **69** (1992), 204.

[110] H. Levine, X.Q. Zhou, *Catalysis at single-crystal Pt(110) surfaces - global coupling and standing waves*, Phys. Rev. E **48** (1993), 50.

[111] M. Falcke, H. Engel, *Influence of global coupling through the gas phase on the dynamics of CO oxidation on Pt(110)*, Phys. Rev. E **50** (1994), 1353.

[112] M. Falcke and H. Engel, *Pattern formation during the CO oxidation on Pt(110) surfaces under global coupling*, J. Chem. Phys. **101** (1994), 6255.

[113] M. Falcke, H. Engel, M. Neufeld, *Cluster formation, standing waves, and stripe patterns in oscillatory active media with local and global coupling*, Phys. Rev. E **52** (1995), 763.

[114] M. Falcke, H. Engel, *Traveling pulses in anisotropic oscillatory media with global coupling*, Phys. Rev. E **56** (1997), 635.

[115] M. Kim, M. Bertram, M. Pollmann, A. von Oertzen, A.S. Mikhailov, H.H. Rotermund, G. Ertl, *Controlling chemical turbulence by global delayed feedback: Pattern formation in catalytic CO oxidation on Pt(110)*, Science **292** (2001), 1357.

[116] M. Bertram, C. Beta, M. Pollmann, A.S. Mikhailov, H.H. Rotermund, G. Ertl, *Pattern formation at the edge of chaos: Experiments with CO oxidation on a Pt (110) surface under global delayed feedback*, Phys. Rev. E **67** (2003), 036208.

[117] D. Battogtokh, A.S. Mikhailov, *Controlling turbulence in the complex Ginzburg-Landau equation*, Physica D **90** (1996), 84.

[118] D. Battogtokh, A.S. Mikhailov, A. Preusser, *Controlling turbulence in the complex Ginzburg-Landau equation. Two-dimensional systems*, Physica D **106** (1997), 327.

[119] M. Bertram, A.S. Mikhailov, *Pattern formation in a surface chemical reaction with global delayed feedback*, Phys. Rev. E **63** (2001), 066102.

[120] M. Bertram and A.S. Mikhailov, *Pattern formation at the edge of chaos: Mathematical modeling of CO oxidation on a Pt (110) surface under global delayed feedback*, Phys. Rev. E **67** (2003), 036207.

[121] J. Christoph, M. Eiswirth, *Theory of electrochemical pattern formation*, Chaos **12** (2002), 215.

[122] N. Mazouz, G. Flätgen, K. Krischer, *Tuning the range of spatial coupling in electrochemical systems: From local via nonlocal to global coupling*, Phys. Rev. E **55** (1997), 2260.

[123] J. Christoph, R.D. Otterstedt, M. Eiswirth, N.I. Jaeger, J.L. Hudson, *Negative coupling during oscillatory pattern formation on a ring electrode*, J. Chem. Phys. **110** (1999), 8614.

[124] J. Christoph, *Musterbildung auf Elektrodenoberflächen-Theorie von Reaktions-Migrations-Systemen*, Ph.D. thesis, FU Berlin, 1999.

[125] J. Christoph, P. Strasser, M. Eiswirth, G. Ertl, *Remote triggering of waves in an electrochemical system*, Science **284** (1999), 291.

[126] P. Strasser, J. Christoph, W. Lin, M. Eiswirth, J.L. Hudson, *Standing wave oscillations in an electrocatalytic reaction*, J. Phys. Chem. **104** (2000), 1854.

[127] P. Grauel, H. Varela, K. Krischer, *Spatial bifurcations of fixed points and limit cycles during the electrochemical oxidation of H_2 on Pt ring-electrodes*, Faraday Discuss. **120** (2002), 165.

[128] F. Plenge, H. Varela, K. Krischer, *Asymmetric target pattern in one-dimensional oscillatory media with genuine Nonlocal coupling*, Phys. Rev. Lett. **94** (2005), 198301.

[129] B. Ermentrout, *Neural networks as spatio-temporal pattern-forming systems*, Rep. Prog. Phys. **61** (1998), 353.

[130] S. Renisch, R. Schuster, J. Wintterlin, G. Ertl, *Dynamics of adatom motion under the influence of mutual interactions: O/Ru(0001)*, Phys. Rev. Lett. **82** (1999), 3839.

[131] C. Sachs, M. Hildebrand, S. Voelkening, J. Wintterlin, G. Ertl, *Spatiotemporal self-organization in a surface reaction: From the atomic to the mesoscopic scale*, Science **293** (2001), 1635.

[132] M. Hildebrand, A.S. Mikhailov, *Mesoscopic modeling in the kinetic theory of adsorbates*, J. Phys. Chem. **100** (1996), 19089.

[133] M. Hildebrand, A.S. Mikhailov, G. Ertl, *Traveling nanoscale structures in reactive adsorbates with attractive lateral interactions*, Phys. Rev. Lett. **81** (1998), 2602.

[134] M. Hildebrand, *Self-organized nanostructures in surface chemical reactions: Mechanisms and mesoscopic modeling*, Chaos **12** (2002), 144.

[135] J. Cisternas, P. Holmes, I.G. Kevrekidis, X. Li, *CO Oxidation on thin Pt crystals: temperature slaving and the derivation of lumped models*, J. Chem. Phys. **118** (2003), 3312–3328.

[136] H.H. Rotermund, *Imaging of dynamics patterns on surfaces*, Curr. Opin. Solid State Mater. **3** (1998), 354.

[137] D. Luss, M. Sheintuch, *Spatiotemporal patterns in catalytic systems*, Catalysis today **105** (2005), 254.

[138] O. Nekhamkina, M. Sheintuch, *Moving waves and spatiotemporal patterns due to weak thermal effects in models of catalytic oxidation*, J. Chem. Phys. **122** (2005), 194701.

[139] M. Sheintuch, O. Nekhamkina, *Stationary fronts due to weak thermal effects in models of catalytic oxidation*, J. Chem. Phys. **123** (2005), 064708.

[140] Y. Kuramoto and H. Nakao, *Power-law spatial correlations and the onset of individual motions in self-oscillatory media with non-local coupling*, Physica D **103** (1997), 294–313.

[141] Y. Kuramoto, *Phase and center manifold reductions for large populations of coupled oscillators with application to non-locally coupled systems*, International Journal of Bifurcation and Chaos **7** (1997), 789–805.

[142] D. Battogtokh, *Pattern formation in nonlocally coupled oscillators*, Prog. of Theor. Phys. **102** (1999), 947–952.

[143] Y. Kuramoto, H. Nakao, D. Battogtokh, *Multi-scaled chemical turbulence in large populations of oscillators in a diffusive medium*, Physica A **288** (2000), 244–264.

[144] D. Battogtokh, Y. Kuramoto, *Turbulence of nonlocally coupled oscillators in the Benjamin-Feir stable regime*, Phys. Rev. E **61** (2000), 3227–3230.

[145] D. Battogtokh, *Phase turbulence in the nonlocally coupled phase equation*, Phys. Lett. A **299** (2002), 558–564.

[146] Y. Kuramoto, D. Battogtokh, *Coexistence of Coherence and Incoherence in Nonlocally Coupled Phase Oscillators*, Nonlinear Phenom. Complex Syst. **5** (2002), 380.

[147] D. Tanaka, *Critical exponents of Nikolaevskii turbulence*, Phys. Rev. E **71** (2005), 025203.

[148] E.M. Nicola, M. Or-Guil, W.Wolf, M. Bär, *Drifting pattern domains in a reaction-diffusion system with nonlocal coupling*, Phys. Rev. E **65** (2002), 055101.

[149] Y. Kuramoto, S. Shima, D. Battogtokh, Y. Shiogai, *Mean-field theory in self-oscillatory fields with non-local coupling*.

[150] Ernesto M Nicola, *Interfaces between Competing Patterns in Reaction-Diffusion Systems with Nonlocal Coupling*, Ph.D. thesis, Technische Universität Dresden, 2001.

[151] R. Courant, D. Hilbert, *Methods of Mathematical Physics*, Interscience Publishers, New York, 1953.

[152] http://www.eccentrix.com/members/chempics/Cell.html.

[153] B. Hess, *Periodic patterns in biology*, Naturwissenschaften **87** (2000), 199–211.

[154] http://www.cs.helsinki.fi/group/sysfys/images/4.html.

[155] H.R. Petty, R.G. Worth, A. Kindzelski, *Imaging sustained dissipative patterns in the metabolism of individual living cells*, Phys. Rev. Lett. **84** (2000), 2754.

[156] B. Hess and A.S. Mikhailov, *Self-organization in living cells*, Ber. Bunsenges. Phys. Chem. **98** (1994), 1198–1201.

[157] A.S. Mikhailov, B. Hess, *Self-organization in living cells: Networks of protein machines and nonequilibrium soft matter*, J. Biolog. Phys. **28** (2002), 655.

[158] B. Hess, A.S. Mikhailov, *Transition from molecular chaos to coherent spiking of enzymic reactions in small spatial volumes*, Biophys. Chem. **58** (1996), 365–368.

[159] L. Stryer, *Biochemistry*, W.H. Freeman, S. Francisco, 1975.

[160] Michaelis L., Menten M., *Die Kinetik der Invertinwirkung*, Biochem. Z. **49** (1913), 333–369.

[161] J. Monod, J. Wyman, J.P. Changeux, *On the nature of allosteric transitions: A plausible model*, J. Mol. Biol. **12** (1965), 88.

[162] D. Koshland, Nemethy G., Filmer D., *Comparison of experimental binding data and theoretical models in proteins containing subunits*, Biochemistry **5** (1966), 365.

[163] A.C. Storer, A. Cornish-Bowden, *Kinetic evidence for a 'mnemonical' mechanism for rat liver glucokinase*, Biochem. J. **165** (1977), 61–69.

[164] K. Kamata, M. Mitsuya, T. Nishimuira, J. Eiki, Y. Nagata, *Structural basis for allosteric regulation of the monomeric allosteric enzyme human glucokinase*, Structure **12** (2004), 429–438.

[165] M.L. Ludwig, R.G. Matthews, *Effector regulation in a monomeric enzyme*, Nature structural biology **9** (2002), 236–238.

[166] P. Ascenzi, A. Bocedi, A. Bolli, M. Fasano, S. Notari, F. Polticelli, *Allosteric modulation of monomeric proteins*, Biochem. Molec. Biolog. Ed. **33** (2005), 169–176.

[167] D.E. Atkinson, G.M. Walton, *Kinetics of regulatory enzymes. Escherichia Coli Phosphofructokinase*, J. Biolog. Chem. **240** (1965), 757–763.

[168] D.E. Atkinson, J.A. Hathaway, *Kinetics of regulatory enzymes. Kinetic order of the yeast diphosphopyridine nucleotide isocitrate dehydrogenase reaction and a model for the reaction*, J. Biolog. Chem. **240** (1965), 2682–2690.

[169] D.E. Atkinson, *Regulation of enzyme function*, Annu. Rev. Microbiol. **23** (1969), 47–68.

[170] T. Schirmer, P.R. Evans, *Structural basis of the allosteric behavior of phosphofructokinase*, Nature **343** (1990), 140–145.

[171] I. Auzat, E. Gawlita, J. Garel, *Slow ligand-induced transitions in the allosteric Phosphofructokinase from Escherichia Coli*, J. Mol. Biol. **249** (1995), 478.

[172] L.A. Blumenfeld, A.N. Tikhonov, *Biophysical Thermodynamics of Intracellular Processes*, Springer Verlag, New York, 1994.

[173] J.A. Adams, *Kinetic and catalytic mechanisms of protein kinases*, Chem. Rev. **101** (2001), 2271.

[174] I. Schlichting, S.C. Almo, G. Rapp, K. Wilson, K. Petratos, A. Lentfer, A. Wittinghofer, , W. Kabsch, E.F. Pai, G. Petsko, R. Goody, *Time-resolved x-ray crystallographic study of the conformational change in HA-Ras p21 protein on GTP hydrolysis*, Nature **345** (1990), 309–315.

[175] I. Schlichting, J. Berendzen, G.N. Phillips Jr, R.M. Sweet, *Crystal structure of photolysed carbonmonoxy-myoglobin*, Nature **371** (1994), 808.

[176] G. Hummer, F. Schotte, P.A. Anfinrud, *Unveiling functional protein motions with picosecond x-ray crystallography and molecular dynamics simulations*, Proc. Natl. Acad. Sci. USA **101** (2004), 15330–15334.

[177] D. Bourgeois, A. Royant, *Advances in kinetic protein crystallography*, Curr. Opinion Struct. Biolog. **15** (2005), 538–547.

[178] M. Eigen, R. Rigler, *Sorting single molecules: Application to diagnostics and evolutionary biotechnology*, PNAS **91** (1994), 5740–5747.

[179] T. Funatsu, Y. Harada, M. Tokunaga, K. Salto, T. Yanagida, *Imaging of single fluorescent molecules and individual ATP turnovers by single myosin molecules in aqueous solution*, Nature **374** (1995), 555.

[180] R.M. Dickson, A.B. Cubitt, R.Y. Tsien, W.E. Moerner, *On/off blinking and switching behavior of single molecules of green fluorescent protein*, Nature **388** (1997), 355.

[181] H.P. Lu, L. Xun, X.S. Xie, *Single-molecule enzymatic dynamics*, Science **282** (1998), 1877.

[182] S. Weiss, *Fluorescence spectroscopy of single biomolecules*, Science **283** (1999), 1676.

[183] L. Edman, Z. Földes-Papp, S. Wennmalm, R. Rigler, *The fluctuating enzyme: A single molecule approach*, Chem. Phys. **247** (1999), 11–22.

[184] E.J. Bjerneld, Z. Földes-Papp, M. Käll, R. Rigler, *Single-molecule surface-enhanced raman and fluorescence correlation spectroscopy of horseradish peroxidase*, J. Phys. Chem. B **106** (2002), 1213.

[185] Y. Jung, E. Barkai, R.J. Silbey, *Current status of single-molecule spectroscopy: Theoretical aspects*, J. Chem. Phys. **117** (2002), 10980.

[186] M. Ishikawa, Y. Maruyama, M. Futamata, *Single molecule imaging and spectroscopy using fluorescence and surface-enhanced raman*, J. Biol. Phys. **28** (2002), 573.

[187] T. Ha, A.Y. Ting, J. Lang, W.B. Caldwell, A.A. deniz, D.S. Chemla, P.G. Schultz, S. Weiss, *Single-molecule fluorescence spectroscopy of enzyme conformational dynamics and cleavage mechanism*, Proc. Natl. Acad. Sci. USA **96** (1999), 893–898.

[188] Y. Chen, D. Hu, E.R. Vorpagel, H.P. Lu, *Probing single-molecule T4 lysozyme conformational dynamics by intramolecular fluorescence energy transfer*, J. Phys. Chem. **107** (2003), 7947–7956.

[189] F.A.A. Mulder, A. Mittermaier, B. Hon, F.W. Dahlquist, L.E. Kay, *Studying excited states of proteins by NMR spectroscopy*, Nature structural biology **8** (2001), 932–935.

[190] A.L. Borovinskiy, A. Yu. Grosberg, *Design of toy proteins capable of rearranging conformations in a mechanical fashion*, J. Chem. Phys. **118** (2003), 5201.

[191] D. Müller-Enoch, H. Gruler, *The activation of cytochrome p-450 dependent monooxygenase system by light*, Z. Naturforschung **41** (1986), 604.

[192] W. Häberle, H. Gruler, Ph. Dutkowski, D. Müller-Enoch, *The activation of the cytochrome p-450 dependent monooxygenase system by light*, Z. Naturforschung **45** (1990), 237.

[193] H. Gruler, D. Müller-Enoch, *Slaving the cytochrome p-450 dependent monooxygenase system by periodically applied light pulses*, Eur. Biophys. J. **19** (1991), 217.

[194] M. Schienbein, H. Gruler, *Enzyme kinetics, self-organized molecular machines, and parametric resonance*, Phys. Rev. E **56** (1997), 7116.

[195] B. Hess and A.S. Mikhailov, *Microscopic self-organization in living cells: A study of time matching*, J. Theor. Biol. **176** (1995), 181–184.

[196] A.S. Mikhailov, B. Hess, *Fluctuations in living cells and intracellular traffic*, J. Theor. Biol. **176** (1995), 185–192.

[197] A.M. Zhabotinsky, M. Dolnik, I.R. Epstein, *Pattern formation arising from wave instability in a simple reaction-diffusion system*, J. Chem. Phys. **103** (1995), 10306–10314.

[198] A.R. Rovinsky, A.M. Zhabotinsky, I.R. Epstein, *Target patterns arising from the short-wave instability in near-critical regimes of reaction-diffusion systems*, Phys. Rev. E **56** (1997), 2412–2417.

Acknowledgments

First of all, I would like to thank Prof. Alexander Mikhailov, for having been such a careful advisor, always ready to answer questions, and to share his scientific knowledge.

I would also like to acknowledge Prof. Gerhard Ertl, who gave me the opportunity to carry out my PhD work under ideal conditions, and showed great understanding of my personal situation. Although I regret not having had more direct collaboration with him, his questions and suggestions about my work always helped me to gain a new viewpoint and deeper insight.

I want to thank Prof. Harald Engel, my advisor at the Technical University, for his support and helpfulness.

I am deeply grateful to all the colleagues whose paths I have crossed in the Physical Chemistry department in the last four years, with whom I shared conference trips, daily life, coffee breaks, asados, and Greek, Chinese, and Japanese dinners, in particular (and in alphabetical order!): Sergio Alonso (aka Sergej Alonsov), Matthias Bertram, Carsten Beta, Katrin Domke, Monika Dornhege, Mads Ipsen, Pablo ”Asador” Kaluza, Hiroshi ”Pepe” Kori, Susanna Manrubia, Thanassis Papathanasiou, Christian Punckt (mein anspruchsvoller Deutschlehrer), Oliver Rudzick, Pablo ”Zen” Sánchez Bodega, Yuichi Togashi, Damián Zanette, and Dai Zhang.

A special mention goes to Michael Stich, for having been a very conscientious guide as I took my first steps both in Germany and in nonlinear dynamics. I would like to thank him for many scientific discussions, especially about birhythmicity, which he tried very patiently to make acceptable to me.

Pedro Stange has been thoughtful and friendly in helping me get started with the enzyme work. Sune Danø, Thomas Mair, and Rudiger Thul have answered several biological questions per email. With Prof. John “Jack” Hudson I had brief but meaningful discussions.

Other people have helped me enormously both with scientific support and friendship: Valentina Beato (la mia stella alpina), Silvia de Monte and Francesco d’Ovidio (i miei fisici preferiti), and Alessandro Torcini.

I want to thank Hiroshi, Yuichi, Katrin, Christian, Pablo, and Jan Christoph for reading and commenting parts of this manuscript.

Without Tiziano this thesis would not have been written, and I truly mean it: He has been the best coworker I could ever wish for in household and child care, as well as a system administrator, computer teacher, proof reader, and consultant for physical, mathematical, and psychological difficulties (and there were many!).

Finally, I want to thank Raffaello for teaching me about chaos and complex systems in real life!